

Deterministic fatigue life simulation of flexible sign structures

by

Khalid Walid Ahmad Al Shboul

B.S., Jordan University of Science and Technology, 2013

M.S., Jordan University of Science and Technology, 2018

AN ABSTRACT OF A DISSERTATION

submitted in partial fulfillment of the requirements for the degree

DOCTOR OF PHILOSOPHY

Department of Civil Engineering
Carl R. Ice College of Engineering

KANSAS STATE UNIVERSITY
Manhattan, Kansas

2022

Abstract

Fatigue failure of highway sign structures has been recognized in many states due to sustained wind loading events. AASHTO specifies that the structural component should be designed for infinite life by maintaining the wind-induced stress below their constant amplitude fatigue threshold (CAFT). However, for the existing structures that are typically not designed for fatigue, it is essential to evaluate the condition of all the critical and fatigue-prone components for safety considerations. The visual inspection consumes a lot of time and effort and may not detect unnoticed fatigue cracks. A need for analytical inspection tools to examine all the critical members and connections in terms of remaining fatigue life has received growing attention to ensure public safety. The reliability of such analytical tools depends on the accuracy of wind loading models applied during the life span of the structure. A fill-interpolate-extend approach is devised to furnish wind loading data ensemble for the entire time span of analysis. This ensemble is utilized to establish a reliable synthetic wind model to generate fatigue cycle counts. A comprehensive analytical framework including structural modeling, stress extraction/processing, and fatigue damage simulation integrated to yield an affordable tool applicable to different sign structures topologies. The resulting software for non-cantilever overhead structure as well as cantilever and butterfly assemblies are successfully verified to predict real cases for fatigue damage reflecting the in-situ condition of the structures.

Deterministic fatigue life simulation of flexible sign structures

by

Khalid Walid Ahmad Al Shboul

B.S., Jordan University of Science and Technology, 2013

M.S., Jordan University of Science and Technology, 2018

A DISSERTATION

submitted in partial fulfillment of the requirements for the degree

DOCTOR OF PHILOSOPHY

Department of Civil Engineering
Carl R. Ice College of Engineering

KANSAS STATE UNIVERSITY
Manhattan, Kansas

2022

Approved by:

Major Professor
Prof. Hayder Rasheed

Copyright

© Khalid Al Shboul 2022.

Abstract

Fatigue failure of highway sign structures has been recognized in many states due to sustained wind loading events. AASHTO specifies that the structural component should be designed for infinite life by maintaining the wind-induced stress below their constant amplitude fatigue threshold (CAFT). However, for the existing structures that are typically not designed for fatigue, it is essential to evaluate the condition of all the critical and fatigue-prone components for safety considerations. The visual inspection consumes a lot of time and effort and may not detect unnoticed fatigue cracks. A need for analytical inspection tools to examine all the critical members and connections in terms of remaining fatigue life has received growing attention to ensure public safety. The reliability of these analytical tools depends on the accuracy of wind loading models applied during the life span of the structure. A fill-interpolate-extend approach is devised to furnish wind loading data ensemble for the entire time span of analysis. This ensemble is utilized to establish a reliable synthetic wind model to generate fatigue cycle counts. A comprehensive analytical framework including structural modeling, stress extraction/processing, and fatigue damage simulation integrated to yield an affordable tool applicable to different sign structures topologies. The resulting software for non-cantilever overhead structure as well as cantilever and butterfly assemblies are successfully verified to predict real cases for fatigue damage reflecting the in-situ condition of the structures.

Table of Contents

List of Figures	ix
List of Tables	xiii
Acknowledgments.....	xiv
Dedication	xv
Chapter 1 - Introduction.....	1
1.1 Background.....	1
1.2 Objective.....	3
1.3 Scope of Dissertation	4
Chapter 2 - Literature Review.....	5
2.1 Overview.....	5
2.2 Fatigue Damage of Highway Sign Structures.....	5
2.3 Analytical Modeling of Natural Wind	8
2.4 Spatial Variation and Interpolation of Wind Speeds	10
2.5 References.....	10
Chapter 3 - Spatial Wind Speed Interpolation Using Isoparametric Shape Functions for Structural Loading	13
3.1 Abstract.....	13
3.2 Introduction.....	14
3.3 Formulation.....	16
3.3.1 Study Area and Dataset.....	16
3.3.2 Meshing the Domain.....	17
3.3.3 The Finite Element Shape Functions	18
3.3.4 Sensitivity Refinement.....	20
3.3.5 Solving for The Shape Functions.....	23
3.4 Synthetic Wind-Time Histories	31
3.5 Rain Flow Counting Technique.....	34
3.6 Interpolation Assessment.....	35

3.7	Results and Discussion	49
3.8	Software Development.....	52
3.8.1	Input Interface.....	53
3.8.2	Results.....	53
3.9	Comparison of Kansas Cities.....	56
3.10	Tracking of Wind Speed Trend.....	59
3.11	Conclusions and Recommendations	61
3.12	References.....	62
Chapter 4 - Intelligent Approach for Accurately Predicting Fatigue Damage in Overhead Highway Sign Structures		
4.1	Abstract.....	66
4.2	Introduction.....	67
4.3	Overhead Sign Structure Model and Automation.....	70
4.3.1	Structural Modeling	70
4.3.2	Model Automation.....	71
4.3.3	Dynamic Amplification Factor (DAF).....	71
4.4	Wind Loading on Overhead Sign Structures	72
4.4.1	Wind Speed Raw and Extended Data	72
4.4.2	Synthetic Wind-Time Histories	73
4.4.3	Validation of The Synthetic Time-History	77
4.4.4	Wind Loading on The Structure	78
4.5	Fatigue Analysis and Life Prediction.....	79
4.5.1	S-N Curve Implementation.....	79
4.5.2	Rainflow Counting and Palmgren-Miner Rule	81
4.5.3	Fatigue Life Calculation Automation	82
4.6	Case Study	83
4.6.1	Results of a Sign Structure Analyzed	83
4.6.2	Further Results and Discussion.....	87
4.7	Additional Examples.....	91
4.8	Conclusions.....	95
4.9	References.....	96

Chapter 5 - Evaluating Fatigue in Steel Cantilevered Sign Structures Under Service Life	
Wind Events Through a Comprehensive Tool for Inspection	99
5.1 Abstract	99
5.2 Introduction.....	100
5.3 Sign Structures Modeling	103
5.3.1 KDOT Highway Structures.....	103
5.3.2 FE Modeling	108
5.3.2.1 Structure.....	108
5.3.2.2 Mast-to-Arm connection.....	108
5.3.2.3 Sign(s) Modeling	115
5.4 Dynamic Amplification Factor (DAF).....	116
5.5 Wind Loading on Sign Structures.....	116
5.5.1 Synthetic Wind Time Histories.....	116
5.5.2 Wind Loading Calculation.....	118
5.6 Fatigue Damage Evaluation.....	118
5.6.1 AASHTO S-N Curves.....	118
5.6.2 Damage Assessment and Palmgren-Miner Rule.....	121
5.7 Analysis Automation	123
5.8 Evaluation of a Damaged Structure and Software Validation	125
5.8.1 Background.....	125
5.8.2 Field Inspection of the Structure.....	126
5.8.3 Analytical Investigation	127
5.9 Conclusions.....	132
5.10 References.....	133
Chapter 6 - Conclusions and Recommendations	136
6.1 Conclusions.....	136

List of Figures

Figure 1.1 Failure of cantilever sign support structure along I-65 in Tennessee [3]	2
Figure 1.2 Fatigue failure at mast arm connection of traffic signal [4]	2
Figure 3.1 Kansas interpolation zones.....	17
Figure 3.2 Mapping (a) the quadrilateral and (b) triangular elements.....	19
Figure 3.3 Revised Kansas triangular interpolation mesh	21
Figure 3.4 High wind speed records for 122 days for Pawnee county resulted from the triangular elements and the quadrilateral elements.....	21
Figure 3.5 Mean wind speed records for 122 days for Pawnee county resulted from the triangular elements and the quadrilateral elements.....	22
Figure 3.6 High wind speed records for 122 days for McPherson county resulted from the triangular elements and the quadrilateral elements.....	22
Figure 3.7 Mean wind speed records for 122 days for McPherson county resulted from the triangular elements and the quadrilateral elements.....	23
Figure 3.8 Illustration of the shape function properties for the quadrilateral element.	24
Figure 3.9 County coordinates in terms of city coordinates	26
Figure 3.10 Area decomposition of a quadrilateral element into four triangles.	27
Figure 3.11 Comparison of the shape function values between the direct solution and the constrained optimization for four different counties.	30
Figure 3.12 Speed vs. Number of cycles for 45 years in Wichita for different cosine waves.....	32
Figure 3.13 Wind-Time histories for various mean wind speeds	33
Figure 3.14 Flowchart for wind-time histories generation	33
Figure 3.15 Rainflow counting example.....	34
Figure 3.16 (a) Wind time histories database (b) Speed-Cycle matrix.....	35
Figure 3.17 New interpolation zones (Zone A and Zone B).....	36
Figure 3.18 Predicted daily high wind speeds for zone A and zone B in Wichita, 1975– 2019.....	37
Figure 3.19 Predicted daily mean wind speeds for zone A and zone B in Wichita, 1975– 2019.....	38

Figure 3.20 Measured vs. Predicted high wind speeds in Wichita for 120 days	39
Figure 3.21 Measured vs. Predicted mean wind speeds in Wichita for 120 days.....	40
Figure 3.22 Measured vs. Predicted High and Mean Wind Speeds for Sedgwick County, 1975, 1980, 1985.....	46
Figure 3.23 Measured vs. Predicted High and Mean Wind Speeds for Sedgwick County, 1990, 1995, 2000.....	47
Figure 3.24 Measured vs. Predicted High and Mean Wind Speeds for Sedgwick County, 2005, 2010, 2015.....	48
Figure 3.25 Zone 8.....	49
Figure 3.26 (A) High wind speeds for zone 8; (B) Medium wind speeds for zone 8.....	50
Figure 3.27 Comparison between the interpolated values for Cowley and Labette County (a) high speed (b) mean speed.	51
Figure 3.28 Wichita cycles distribution.....	52
Figure 3.29 Speed-Cycle Generation interface.....	54
Figure 3.30 Results Screen	54
Figure 3.31 (A) Save Box Screen; (B) Sample File.....	55
Figure 3.32 Database Mirroring.....	55
Figure 3.33 45-Years Damaging Index for Main Cities in Kansas.....	57
Figure 3.34 The 10-Years Damaging Index for Main Cities in Kansas	58
Figure 3.35 Average mean and high wind speeds in winter from 1975-2015 for (A) Wichita (B) Garden City (C) Dodge City (D) Goodland.....	60
Figure 3.36 Average mean and high wind speeds in spring from 1975-2015 for (A) Wichita (B) Garden City (C) Dodge City (D) Goodland.....	61
Figure 4.1 Model of four-chord box truss.....	70
Figure 4.2 (A) The modeler interface, (B) adding sign(s) option interface.....	71
Figure 4.3 Frequency-response curve and average DAF ($\xi = 0.02$).....	72
Figure 4.4 Speed vs. number of cycles for 45-years in City of Wichita.....	76
Figure 4.5 Real and synthetic wind comparison for mean 7 mph and high 13.8 mph, (1 mph = 1.609 km/h). (a) Time domain (b) Frequency domain	78
Figure 4.6 S-N curve for welded aluminum adapted from [23]	80
Figure 4.7 Fatigue life software interface	83

Figure 4.8 Fatigue life calculation flowchart.....	84
Figure 4.9 Wichita Staad model (Model 2)	85
Figure 4.10 Fatigue life results sample for Wichita model.....	87
Figure 4.11 Damaged members in the model	88
Figure 4.12 Member’s connection type per AASHTO.....	88
Figure 4.13 damage variation with speed in member 259	89
Figure 4.14 damage in member 260 after exposing it to extra 4 years of wind speeds....	90
Figure 4.15 damaged members in the overhead sign truss under investigation (Wichita) courtesy of KDOT (Bureau of structural and geotechnical services).....	91
Figure 4.16 Examples for three models and location of the evaluated members	93
Figure 4.17 (A) Stress variation in the critical members with wind speed (B) Damage index for the critical members resulted from 45 years of wind loading	94
Figure 5.1(a) Cantilever model (b) Butterfly model.....	105
Figure 5.2 Support Connection, (A) Gusseted box connections. (B) Ring-stiffened box connection	106
Figure 5.3 (a) post-to-chord connection (b) The model.....	109
Figure 5.4 (A) rigid model (B) rigid-dead load (C) gusseted-normal wind (D) gusseted-dead load (E) ring stiffened-normal wind (F) gusseted-dead load.	110
Figure 5.5 Key nodes deflection for three models (A) Dead load case (B) Normal wind load case.....	112
Figure 5.6 Stress at center of the plate vs. mesh density	114
Figure 5.7 The calibrated beam connection.....	114
Figure 5.8 Stress comparison in different locations for the beam model vs. the fine-meshed model	115
Figure 5.9 Frequency-response curve and average DAF ($\xi = 0.02$).....	116
Figure 5.10 Flowchart of the automation algorithm	124
Figure 5.11 The modeling software interface	125
Figure 5.12 Sedgwick structure geometry (all dimensions are in feet/inches).....	126
Figure 5.13 Crack in the weld toe in Sedgwick structure, courtesy of KDOT (Bureau of structural and geotechnical services).	127
Figure 5.14 Fatigue life results in Sedgwick structure.	130

Figure 5.15 Stress variation with wind speed in the connection.....	130
Figure 5.16 (a) the actual structure (b) the model.....	132
Figure 5.17 Damage in the butterfly member's model.....	132

List of Tables

Table 3-1 City center coordinates	24
Table 3-2 Coordinates of County Centers	25
Table 3-3 Main parameters in Wind-Speed simulation	32
Table 3-4 Measured vs. Predicted high wind speeds in Wichita	41
Table 3-5: Measured vs. Predicted mean wind speeds in Wichita	41
Table 3-6 Chi-Square Goodness of fit results all year-groups.....	44
Table 3-7: Chi-Square Goodness of fit results for all seasons in 1975.....	44
Table 4-1: Representation of Kansas regions using eight cities	73
Table 4-2 Results color code.....	83
Table 4-3 Case study model information.....	85
Table 5-1 Geometric properties for cantilever models	107
Table 5-2 Geometry and loading data for the test model.....	109
Table 5-3 Key nodes deflection for the three models.	111
Table 5-4 <i>S-N</i> equations for different structure components used by AASHTO	120
Table 5-5. Stress calculation in different structure spots.....	122
Table 5-6. Sedgwick structure information	126
Table 5-7. Stress and damage in connection associated to each wind speed.....	131
Table 5-8 Wyandotte structure information.....	131

Acknowledgments

I would like to thank the Kansas Department of Transportation (KDOT) for funding and making possible the research this dissertation is based on.

To my advisor, Prof. Hayder Rasheed. Thank you for the opportunity to work on such an exciting and challenging project. Thank you for being so confident in me and, more importantly, for your endless guidance and support. Thanks are further extended to my committee members: Dr. Christopher Jones, Dr. Bacim Alali, and Dr. Krishna Ghimire, for giving me helpful instructions and suggestions in my research.

Thank you to my mother, Nahla Nabhan, for her unlimited support, love, and prayers. A special feeling of gratitude to my Father, Walid Al Shboul, for his wise guidance, continued encouragement, and outstanding support, whose words of encouragement and push for tenacity are the reason for what I have become today. I just hope I can do the same for my children

To my wife, Ayah. Thank you for supporting me and believing in me. Thank you for your patience, understanding, love, and devotion, in addition to my children, Waleed and Ayla, for being in my life on this journey. It was a long journey, but we made it.

Dedication

To my parents, who sacrificed everything for their children's education

and

My wonderful wife for her endless love

and

My children

Chapter 1 - Introduction

1.1 Background

Full-span sign support structures are extensively used on major highways to guide road users. They are usually extended over multi-lanes to provide the necessary information and to prevent any hazard resulting from collisions. Sign structures are considered very flexible because of their long span length and relatively small cross-sectional area and mass. Thus, these structures have very low natural frequencies, and the damping is also very low. These characteristics make the sign structure very susceptible to significant large amplitude vibration. Large-amplitude vibration is not necessarily a problem concerning the integrity of the design. However, a large number of motorist complaints occur when the displacement range exceeds 200 mm (8 in.) [1]. Motorists cannot see the signals or signs and are concerned about driving under the vibrating structures. More significant issues resulted from the fact that the stress fluctuations in various structure details caused fatigue cracking in these details. Many states agencies have been reported cracks in sign structures due to fatigue damage, and in a few cases, sign structure failures have also been reported [2]. Figure 1.1 and Figure 1.2 show fatigue failure in highway sign structures. Kansas Department of transportation used different sign structures topology in the Kansas transportation system. Most of them have been in service for more than 45 years. These structures could be classified as cantilevered, double cantilevered, and overhead sign structures. Each type of structure has the most fatigue-sensitive connections at which the fatigue damage tends to occur. Due to the old age of these structures, most of them were not designed for fatigue. Thus, it is essential to perform routine fatigue inspections in all



Figure 1.1 Failure of cantilever sign support structure along I-65 in Tennessee [3]



Figure 1.2 Fatigue failure at mast arm connection of traffic signal [4]

structural components to ensure structural integrity and repair/replace any defective elements. The inspection in this regard should be thorough and comprehensive to eliminate any possible un-noticed fatigue cracks. This makes the inspection plans tedious and complex to implement due to the large number of members that should be evaluated. A more reliable methodology to assist in the inspection and evaluation of these structures should be developed to save time and guide inspectors to identify fatigue cracks in different critical spots. This study aims to develop a comprehensive approach for fatigue inspection from wind loading development to modeling, analysis, and structural assessment of various components in the highway structures.

1.2 Objective

Cantilevered and butterfly sign support structures can be an attractive option due to their lower cost and reducing the probability of vehicle collision compared to the overhead sign structures. Over the last few decades, the span of cantilevered support structures has been increased due to installing the upright further away from the road for safety reasons. These structures are being used for roads of multi lanes, thereby increasing the susceptibility of these structures to large amplitude oscillations resulting from different wind loading scenarios. Therefore, a study was initiated to evaluate the remaining fatigue life of cantilevered and butterfly structures. This study is intended to build a comprehensive tool to accurately predict the remaining fatigue life of cantilevered and butterfly highway sign support structures subjected to prolonged and sustained wind fluctuations. The specified objectives of the analytical study are as follows:

- Develop a spatial interpolation technique using Isoparametric finite element shape functions to derive wind speed records for all unsampled Kansas counties from actual data recorded at 17 city locations within and around Kansas and make this wind dataset projectable into the future by mirroring the data about the end of December 2019-beginning of the January 2020 line.
- Develop fatigue analysis procedures to estimate the fatigue life expectation of cantilevered and butterfly sign structures and evaluate the remaining fatigue life of these structures based on the wind loading dataset generated above.
- Identify and mark the most critical members in the various sign structures for further field investigation concerning fatigue life consumption.

- Project the number of years in the future that these structures would experience total fatigue damage and guide the highway agencies to prioritize their inspection plans.
- Develop a computationally affordable simulation package using object-oriented programming language C# interacting with the finite element software STAAD Pro to predict fatigue life.

1.3 Scope of Dissertation

This dissertation consists of six chapters. The first chapter presents an introduction of the topic, objectives of this work, and dissertation scope. Chapter two includes the literature review undertaken on the topics related to the dissertation scope. Chapter three introduces the methodology of preparing wind loading cycles for structural application using Isoparametric finite element shape functions interpolation. In chapter four, the developed wind loading was used to validate the damage in defected overhead highway sign structures and to examine the applicability of the developed approach in detecting the damaged members. In chapter five. The developed methodology was extended to other flexible structures, namely, the cantilevered and butterfly highway structures, and evaluated the applicability of this method in identifying the fatigue damage in different connection members. In addition to that, structural software development was discussed. Conclusions and recommendations of the present study are presented in chapter six.

Chapter 2 - Literature Review

2.1 Overview

A brief overview regarding the work conducted on the fatigue inspection of highway sign structures is introduced in this chapter.

2.2 Fatigue Damage of Highway Sign Structures

The repeated loading and unloading of members and connections in highway sign structures leads to the susceptibility of these structures to the accumulation of fatigue damage, which can ultimately lead to fatigue failure. Therefore, it is important that these structures be designed adequately to endure typical in-service loading scenarios while maintaining a level of accumulated fatigue damage below an acceptable limit. In order to ensure that the support structures are proportioned to withstand all wind-induced loading scenarios, and the wind-induced stresses are below the constant amplitude fatigue threshold (CAFT), AASHTO 2015 [5] specifications require the support structures to be designed for fatigue using two approaches: the nominal stress-based classifications of typical connection details or experiment-based methodologies. Past research studies were conducted to provide reasonably detailed methods of quantifying fatigue damage in highway sign structures. Many researchers also performed fatigue simulations using different wind loading scenarios, types of structures, and analysis methods [2,6–11].

Creamer et al. [7] studied the effects of vehicle-induced gusts on cantilever sign structures. In this study, truck-induced gusts were experimentally studied for one double cantilever (i.e., “butterfly”) structure and two standard double-mastarm cantilever structures. The structure response and member forces due to vehicle-induced gusts were experimentally investigated. In addition, they analytically and numerically studied the static and dynamic

behavior of the sign structures and determined an appropriate gust load to simulate the measured field response. In order to provide “infinite” lives for the sign structure anchor bolts, they suggested that Category C Constant Amplitude Fatigue Limit be used for double-nutted anchor bolts.

Kaczinski et al. [12] authored the NCHRP Report 412, and the main goals were to characterize the susceptibility of cantilevered structures to excessive displacement or fatigue damage, to develop equivalent static load ranges for the four common wind-related causes of fatigue, to identify the fatigue sensitive connection details in a sign structure, and to determine the fatigue strength of anchor bolts. They indicated that at least four wind-loading phenomena could produce significant displacements and stress ranges in cantilever sign structures: galloping, vortex shedding, natural wind gusts, and truck-induced wind gusts. These four types of loading are considered to make the most contribution to fatigue damage of sign structures. In order to determine the susceptibility to galloping and vortex shedding, the authors undertook wind tunnel testing of scale models of five representative structures. Three structures were cantilevered mast arms (one supporting two traffic lights, one supporting one traffic light, and one with a sign), while the others were two-chord trusses (both supporting a single sign). The structures were tested with and without the sign attachments. It was found that galloping-induced vibrations depend on the condition of the specific structure and do not occur frequently, but once they do occur, vibration can persist. The authors recommended that a shear pressure range of 21 psf (1000 Pa) be applied vertically to the vertically projected area of any attachment when designing for galloping of cantilevered structures. The authors reported that overhead structures are likely not susceptible to galloping. In regards to vortex shedding, they found that it only needs to be

considered before the attachments (such as signs or lights) are attached to the structure and that only structures with horizontal supports of large diameter are prone to such phenomena. A second goal of the research was to categorize the fatigue-sensitive connection details with respect to the AASHTO fatigue design curves (AASHTO 1994). They grouped together those details with similar cracking modes and similar stress concentrations into categories A-E', where the fatigue threshold of the detail decreases as you move from letter A to letter E'. The majority of details on a cantilevered sign were put into the E or E' category, though anchor bolts were put into category *D*. Repetto and Solari [13] proposed a mathematical model aimed at deriving a histogram of the stress cycles, the accumulated damage and the fatigue life of slender vertical structures in the along-wind vibration direction. In the research, the response of the vertical structures was treated as a narrow-band process, which greatly simplified the representation of wind velocity. The method broke down the broad-band process of wind velocity and considered each small-time span as a narrow-band process of a mean wind speed plus variations. Natural wind was considered as the load causing fatigue damage.

Ginal [14] investigated the fatigue performance of three full-span overhead sign support structures using ANSYS considering natural wind load and truck-induced pressures. It was concluded that the truck-induced pressure has a minimal damaging effect in most full-span overhead sign structures. On the contrary, the natural wind loading ranging from 20-50 mph has the most damaging effect on these structures, and the predicted remaining life for these structures under investigation ranges from 4-27 years. Kacin et al. [15] performed fatigue analysis of pristine and damaged overhead four-chord truss sign structure using stress histories obtained from finite element solution to identify the critical structural members, using the Kaimal wind spectrum for base wind speeds in the range of 5-25 mph.

The infinite fatigue life was predicted for the welded diagonal members. However, they recommended that field monitoring of the real structure and accurate field measuring of the wind loading should be necessary to confirm the exact conditions of the structures.

2.3 Analytical Modeling of Natural Wind

The literature has investigated several techniques to model the power spectral density function for turbulent wind speed for practical engineering applications. The “classical” model of the wind turbulence spectrum is attributed to Davenport [16]. He used approximately 70 spectra results of horizontal components of gust in intense wind events in various locations and circumstances worldwide. The Davenport model is given by:

$$\begin{aligned}
 Sd(f) &= \frac{4U_*^2 x^2}{f(1+x^2)^{4/3}} \\
 x &= \frac{4000f}{U_z} \\
 V(z) &= V_{10} \cdot \left(\frac{z}{10}\right)^\alpha
 \end{aligned} \tag{1}$$

Where $S_D(n)$ is the fluctuation wind-speed spectrum; n is the frequency; z is the height; $V(z)$ is the mean wind speed at the height of z ; V_{10} is the mean wind speed at the standard height of 10 m; α is the ground roughness exponent, and k is the terrain roughness factor, and U_* is the friction (or shear) velocity. The friction velocity accounts for the wind speed turbulence resulting from interference with the ground surface. From Eq. (1), it is evident that the Davenport model is independent of height above the ground surface. Therefore, the wind turbulence generated with this spectrum is fixed to a mean velocity at a particular reference height. This reference height may not coincide with the height of the structure under consideration. In order to account for such scenarios, several improved models, which are height-dependent, have been suggested.

Several modifications have been made to the Davenport model in order to account for both the structure height above the ground surface and the accuracy of structural response within different frequency ranges. The spectral density of the turbulent wind component proposed by Kaimal [17] takes the height of the structure into account, and it is given by:

$$S_K(f) = \frac{200U_*^2 z}{U_z(1 + 50 \frac{fz}{U_z})^{5/3}} \quad (2)$$

Where S_K is the Kaimal spectrum, z is the height above the ground (10 m (33 ft.)), U_* is shear velocity, U_z is the mean wind velocity at z , and f is the specified frequency.

The wind turbulence spectrum given by Eq. (2) is superior to the Davenport spectrum and is a good model for most structural engineering applications for several reasons. The Kaimal spectrum includes the effect of height on the turbulent wind component, and it has been found to be quite accurate in the higher frequency range to which most engineered structures respond [18].

Kumar and Stathopoulos [19] presented a general approach for representing Gaussian as well as non-Gaussian wind pressure characteristics using the fast Fourier transform algorithm. The simulation procedure needed both Fourier amplitudes and phases in order to generate pressure time histories. The amplitudes were constructed from pressure spectra. The phases were obtained from a stochastic model. Ginal [14] also modeled a time history of randomly varying wind speeds to be applied to the finite element models of three overhead sign structures. A wide range of mean wind speeds (5-50 mph) was used in the analysis, and a fluctuating component of wind was modeled using the Kaimal wind spectrum. This was chosen because, unlike the Davenport spectrum used in Dexter and Ricker [2], the Kaimal spectrum takes elevation into account. An equation based on the superposition of cosine waves was then used to combine the mean and fluctuating components of wind into a wind speed time history.

Li [20] developed a wind load time history to be used in a finite element analysis of sign structures located in Indiana. The range of wind speeds used in the analysis varied from 0-30 mph. In order to create the time history, a fast Fourier transform-based method was employed. Doing this involves choosing a number of frequencies within the range of the natural frequencies of different mode shapes of the structure. The Kaimal spectrum was then used to find the fluctuating component of the wind.

2.4 Spatial Variation and Interpolation of Wind Speeds

Weather data are generally recorded at specific locations, but spatial interpolation can be used to estimate wind speed values at other locations. Various deterministic and geostatistical interpolation methods can approximate values for spatially continuous phenomena from measured values at limited sample points. Most spatial interpolation techniques are based on the concept that derived values are represented as the weighted average of measured values at the sample points. The general interpolation formula is

$$\hat{Z}(x_0, y_0) = \sum_{i=1}^n w_i Z(x_i, y_i) \quad (3)$$

Where $\hat{Z}(x_0, y_0)$ represents the predicted value at a specific location (x_0, y_0) , $Z(x_i, y_i)$ represents the measured value at the sample point (x_i, y_i) , w_i is the weight assigned to the sample point, and n is the number of sampling points used in the [21,22]

2.5 References

- [1] American Welding Society, AWS D1.1-2000. Structural Welding Code—Steel. Miami: American Welding Society,; 2000.
- [2] Dexter RJ. Fatigue-resistant design of cantilevered sign, sign, and light supports. vol. 469. Transportation Research Board; 2002.
- [3] Beneberu E, Goode J, Yazdani N. Computational fluid dynamics application for design of highway sign support structures. Int J Civ Struct Eng 2014;5.

<https://doi.org/10.6088/ijcser.2014050010>.

- [4] Florea MJ, Manuel L, Frank KH, Wood SL. Field tests and analytical studies of the dynamic behavior and the onset of galloping in traffic signal structures. 2007.
- [5] AASHTO. 2015 Interim Revisions to Standard Specifications for Structural Supports for Highway Signs , Luminaires , and Traffic Signals Sixth Edition 2013. 2015.
- [6] Chen G, Wu J, Yu J, Dharani LR, Barker M. Fatigue Assessment of Traffic Signal Mast Arms Based on Field Test Data Under Natural Wind Gusts. *Transp Res Rec* 2001;1770:188–94. <https://doi.org/10.3141/1770-24>.
- [7] Creamer BM, Frank KH, Klingner RE. Fatigue loading of cantilever sign structures from truck wind gusts. 1979.
- [8] Fouad FH, Hosch IE. Design of Overhead VMS Structures for Fatigue Loads. University Transportation Center for Alabama; 2011.
- [9] Letchford C, Cruzado H. Risk assessment model for wind-induced fatigue failure of cantilever traffic signal structures. 2008.
- [10] Hong HP, Zu GG, King JPC. Estimating fatigue design load for overhead steel sign support structures under truck-induced wind pressure. *Can J Civ Eng* 2016;43:279–86. <https://doi.org/10.1139/cjce-2015-0158>.
- [11] DeSantis P V, Haig PE. Unanticipated loading causes highway sign failure. *Proc. ANSYS Conv.*, 1996.
- [12] Kaczinski MR, Dexter RJ, Van Dien JP. Fatigue-resistant design of cantilevered signal, sign and light supports. vol. 412. Transportation Research Board; 1998.
- [13] Repetto MP, Solari G. Dynamic alongwind fatigue of slender vertical structures.

- Eng Struct 2001;23:1622–33.
- [14] Ginal S. Fatigue Performance of Full-Span Sign Support Structures Considering Truck-Induced Gust And Natural Wind Pressures. MS Thesis 2003:393.
- [15] Kacin J, Rizzo P, Tajari M. Fatigue analysis of overhead sign support structures. Eng Struct 2010;32:1659–70. <https://doi.org/10.1016/j.engstruct.2010.02.014>.
- [16] Davenport AG. The spectrum of horizontal gustiness near the ground in high winds. Q J R Meteorol Soc 1962;88:197–8. <https://doi.org/https://doi.org/10.1002/qj.49708837618>.
- [17] Kairnal JC, Wyngaard JC, Izumi Y, Force A. c) u ; ssJ... , " . n.d.
- [18] Simiu E, Scanlan RH. Wind effects on structures: fundamentals and applications to design. vol. 688. John Wiley New York; 1996.
- [19] Kumar KS, Stathopoulos T. Computer simulation of fluctuating wind pressures on low building roofs. J Wind Eng Ind Aerodyn 1997;69:485–95.
- [20] Li X, Whalen TM, Bowman MD. Fatigue Strength and Evaluation of Double–Mast Arm Cantilevered Sign Structures. Transp Res Rec 2005;1928:64–72. <https://doi.org/10.1177/0361198105192800107>.
- [21] Luo W, Taylor MC, Parker SR. A comparison of spatial interpolation methods to estimate continuous wind speed surfaces using irregularly distributed data from England and Wales. Int J Climatol A J R Meteorol Soc 2008;28:947–59.
- [22] Webster R, Oliver MA. Geostatistics for environmental scientists. John Wiley & Sons; 2007.

Chapter 3 - Spatial Wind Speed Interpolation Using Isoparametric Shape Functions for Structural Loading

Khalid W. Al Shboul¹, Hayder A. Rasheed², Abdulkareem AlKhiary³

3.1 Abstract

This study developed a spatial interpolation technique using Isoparametric finite element shape functions to derive wind speed records for all unsampled Kansas counties from actual data recorded at 17 city locations within and around Kansas. A computational method using the Kaimal spectrum is presented for generating artificial time histories of wind speeds. This is done to extract wind-cycle distribution using the Rainflow counting technique, which can be used as input for fatigue analysis procedures of highway sign structures. A user-friendly software was designed using C# to extract wind-speed cycles for all Kansas counties related to different time spans. This software is expected to facilitate fatigue-life prediction because it generates a full range of wind-loading output files that can be used for other fatigue-life simulators (e.g., cantilever sign structures and butterfly sign structure simulators).

¹ Ph.D. Candidate, Department of Civil Engineering, Kansas State University, Manhattan, KS

² Professor, Department of Civil Engineering, Kansas State University, Manhattan, KS

³ Department of Electrical and Computer Engineering, Kansas State University, Manhattan, KS

3.2 Introduction

Fatigue has been recognized as the primary failure mode in many highway sign support structures. Even though these structures would probably withstand larger loads if the loading was static, their response due to wind-load fluctuations should be monitored and analyzed to predict remaining structural fatigue life and prevent any pre-mature damage or failure. Generally, metal structures that are exposed to repetitive loading are expected to yield fatigue damage. Many studies have been conducted to develop inspection procedures to evaluate the status of different structural components during their respected service life [1–4]. However, the fatigue failure involves considerable uncertainties resulting from both materials and the nature of loadings [5,6]. Wind turbulence is considered the leading cause of repeated stress fluctuations in highway sign structures. Therefore, it is essential to be considered in the analysis of these structures. Some facilities may exhibit resonant responses produced by velocity fluctuations of wind turbulency. In addition, the aerodynamic behavior of a structure may be highly dependent upon airflow turbulence. Therefore, wind simulations generated during the structural analysis must accurately capture the characteristics of natural turbulent wind. Unfortunately, however, because the wind is dynamic in nature, the accurate estimation of turbulent wind characteristics during any wind event is cumbersome since these processes are not stationary [1,7]. Quantifying wind loading is a crucial stage in designing engineering structures prone to wind. Wind loading typically focuses on the strongest winds or extreme wind speeds that occur during a structure's lifetime. However, robust wind structural analysis and design require an accurate estimation of extreme wind-speed values and wind-speed variations over time. Although wind behavior is assumed to be a stochastic process, many researchers have

attempted to model and simulate its behavior over time [8–10]. These simulations require building a complete database of continuous wind speed measurements to utilize it as input for the simulations.

The needed wind speed data are obtained from recording metrological stations, which are usually distributed over various locations to record wind-speed measurements. Extreme wind speeds are estimated from these records. However, it is impractical to distribute and set up metrological stations everywhere. For uncovered geographical areas, wind-speed records can be spatially interpolated from those of the measured locations by different means of spatial interpolation methods. These methods assume a more robust correlation among points that are closer to the location of interest than those farther apart. Moreover, most spatial interpolation techniques are based on the concept that derived values are represented as the weighted average of measured values at the sample points. The general interpolation formula is

$$\hat{Z}(x_0, y_0) = \sum_{i=1}^n w_i Z(x_i, y_i) \quad (1)$$

Where $\hat{Z}(x_0, y_0)$ represents the predicated value at a specific location (x_0, y_0) , $Z(x_i, y_i)$ represents the measured value at the sample point (x_i, y_i) , w_i is the weight assigned to the sample point, and n is the number of sampling points used in the interpolation [11,12]. Various spatial and Spatio-temporal methods were developed, and they are characterized as either deterministic or geostatistical interpolation methods, such as trend surface analysis, natural neighbors, splines, Inverse distance weighting (IDW) [12], and Kriging [13]. They are widely used to derive and approximate spatially continuous phenomena from measured values at limited sample points in various disciplines. For Example, Air

pollution exposure [14], indoor temperature distribution [15], surface wind pressure [16] wind speed records [17–19].

Generally, in fatigue life analysis and structural engineering, there is a need to estimate wind speed fluctuations at the location of interest and quantify the number of cycles associated with each stress level induced on the structure in case of the absence of data for any site, rather than using the wind speed values from the nearest available point, which might over or underestimate the reality. A more robust approach would be to systematically interpolate the wind speed values.

This paper implements and treats the Isoparametric finite element shape functions as spatial interpolators to generate wind speed records for unsampled areas from surrounding sampled locations in the state of Kansas. The conventional Finite Element analysis procedures are depicted herein, including meshing the domain, evaluating the shape functions, and solving the unknowns. After deriving the wind speed records, namely, mean and high wind speeds for all counties in the state of Kansas, the synthetic daily wind time history is generated, and the Rain Flow analysis is conducted to transform the irregular histories into constant-amplitude cycle-loading to produce a complete database of wind speed vs. the number of cycles for fatigue analysis. This database was implemented in a computer program to quickly generate the needed data over any period for any county in Kansas.

3.3 Formulation

3.3.1 Study Area and Dataset

Kansas is located between 37° and 40° to the north and $94^{\circ} 35'$ to $102^{\circ} 3'$ to the west. The area of Kansas is 213,100 km² and is made up of 105 counties, and it is included in the

tornado alley. The complete wind-speed records for the 45-year interpolation period were collected and extended for all cities inside and around the Kansas borders, as represented by red dots in Figure 3.1. These cities represent the sampled locations that were used to interpolate county data throughout the study area. The complete records for these cities were obtained [20] and used as base interpolation data to approximate and precisely build wind-time histories for all Kansas counties in a piecewise manner.

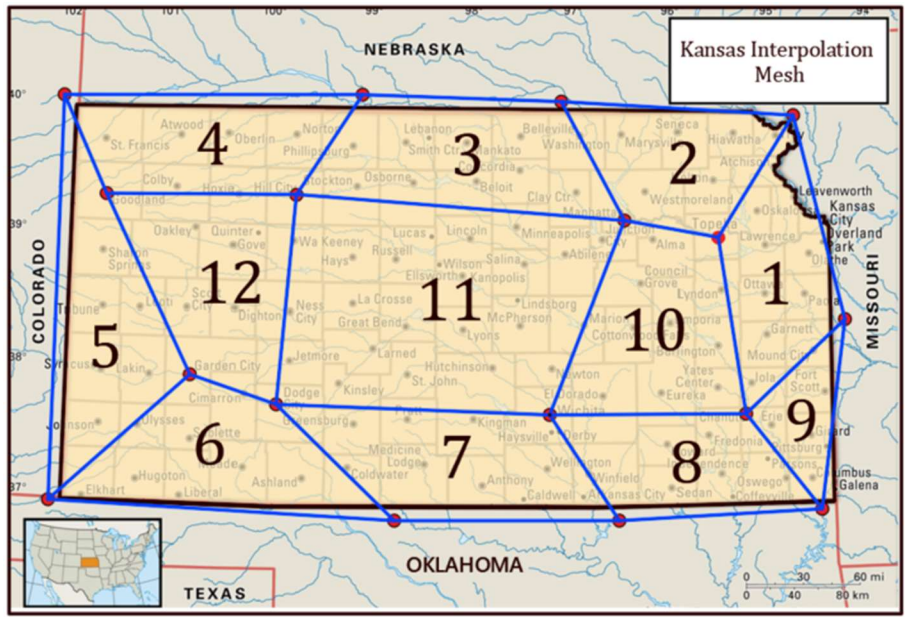


Figure 3.1 Kansas interpolation zones.

3.3.2 Meshing the Domain

In the generalized finite element analysis, discretizing the problem domain is the first step in formulating the procedure. It is of most importance as the elements' number, size, and shape are responsible for the FE solution's accuracy [21]. However, in the current problem, the domain is discretized in a limited number of elements to fully utilize the available data records ("nodal solutions"), and no further refinement could be realized. This varies from one problem to another depending on the availability of the data that is being used in the interpolation. Therefore, Kansas was divided into twelve geometrical interpolation zones

to cover the entire domain, combined with quadrilateral and triangular shapes, as shown in Figure 3.1

3.3.3 The Finite Element Shape Functions

As shown in Figure 3.1, the discretized domain revealed twelve geometrical interpolation zones (elements) with quadrilateral and triangular shapes. Two zones were triangular (zones 5 and 9), whereas the other zones were quadrilateral. Knowing the nodal high and medium wind-speed values at the corner of each zone allowed us to mimic the FE shape functions on obtaining the solution within the domain from the nodal values. The shape functions corresponding to each element were used to approximate these specific wind speed quantities within the zone. The Isoparametric quadrilateral element, a two-dimensional element with natural and global coordinates, was used to model quadrilateral zones in the discretized domain. This element is characterized by linear shape functions in the x and y directions, and it is a generalization of the 4-node rectangular element. Each Isoparametric quadrilateral element has four nodes with two in-plane degrees of freedom at each node, as shown in Figure 3.2a, with global coordinates of the four nodes denoted by (x_1, y_1) , (x_2, y_2) , (x_3, y_3) , and (x_4, y_4) . The node order for each element is essential—they must be listed in a counterclockwise direction starting from any node. The element was mapped to a master square using the natural coordinates ξ and η , as shown in Figure 3.2a, where $\xi \in [-1, 1]$ and $\eta \in [-1, 1]$ and the four Lagrangian shape functions for this element are listed in Eq. (2) in terms of the natural coordinates ξ and η . Similarly, the linear triangular element, a two-dimensional finite element with natural and global coordinates, was used to model the triangular shapes. This element is characterized by linear shape functions. Each linear triangle has three nodes with two in-plane degrees of freedom at

each node, and the global coordinates of the three nodes are denoted by (x_1, y_1) , (x_2, y_2) , and (x_3, y_3) . The element was mapped into a master triangle using the natural coordinates ξ and η , as shown in Figure 3.2b, Eq. (3) details the three shape functions for this element [22].

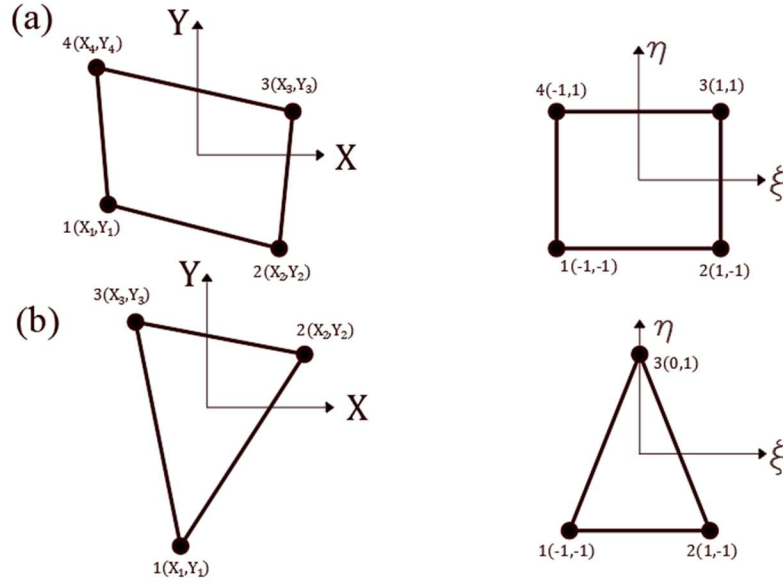


Figure 3.2 Mapping (a) the quadrilateral and (b) triangular elements

$$\left\{ \begin{array}{l} N_1 = \frac{1}{4}(1 - \xi)(1 - \eta) \\ N_2 = \frac{1}{4}(1 + \xi)(1 - \eta) \\ N_3 = \frac{1}{4}(1 + \xi)(1 + \eta) \\ N_4 = \frac{1}{4}(1 - \xi)(1 + \eta) \end{array} \right\} \quad (2)$$

$$\left\{ \begin{array}{l} N_1 = \frac{1}{4}(1 - \xi)(1 - \eta) \\ N_2 = \frac{1}{4}(1 + \xi)(1 - \eta) \\ N_3 = \frac{1}{2}(1 + \eta) \end{array} \right\} \quad (3)$$

3.3.4 Sensitivity Refinement

The meshed Kansas map revealed twelve geometrical interpolation zones (elements) with quadrilateral and triangular shapes. Two zones were triangular (zones 5 and 9), whereas the other zones were quadrilateral. Mesh refinement is crucial in obtaining accurate results. This section compares the results obtained from the quadrilateral elements with another way of discretizing the domain using triangular elements. One quadrilateral element (Zone 11 in the original disseized map) was selected and divided into two triangles, 11a, and 11b, as shown in Figure 3.3, then a known county was selected into each triangular element to obtain the new shape functions using the triangular shape functions relation as in Eq. (3). The computed shape functions were used to calculate the high and mean wind speeds for these two counties then the results were compared with those obtained from the quadrilateral elements. The high and mean wind speed values obtained for Pawnee county (element 11a) are shown in Figure 3.4 and Figure 3.5, respectively, and in Figure 3.6 and Figure 3.7 for McPherson county (element 11b). It is evident from the figures that both meshing techniques revealed nearly the same results implying that using the quadrilateral elements provides accurate results, and no more refinement should be made. This is considered an affordable meshing technique since it offers fewer elements to solve.

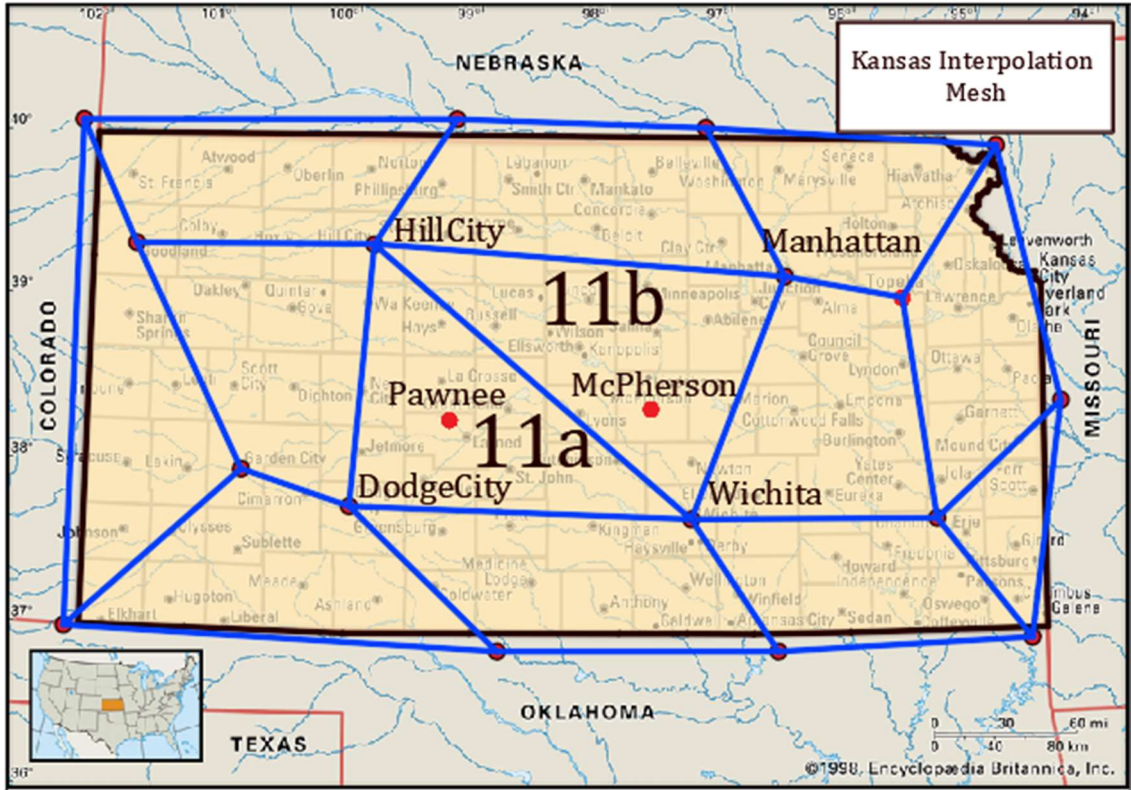


Figure 3.3 Revised Kansas triangular interpolation mesh

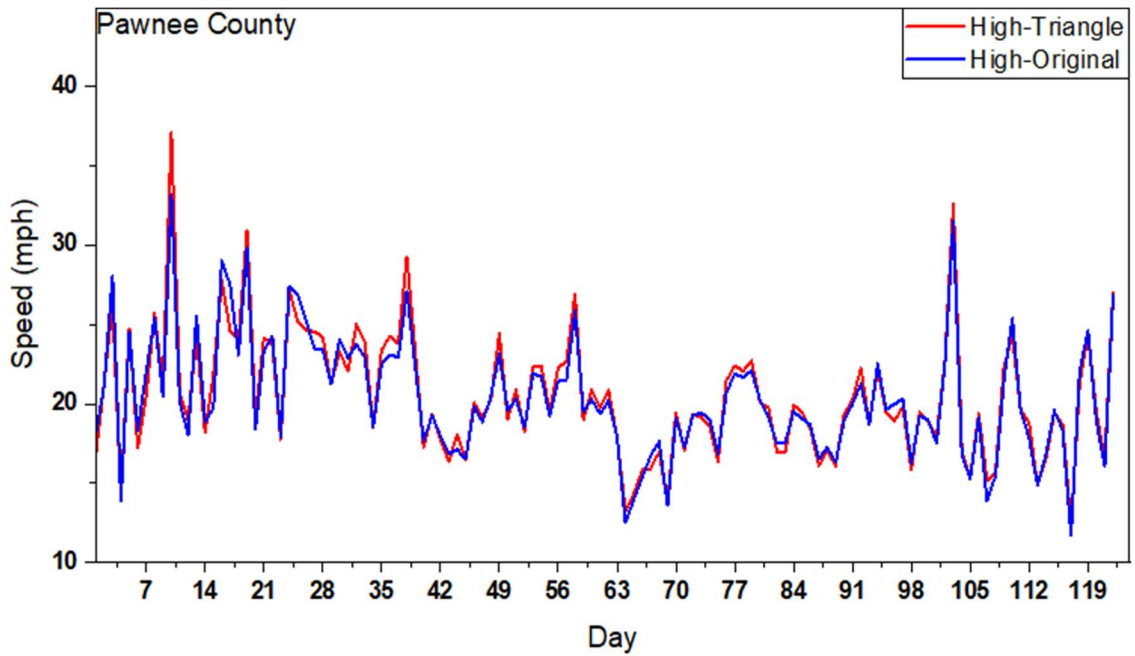


Figure 3.4 High wind speed records for 122 days for Pawnee county resulted from the triangular elements and the quadrilateral elements

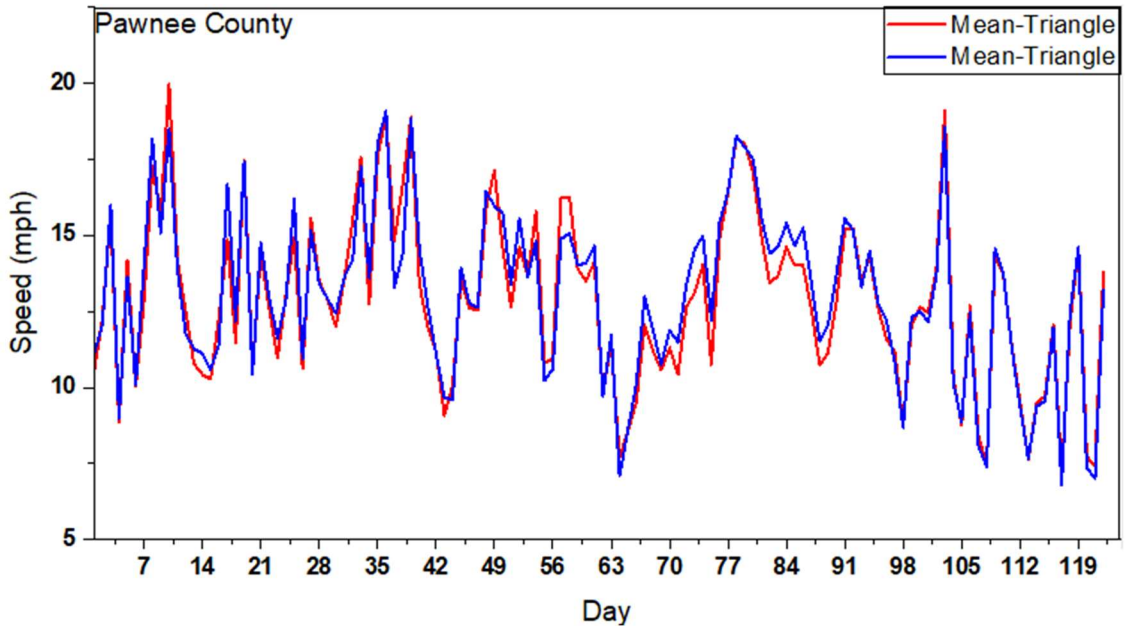


Figure 3.5 Mean wind speed records for 122 days for Pawnee county resulted from the triangular elements and the quadrilateral elements

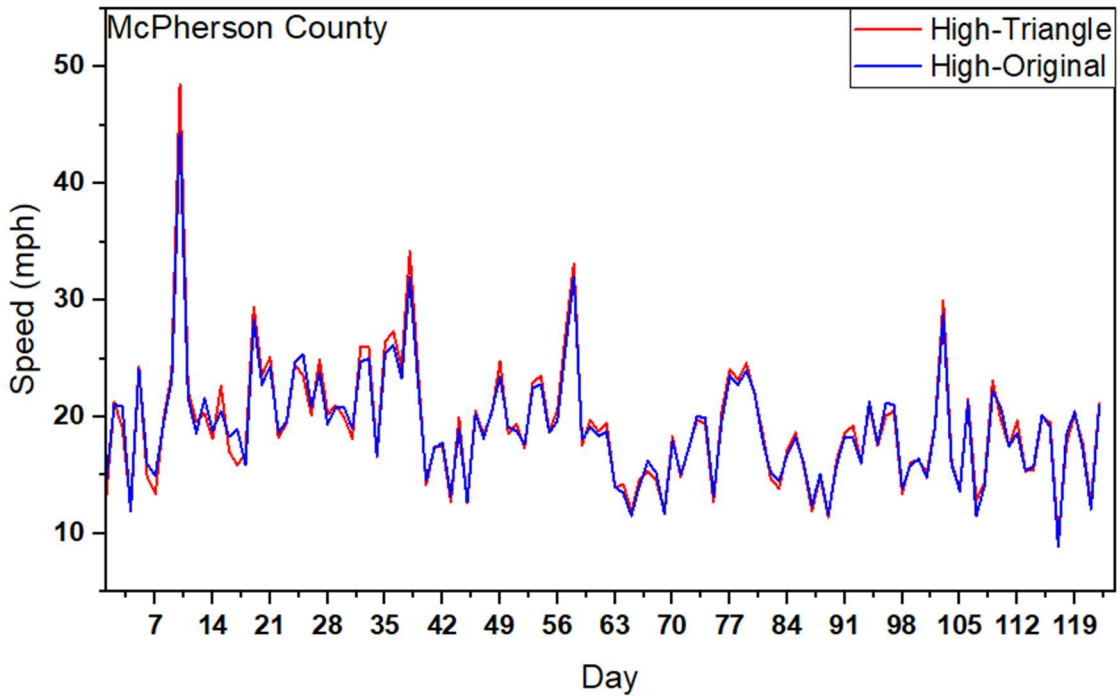


Figure 3.6 High wind speed records for 122 days for McPherson county resulted from the triangular elements and the quadrilateral elements

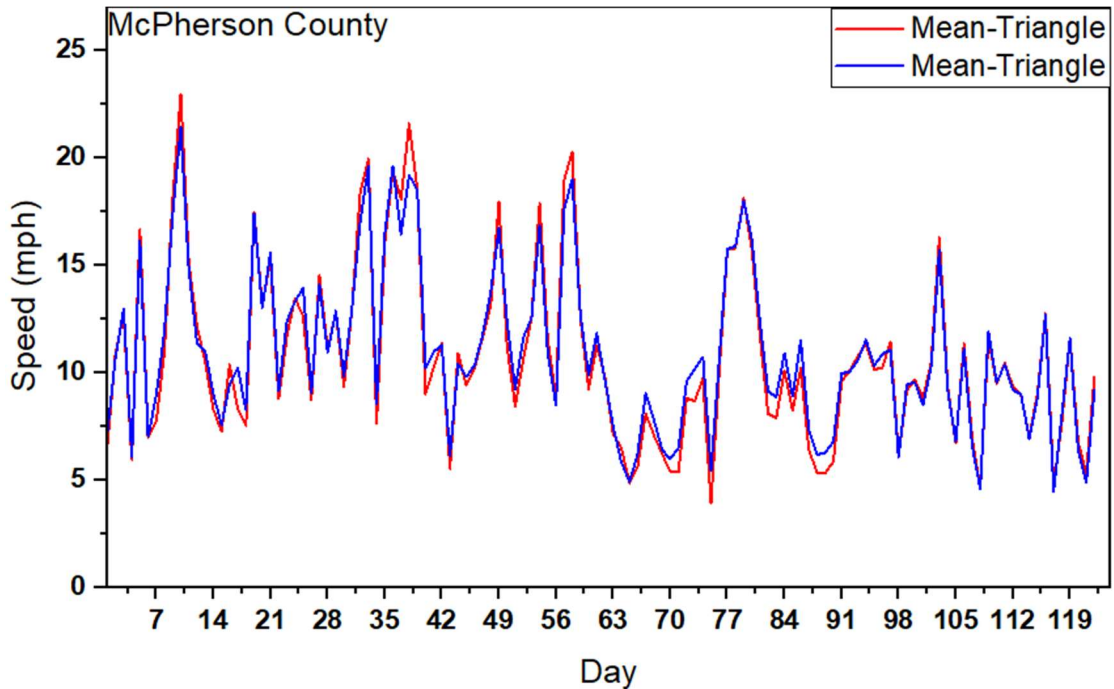


Figure 3.7 Mean wind speed records for 122 days for McPherson county resulted from the triangular elements and the quadrilateral elements

3.3.5 Solving for The Shape Functions

The shape function N_i has a value of 1 at node i and zero at the other nodes. This is a property of exact interpolation that allows recovering the value observed at the sampling point. Moreover, the pointwise shape functions can be linearly combined, and their sum is equal to 1, as illustrated in Figure 3.8. The coordinates of the center of main cities (element corners) and central coordinates of the county within the element were obtained using ArcGIS [23] in terms of latitude and longitude (x,y) as shown in Table 3-1 and

Table 3-2. The county's coordinates could be written as a linear combination of the four corner coordinates as in Eq. (4). The shape functions were used to express the coordinates of the center of the county in terms of the coordinate of the cities in each element, as shown in Figure 3.9.

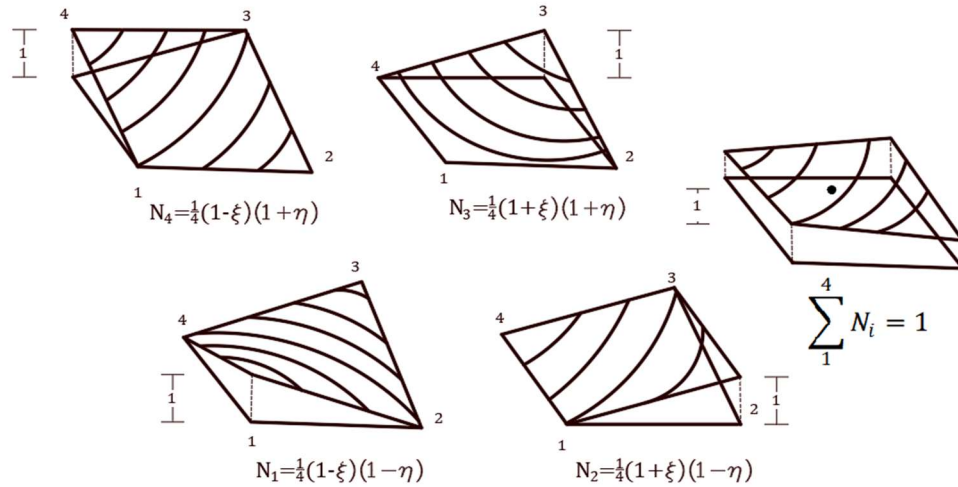


Figure 3.8 Illustration of the shape function properties for the quadrilateral element.

Table 3-1 City center coordinates

City	X(Global)	Y(Global)
Akron	131.12	93.96
Kearney	442.608	98.64
Goodland	169.808	196.92
Hill City	409.872	204.72
Beatrice	729.736	108
Manhattan	803.144	245.28
Topeka	926.152	254.64
Cameron	1009.48	120.48
Elkhart	136.088	562.56
Garden City	283.896	425.28
Dodge City	387.064	451.8
West Woodward	461.464	584.4
Wichita	691.736	470.52
Ponca	738.36	582.84
Chanute	931.8	493.92
El Dorado Springs	1033.976	359.76
Monett	1021.08	573.48

Table 3-2 Coordinates of County Centers

County	x	y	County	x	y	County	x	y
Allen	958	430	Ellsworth	610	308	Lincoln	612	257
Anderson	958	379	Finney	300	401	Linn	1009	380
Atchison	949	176	Ford	408	461	Logan	263	274
Barber	551	530	Franklin	955	326	Lyon	853	345
Barton	549	341	Gearry	782	264	McPherson	674	360
Bourbon	1007	433	Gove	340	273	Marion	742	362
Brown	920	133	Graham	412	210	Marshall	806	143
Butler	772	450	Grant	239	479	Meade	349	529
Chase	801	371	Gray	343	455	Miami	1009	327
Chautauqua	844	543	Greeley	176	341	Mitchell	610	204
Cherokee	1008	538	Greenwood	843	434	Montgomery	904	536
Cheyenne	188	141	Hamilton	177	412	Morris	792	313
Clark	414	530	Harper	624	538	Morton	175	534
Clay	731	210	Harvey	701	411	Nemaha	867	147
Cloud	674	192	Haskell	289	479	Neosho	956	481
Coffey	900	376	Hodgeman	405	401	Ness	405	341
Comanche	482	538	Jackson	894	197	Norton	408	143
Cowley	771	530	Jefferson	940	222	Osage	903	316
Crawford	1008	486	Jewell	611	142	Osborne	544	210
Decatur	346	142	Johnson	1009	275	Ottawa	675	246
Dickinson	735	285	Kearny	240	412	Pawnee	488	387
Doniphan	970	137	Kingman	620	483	Phillips	474	142
Douglas	955	276	Kiowa	485	483	Pottawatomie	827	204
Edwards	481	435	Labette	957	534	Pratt	548	472
Elk	843	495	Lane	343	339	Rawlins	268	140
Ellis	478	273	Leavenworth	986	224	Reno	623	423
Rice	611	364	Shawnee	898	252	Republic	672	136
Riley	777	214	Sheridan	346	211	Trego	415	273
Rooks	479	209	Sherman	185	208	Wabaunsee	848	264
Rush	480	335	Smith	542	141	Wallace	184	273
Russell	544	272	Stafford	553	410	Washington	741	141
Saline	674	360	Stanton	180	479	Wichita	228	339
Scott	289	340	Stevens	239	536	Wilson	904	479
Sedgwick	697	466	Sumner	699	531	Woodson	905	430
Seward	293	536	Thomas	275	208	Wyandotte	1019	237

$$\begin{Bmatrix} X \\ Y \end{Bmatrix} = \begin{bmatrix} X_1 & X_2 & X_3 & X_4 \\ Y_1 & Y_2 & Y_3 & Y_4 \end{bmatrix} \begin{Bmatrix} N_1 \\ N_2 \\ N_3 \\ N_4 \end{Bmatrix} \quad (4)$$

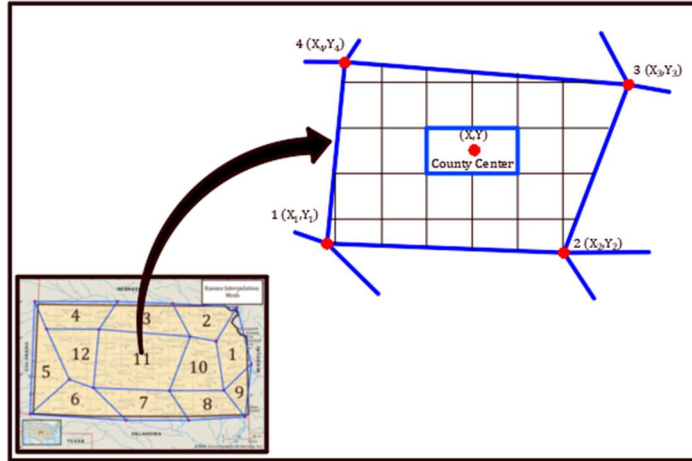


Figure 3.9 County coordinates in terms of city coordinates

Using the unity property of the shape functions, Eq. (4) could be re-written as

$$\begin{Bmatrix} X \\ Y \\ 1 \end{Bmatrix} = \begin{bmatrix} X_1 & X_2 & X_3 & X_4 \\ Y_1 & Y_2 & Y_3 & Y_4 \\ 1 & 1 & 1 & 1 \end{bmatrix} \begin{Bmatrix} N_1 \\ N_2 \\ N_3 \\ N_4 \end{Bmatrix} \quad (5)$$

This is an underdetermined system of equations; we wish to derive a fourth continuity equation using the physical area of the element. The total area of a quadrilateral element is composed of summation of the area of four triangles intersected at an arbitrary point inside the element at (X, Y) , which represents the coordinates of the county as shown in Figure 3.10.

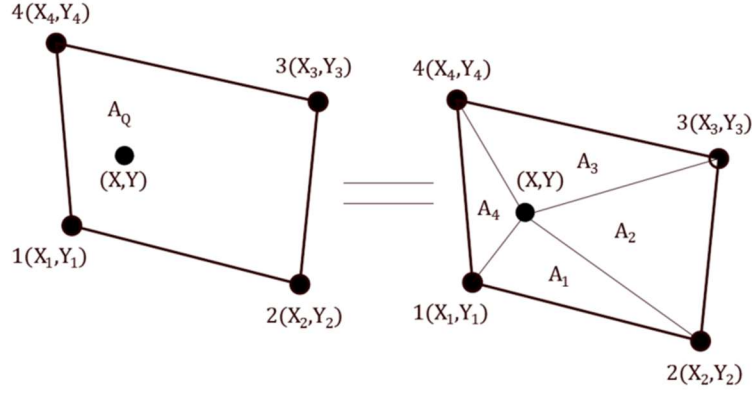


Figure 3.10 Area decomposition of a quadrilateral element into four triangles.

The area of quadrilateral could be calculated using the Gauss quadrature formula in two-dimensional regions as

$$A_Q = \int_{-1}^1 \int_{-1}^1 |\mathbf{J}(\xi, \eta)| d\xi d\eta = \sum_{i=1}^2 \sum_{j=1}^2 w_i w_j |\mathbf{J}(\xi_i, \eta_j)| \quad (6)$$

where $|\mathbf{J}(\xi, \eta)|$ is the determinant of the Jacobian matrix evaluated at the integration points $(\pm \frac{1}{\sqrt{3}}, \pm \frac{1}{\sqrt{3}})$, and $w_i = 1$, $w_j = 1$, and the Jacobian matrix is given by Eq. (7).

$$[\mathbf{J}] = \begin{bmatrix} \frac{\partial x}{\partial \xi} & \frac{\partial y}{\partial \xi} \\ \frac{\partial x}{\partial \eta} & \frac{\partial y}{\partial \eta} \end{bmatrix} \frac{1}{4} \begin{bmatrix} -(1-\eta) & (1-\eta) & (1+\eta) & -(1+\eta) \\ -(1-\xi) & -(1+\xi) & (1+\xi) & (1-\xi) \end{bmatrix} \begin{bmatrix} x_1 & y_1 \\ x_2 & y_2 \\ x_3 & y_3 \\ x_4 & y_4 \end{bmatrix} \quad (7)$$

evaluating Eq. (6) and Eq. (7) yields

$$A_Q = \frac{1}{2} x_4 (y_1 - y_3) + \frac{1}{2} y_2 (-y_1 + y_3) + \frac{1}{2} x_1 (y_2 - y_4) + \frac{1}{2} x_3 (-y_2 + y_4) \quad (8)$$

At the same time, the area of a triangle is given by Eq. (9)

$$\mathbf{A}_T = 0.5 * \begin{vmatrix} 1 & x_i & y_i \\ 1 & x_j & y_j \\ 1 & x & y \end{vmatrix} \quad (9)$$

Where (x_i, y_i) , (x_j, y_j) , the coordinates of the base and they change for each triangle while the (x, y) are the coordinates of the apex and they are constant for all the triangles. The area of all triangles could be written as:

$$\mathbf{A}_1 = \frac{1}{2} \begin{vmatrix} 1 & x_1 & y_1 \\ 1 & x_2 & y_2 \\ 1 & x & y \end{vmatrix} \quad \mathbf{A}_2 = \frac{1}{2} \begin{vmatrix} 1 & x_2 & y_2 \\ 1 & x_3 & y_3 \\ 1 & x & y \end{vmatrix} \quad \mathbf{A}_3 = \frac{1}{2} \begin{vmatrix} 1 & x_3 & y_3 \\ 1 & x_4 & y_4 \\ 1 & x & y \end{vmatrix} \quad \mathbf{A}_4 = \frac{1}{2} \begin{vmatrix} 1 & x_4 & y_4 \\ 1 & x_1 & y_1 \\ 1 & x & y \end{vmatrix} \quad (10)$$

Replacing the x in A_I by

$$x = \sum_{i=1}^4 x_i N_i \quad (11)$$

Then we have

$$A_Q - A_2 - A_3 - A_4 = \frac{1}{2} \begin{vmatrix} 1 & x_1 & y_1 \\ 1 & x_2 & y_2 \\ 1 & \sum_{i=1}^4 x_i N_i & y \end{vmatrix} \quad (12)$$

After substituting Eq. (10) and Eq. (11) in Eq. (12) and rearranging terms, we get

$$m = AN_1 + BN_2 + CN_3 + DN_4 \quad (13)$$

Where:

$$m = \frac{1}{2}(xy_1 - xy_2) \quad A = \frac{1}{2}x_1(y_1 - y_2) \quad B = \frac{1}{2}x_2(y_1 - y_2) \quad C = \frac{1}{2}x_3(y_1 - y_2) \quad D = \frac{1}{2}x_4(y_1 - y_2)$$

Then the Eq. (5) could be re-written as

$$\begin{Bmatrix} X \\ Y \\ 1 \\ \frac{1}{2}(xy_1 - xy_2) \end{Bmatrix} = \overbrace{\begin{bmatrix} X_1 & X_2 & X_3 & X_4 \\ Y_1 & Y_2 & Y_3 & Y_4 \\ 1 & 1 & 1 & 1 \\ \frac{1}{2}X_1(Y_1 - Y_2) & \frac{1}{2}X_2(Y_1 - Y_2) & \frac{1}{2}X_3(Y_1 - Y_2) & \frac{1}{2}X_4(Y_1 - Y_2) \end{bmatrix}}^{\mathbf{A}} \begin{Bmatrix} N_1 \\ N_2 \\ N_3 \\ N_4 \end{Bmatrix} \quad (14)$$

Eq. (14) cannot be solved directly since it produces a singular matrix. However, the Moore-Penrose [24] inverse A^+ could be calculated easily for this square matrix. Eq. (14) is written in compact form as

$$\mathbf{b} = \mathbf{A}\mathbf{x} \quad (15)$$

The Pseudo-inverse of the singular matrix \mathbf{A} is

$$\mathbf{A}^+ = (\mathbf{A}^T \mathbf{A})^{-1} \mathbf{A}^T \quad (16)$$

And the solution of Eq. (15) will therefore be approximately obtained as

$$\mathbf{x} = \mathbf{A}^+ \mathbf{b} \quad (17)$$

The solution \mathbf{x} , in this case, is not exact. Instead, it minimizes the quantity

$$\|\vec{b} - A\vec{x}\|$$

By knowing the county center coordinates X and Y and the nodal cities' coordinates (x_1, y_1) , (x_2, y_2) , (x_3, y_3) , and (x_4, y_4) , the shape functions (N_1, N_2, N_3, N_4) could be calculated by solving Eq. (17). An alternative way to solve Eq. (4) is by using linear programming in Excel. Figure 3.11 shows a comparison between the values of shape functions obtained by

the direct solution of Eq. (17) and the constrained optimization solution obtained from excel for five different counties. The values are in good agreement with each other. Some slight differences are noticed due to the fact that there is no exact solution for the prescribed system of equations, and both methods to optimize the solution since excel provides a quick way to solve for the shape functions, all the values were obtained using Excel. After calculating the shape functions $\{N_i\}$, medium and high wind speeds were interpolated using the nodal values for the element surrounding the county as follows:

$$HWS = N_1 * HWS_1 + N_2 * HWS_2 + N_3 * HWS_3 + N_4 * HWS_4 \quad (18)$$

$$MWS = N_1 * MWS_1 + N_2 * MWS_2 + N_3 * MWS_3 + N_4 * MWS_4 \quad (19)$$

It is worth mentioning that this work is not intended to produce wind speed surfaces.

Instead, it produces discrete wind speed records at the center of each county.

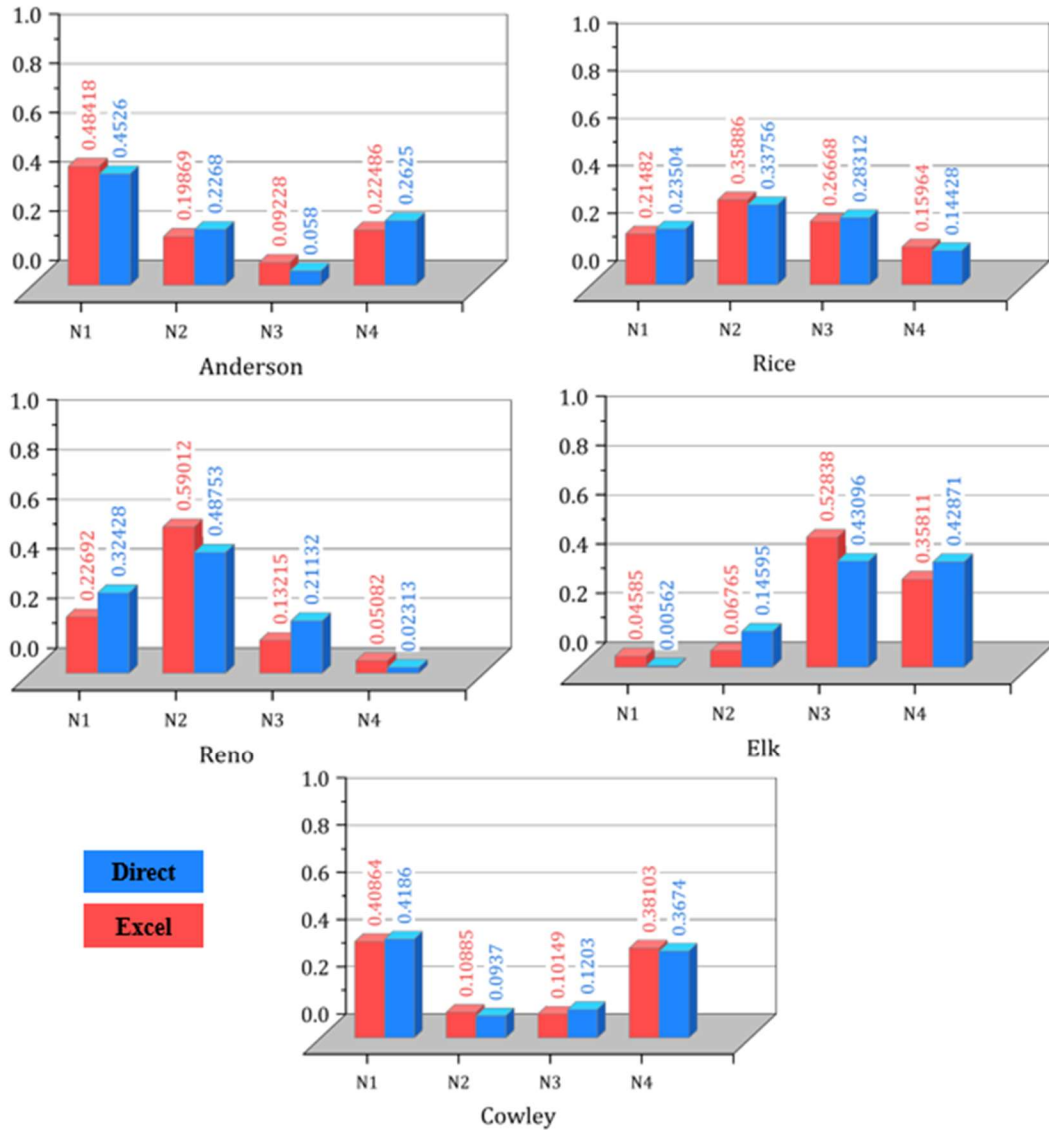


Figure 3.11 Comparison of the shape function values between the direct solution and the constrained optimization for four different counties.

For the triangular element, the county coordinates could be written in terms of the nodal coordinates as

$$\begin{Bmatrix} X \\ Y \\ 1 \end{Bmatrix} = \begin{bmatrix} X_1 & X_2 & X_3 \\ Y_1 & Y_2 & Y_3 \\ 1 & 1 & 1 \end{bmatrix} \begin{Bmatrix} N_1 \\ N_2 \\ N_3 \end{Bmatrix} \quad (20)$$

The shape functions could be easily calculated by inverting the coordinates matrix and multiplying it by the county coordinates vector.

$$\begin{Bmatrix} N_1 \\ N_2 \\ N_3 \end{Bmatrix} = \begin{bmatrix} X_1 & X_2 & X_3 \\ Y_1 & Y_2 & Y_3 \\ 1 & 1 & 1 \end{bmatrix}^{-1} \begin{Bmatrix} X \\ Y \\ 1 \end{Bmatrix} \quad (21)$$

It is worth mentioning that the shape functions obtained from Eq. (21) match exactly the corresponding values obtained from Excel since the coefficient matrix of Eq. (21) is not singular.

3.4 Synthetic Wind-Time Histories

The spatial and temporal variation of wind velocity has two components: a daily mean component $U(z)$ and daily fluctuating component $u(z, t)$, expressed through $U(z, t) = U(z) + u(z, t)$, where $U(z, t)$ is the varying wind speed profile during the day [25]. Because wind is a random process with dynamic behavior that cannot be entirely predicted, the well-established Kaimal spectrum [9] was utilized to simulate the power spectral density, Eq. (22) and the weighted amplitude wave superposition represented by Eq. (23) [10] was used to generate daily time history for the entire 45 years.

$$S_K(f) = \frac{200U_*^2 z}{U_z (1 + 50 \frac{fz}{U_z})^{5/3}} \quad (22)$$

Where S_K is the Kaimal spectrum, z is the height above the ground (10 m (33 ft.)), U_* is shear velocity, U_z is the mean wind velocity at z , and f is the specified frequency.

$$u(t) = \sum_{i=1}^N \sqrt{2S_i f_i \Delta f} \cdot \cos(2\pi f_i t + \phi_i) \quad (23)$$

In Eq. (23), a sensitivity calculation was performed in which 798, 80, and 40 cosine waves were used to build synthetic wind speed histories for the city of Wichita over a 45-year period and extract the number of wind cycles corresponding to each speed. The Rain Flow method was used to establish the distribution of speed versus the number of cycles for the three cosine waves (Figure 3.12). The figure shows that the overall distribution was precisely identical, and the cycle variation followed a Gaussian distribution. Discretization

using 80 waves was an excellent trade-off between computational speed and accuracy of results to generate the 45-year wind database. More details are in [4]. Table 3-3 summarizes the main parameters used in the final wind-speed simulation. Figure 3.13 shows a sample of generated wind-time histories for various mean wind speeds.

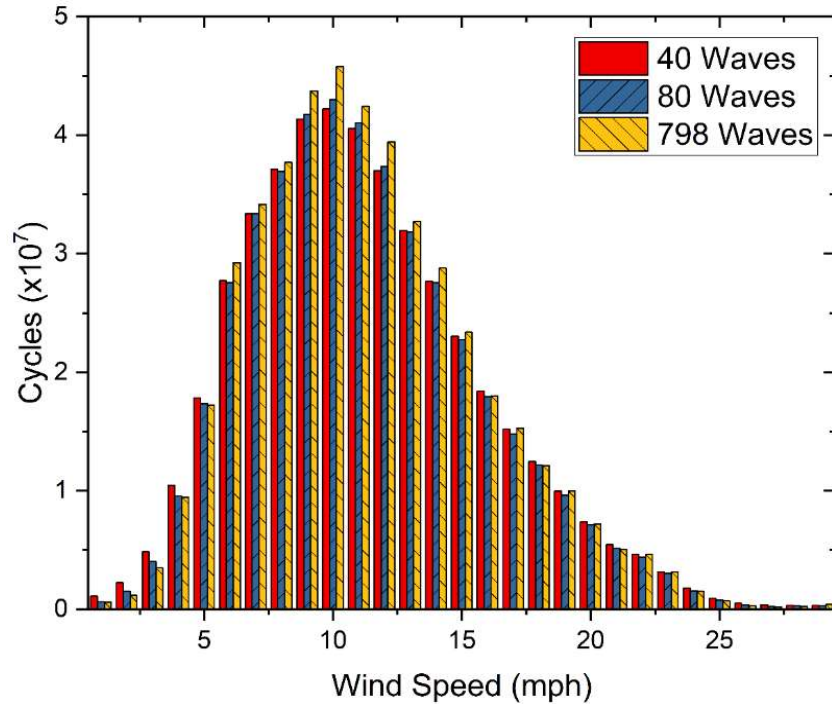


Figure 3.12 Speed vs. Number of cycles for 45 years in Wichita for different cosine waves

Table 3-3 Main parameters in Wind-Speed simulation

Parameter	Value
Surface roughness class	Open terrain ($k = 0.005$)
Height above ground	33 ft.
U_z	Vary
U_{max}	Vary
Fluctuation wind speed spectrum	Kaimal
Length of time history	One day
Time step	1 s
Frequency range	3–300 Hz
Number of cosine waves in superposition	80

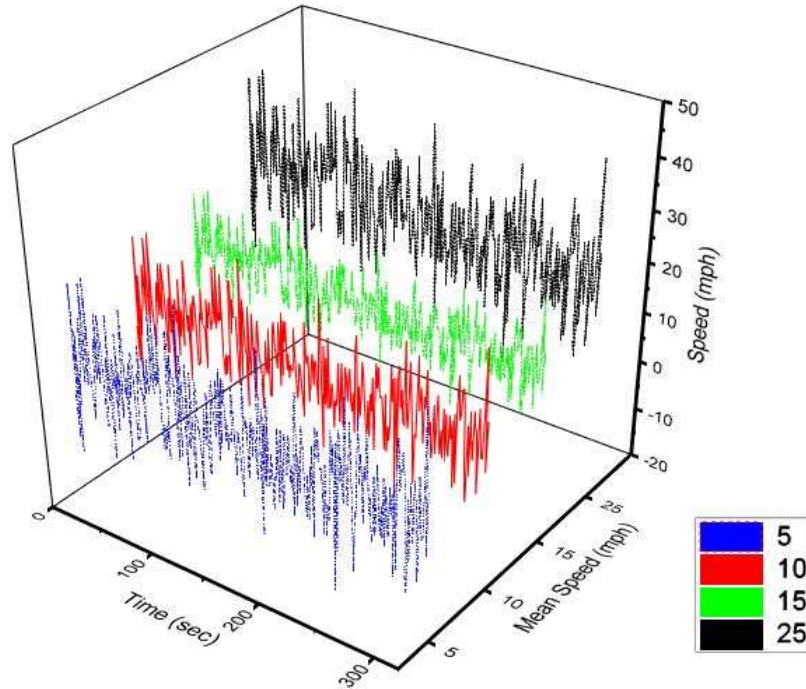


Figure 3.13 Wind-Time histories for various mean wind speeds

The complete procedures for generating single daily time history are shown in Figure 3.14 and were implemented in C# code to produce a 45-year database of wind-time histories and daily synthetic wind profiles for all counties in Kansas. After generating the database, the Rain Flow counting technique [26,27] described in detail below was implemented to convert the irregular wind-time histories into a usable number of constant amplitude cycles.

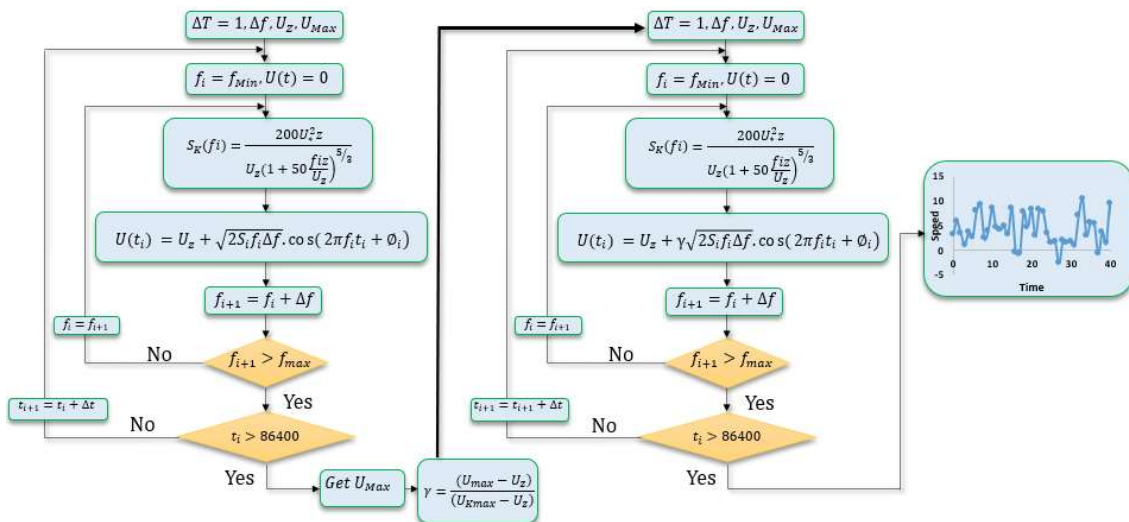


Figure 3.14 Flowchart for wind-time histories generation

3.5 Rain Flow Counting Technique

The wind-time histories generated for the 45 years of data represented highly irregular variations of speed with time. To identify how each wind speed cycle was extracted, the Rainflow counting technique, developed by Matsuishi and Endo [27], was adapted to convert the irregular time histories to cycles. The approach identified closed hysteresis loops in a non-periodic stress response. The algorithm was borrowed from ASTM E1049 [26] and implemented into a computer code to extract the cycle database for 45 years. Figure 3.15 demonstrates the Rainflow counting technique through an example. Implementing the Rainflow counting technique for each daily wind-time history resulted in a speed-cycle matrix that represented the number of cycles for each wind speed in a day, obtained from grouping the cycles in 0.5 range scale. Figure 3.16 a and b show the layout database for wind time histories for any county in Kansas stored in a matrix form and the speed-cycle matrix, respectively.

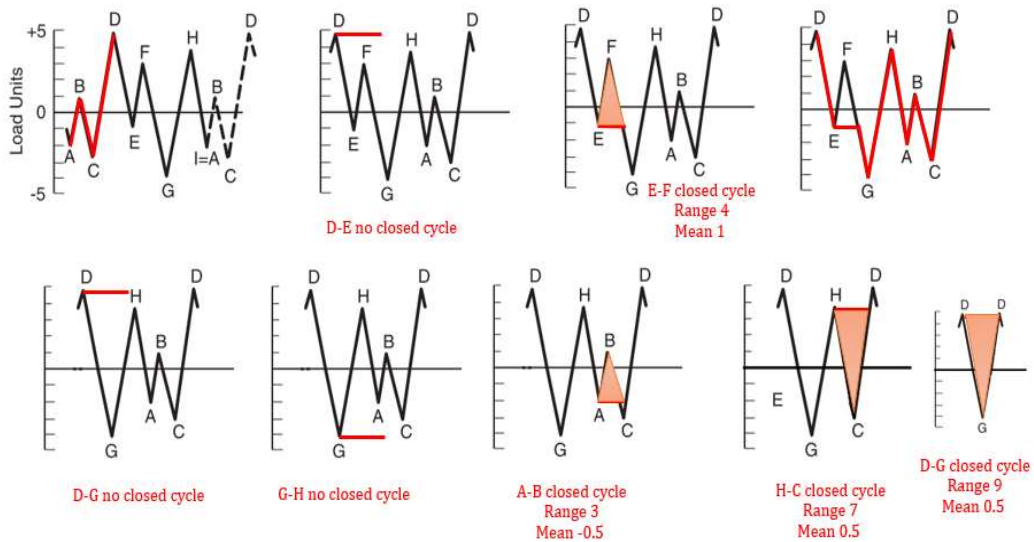


Figure 3.15 Rainflow counting example

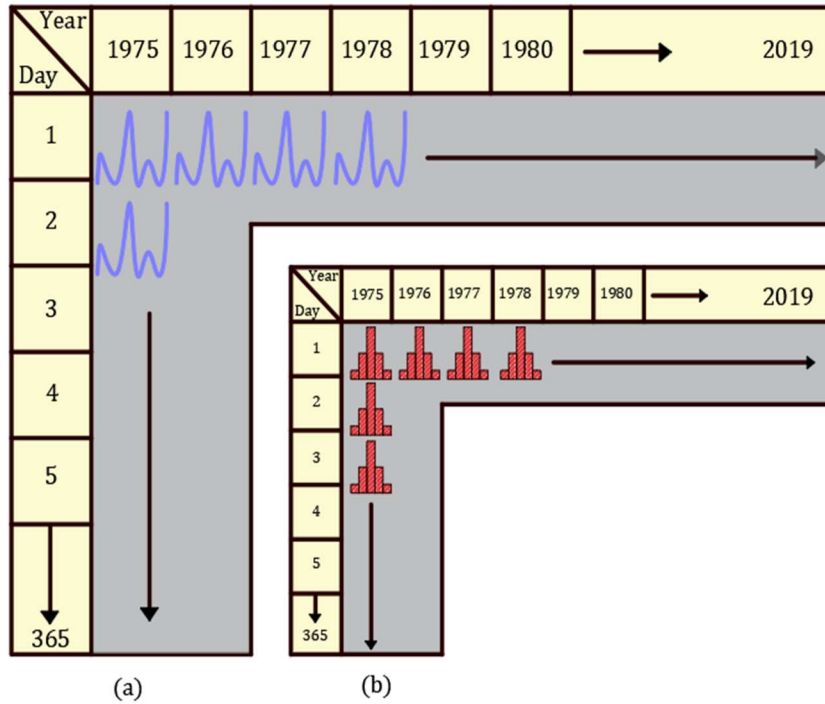


Figure 3.16 (a) Wind time histories database (b) Speed-Cycle matrix

3.6 Interpolation Assessment

The accuracy of the shape function interpolation method depends on mesh size. A smaller mesh size results in more accurate, reliable results because the spatial dependency of the interpolated phenomena is minimal. On the other hand, larger areas result in deviation of the interpolated data from the actual measurements. In the absence of actual data, the Kansas map was re-meshed, as shown in Figure 3.17, to form two new zones to recover wind records for the city of Wichita. Wind-speed records from the four nodal cities bounding each zone were interpolated and compared to the actual measured values at the city of Wichita, and the high/mean wind speeds were evaluated for four months for all the year groups to assess the reliability of results of the developed method statistically.

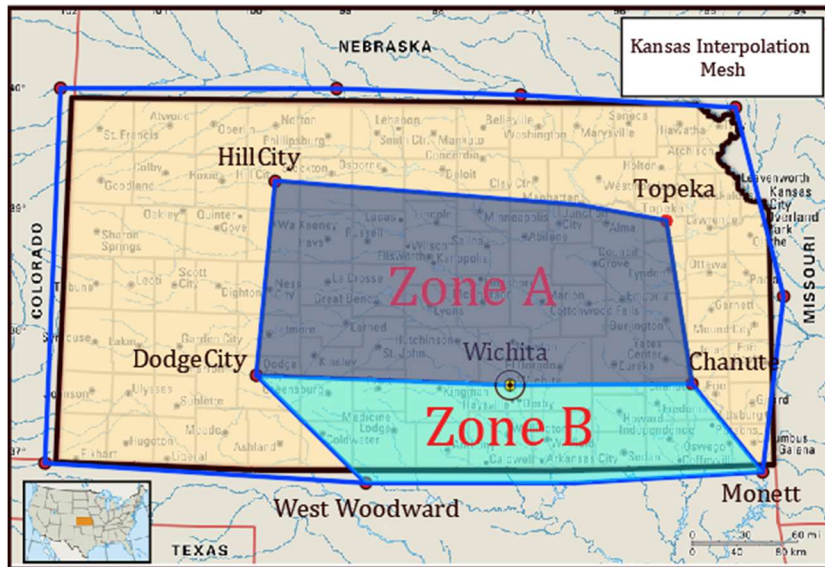


Figure 3.17 New interpolation zones (Zone A and Zone B)

Accurate interpolation zone selection is essential to achieve accurate results. Zones should be selected as closely as possible to the interpolated city since measured values closest to the prediction location have more influence on predicted values than those far from the prediction location. Figure 3.18 and Figure 3.19 show the correlation between predicted high and mean wind speeds in Zones A and B, respectively, for the years 1975–2019. As shown in the plots, the high and mean daily wind speed values are identical regardless of the zone used in the interpolation. Because the shape function values differ in both cases to account for the distance between the interpolated cities and the city of Wichita, their agreement along the 45° line testifies to the reliability of the formulated interpolation.

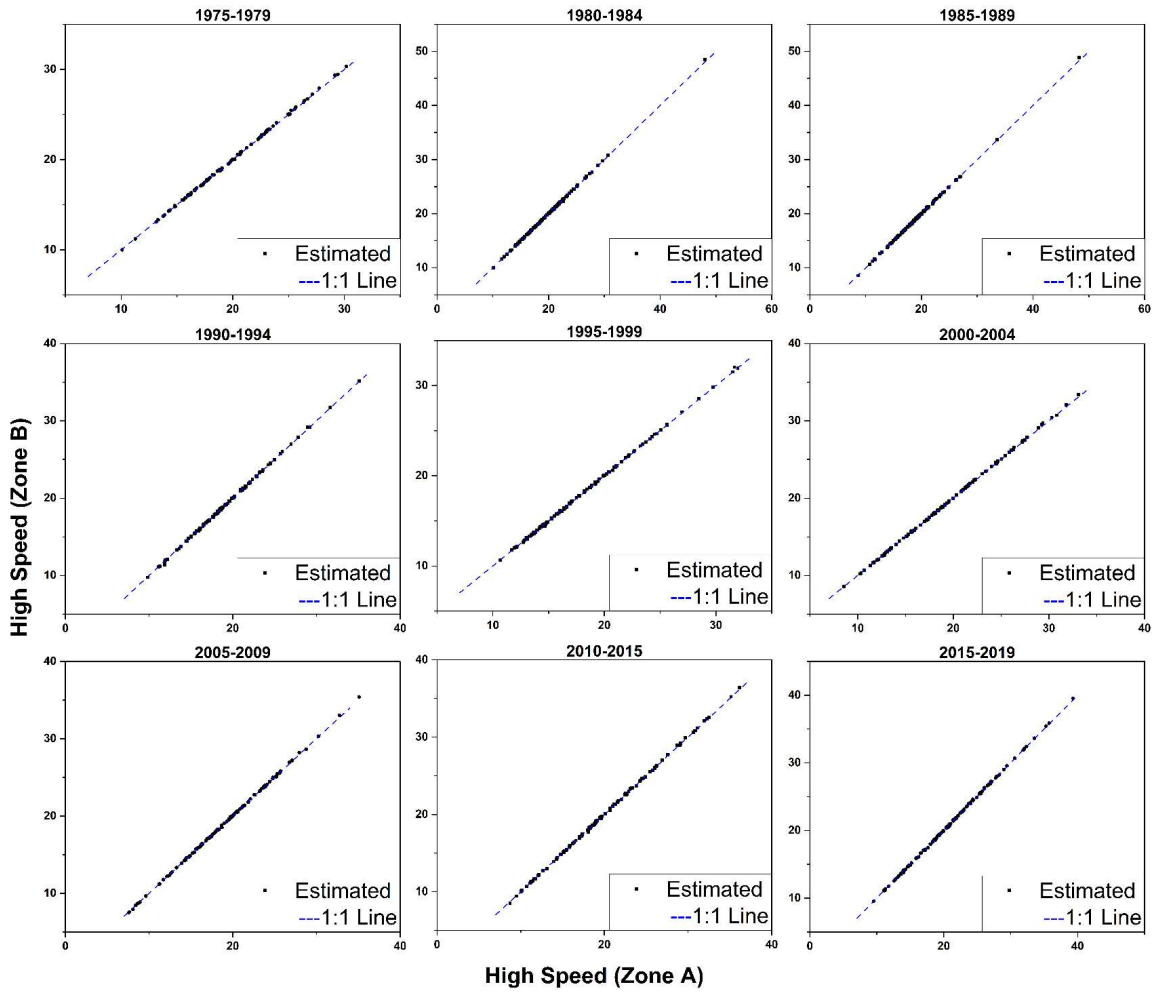


Figure 3.18 Predicted daily high wind speeds for zone A and zone B in Wichita, 1975–2019

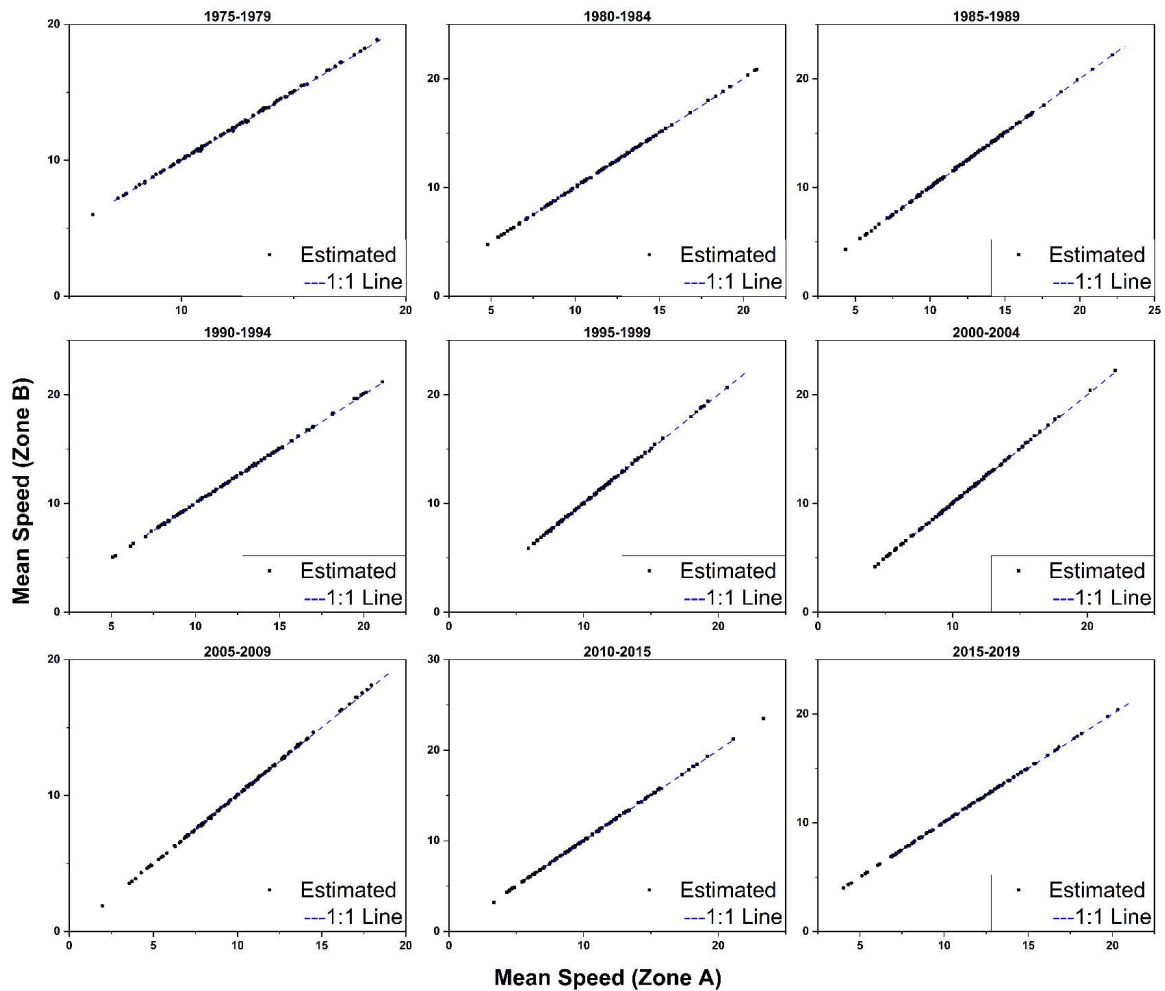


Figure 3.19 Predicted daily mean wind speeds for zone A and zone B in Wichita, 1975–2019

Since zones A and B displayed the same results, the predicted values obtained from zone A were compared to the actual measured values. Figure 3.20 and Figure 3.21 present the measured and the predicted high and mean wind-speed values, respectively, for 120 days in Wichita.

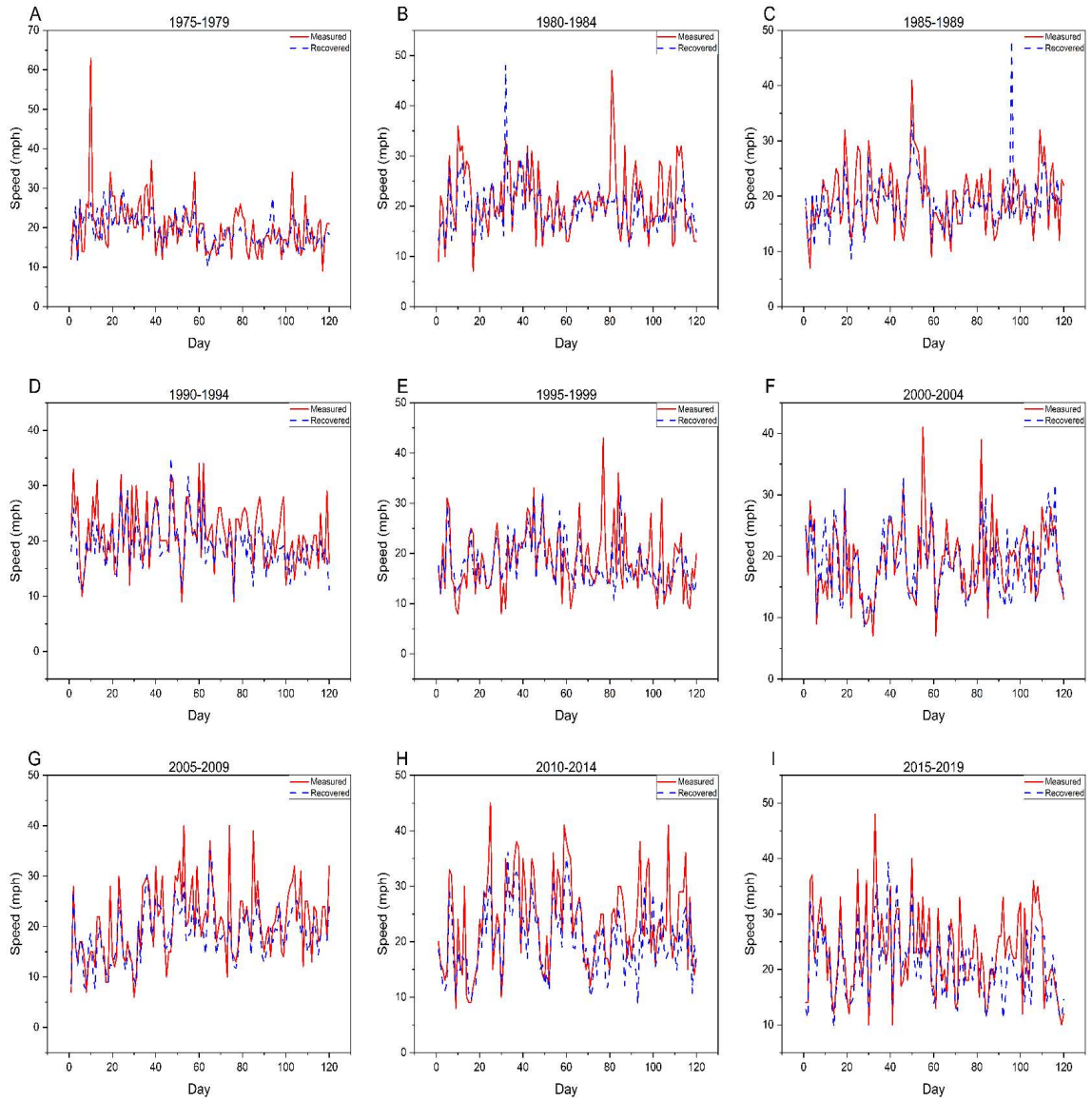


Figure 3.20 Measured vs. Predicted high wind speeds in Wichita for 120 days

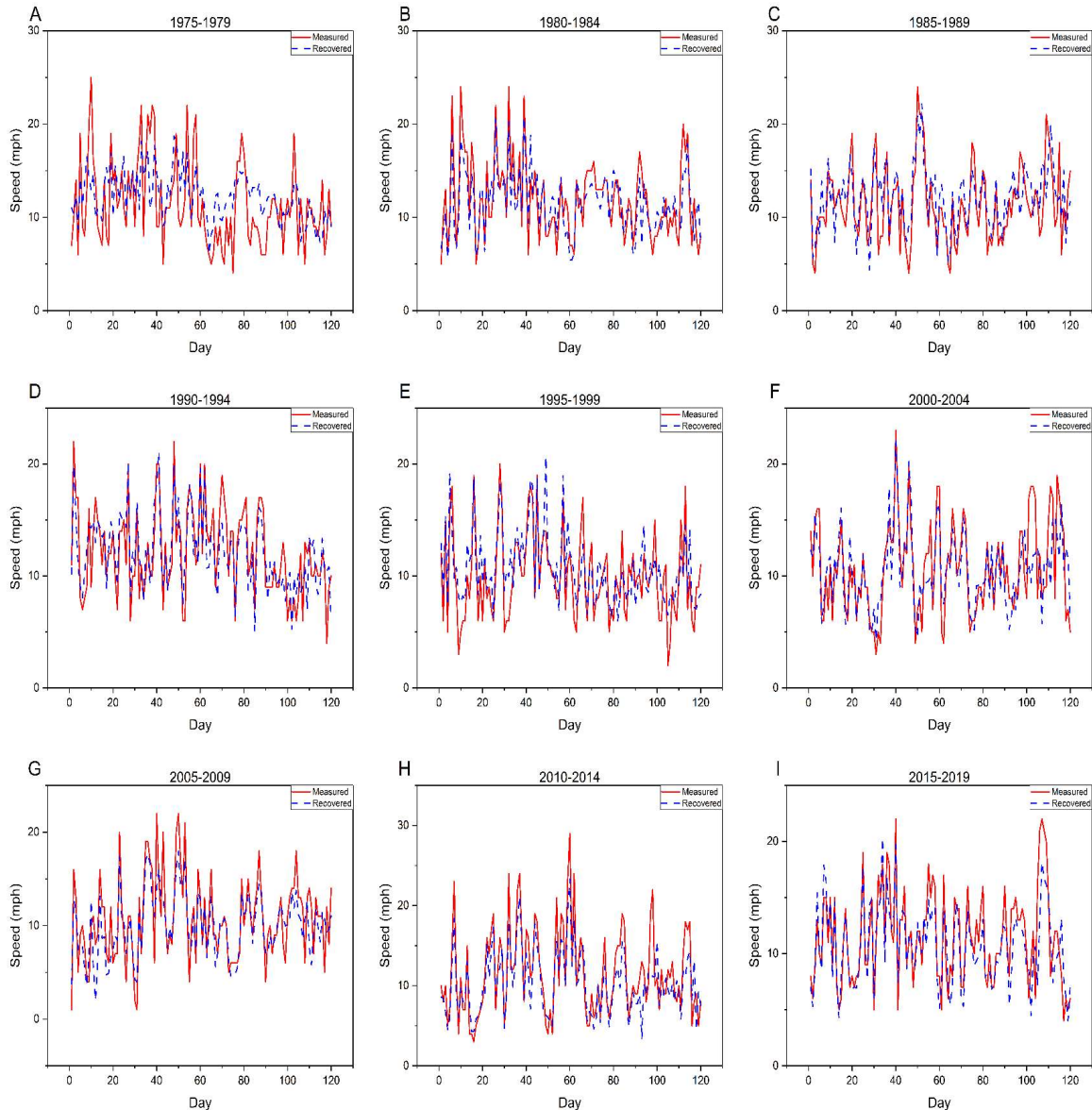


Figure 3.21 Measured vs. Predicted mean wind speeds in Wichita for 120 days

Comparing the predicted and measured high wind speeds showed that the global trend of the predicted values captured the measured numbers with slightly less reliability than the mean values (Figure 3.20 and Figure 3.21). For example, some high wind-speed points were evident in all-year groups due to high wind-speed values, representing single-peak measurements. However, the interpolated values represented the weighted averages for all the high measurements in the four corner cities at any given time. On the other hand, the mean wind-speed values represent the average daily wind-speed readings. Due to the fact

that, wind speed is highly affected by location and is more variable over short distances, this variation is expected to diminish if a denser network of sampled sites is available, leading to more accurate interpolated values. Table 3-4 and Table 3-5 compare high and mean wind speeds, respectively, for Wichita, using Minimum, Maximum, Average, Standard Deviation, Root Mean Square Error (RMSE), and Mean Error (ME).

$$RMSE = \sqrt{\frac{1}{N} \sum_1^N [\hat{Z}(x_o, y_o)_i - Z(x_o, y_o)_i]^2} \quad (24)$$

$$ME = \frac{1}{N} \sum_1^N [\hat{Z}(x_o, y_o)_i - Z(x_o, y_o)_i] \quad (25)$$

Where $\hat{Z}(x_o, y_o)$ is the predicted value at a specific location (x_o, y_o) , and $Z(x_i, y_i)$ is the measured value at the sample point (x_i, y_i) .

Table 3-4 Measured vs. Predicted high wind speeds in Wichita

Year group	Measured high				Predicted high				RMSE	ME
	Min	Max	Mean	St. dev.	Min	Max	Mean	St. dev.		
1975-1979	9	63	20	7	10.1	30.2	19.5	3.9	5.6	-0.7
1980-1984	7	47	21	7	10.1	48.0	19.4	4.8	5.2	-1.7
1985-1989	7	41	20	5	8.6	48.2	19.1	4.6	3.5	3.5
1990-1994	9	34	21	5	9.8	35.1	19.3	4.3	4.1	-1.8
1995-1999	8	43	19	6	10.7	32.0	17.9	4.4	5.5	-0.9
2000-2004	7	41	19	6	8.6	33.1	18.9	5.3	4.4	-0.5
2005-2009	6	40	21	7	7.6	35.1	18.6	5.3	5.0	-2.2
2010-2014	8	45	23	8	8.7	36.2	20.1	6.2	6.1	-3.2
2015-2019	10	48	23	7	9.6	39.3	20.7	5.9	5.8	-2.3

Table 3-5: Measured vs. Predicted mean wind speeds in Wichita

Year group	Measured mean				Predicted mean				RMS E	ME
	Min	Max	Mean	St. dev.	Min	Max	Mean	St. dev.		
1975-1979	4	25	11.44	4.51	6.0	18.7	12.21	2.63	3.83	0.77
1980-1984	4	24	11.82	4.18	4.8	20.7	11.43	3.32	2.36	-0.38
1985-1989	4	24	11.44	4.00	4.3	22.1	12.22	3.25	3.38	3.38
1990-1994	4	22	12.12	3.86	5.1	21.1	12.03	3.29	2.29	-0.10
1995-1999	2	20	10.16	3.87	5.9	20.6	10.66	3.17	2.68	0.71
2000-2004	3	23	10.80	4.07	4.2	22.0	10.56	3.33	2.63	-0.24
2005-2009	1	22	10.72	4.41	1.9	17.9	9.99	3.34	2.58	-0.73
2010-2014	3	29	11.52	5.34	3.3	23.3	10.33	4.00	2.87	-1.20
2015-2019	4	22	11.42	4.07	4.0	20.3	10.69	3.46	2.32	-0.72

The Chi-square goodness of fit test is a hypothesis testing method that assesses the goodness of fit and measures the significant difference between observed values and theoretical values to determine whether or not the sample data matches the population. In other words, the test shows how well the sample data fits a set of observations. To assess the goodness of fit of the interpolated wind-speed values and how close they align with the measured values, the null hypothesis H_0 , stated as $(V_i)_{Predicted} = (V_i)_{Measured}$ and the alternate hypothesis, H_1 stated that some predicted mean and high wind speeds differed from measured values. The significance level was chosen as $\alpha = 0.05$ based on engineering judgment. The critical value was calculated from the Chi-distribution to be 146.6. Then the value of the test was calculated based on Eq. (26). If χ^2 is less than the critical value, then the null hypothesis H_0 should be accepted, otherwise it should be rejected.

$$\chi^2 = \sum \frac{(O - E)^2}{E} \quad (26)$$

Where O represents observed values, and E represents expected values.

Table 3-6 presents the Chi-square goodness of fit test analysis results used to determine effective prediction. Decision-rule results revealed that, although mean wind-speed prediction was acceptable according to Chi-square for all year groups, the high wind speed

was only acceptable for three-year groups (1985–1989, 1990–1994, and 2000–2004) and rejected for the rest of the groups. However, this does not mean that the predicted high wind speed did not reflect the measured values; as stated before, high wind speeds, which are high peaks, could not be recovered exactly from the corner cities. Moreover, the decisions were made at a 95% confidence level ($\alpha = 0.05$), which is considered a tight criterion for assessing high wind speeds, so it is inaccurate to state that the interpolated wind speeds do not represent the measured speeds. A more precise result could be achieved by refining the interpolation mesh to recover exact values. Results also may differ slightly because wind-speed measurements may be taken at specific locations in the cities, but the interpolation method assumes a central coordinate of the cities. However, if sufficient data is lacking, this method can adequately predict wind speeds.

It can be reliably argued that the goodness of fit assessment, which was made for the entire year in all year groups, may be unrealistic because the FE interpolation technique is easily affected by an uneven distribution of observational data points since the same weight is assigned to each city regardless of the season. In the winter, even though the high wind-speed measurements drastically change from one location to another, the weights are similar and assume even contributions. A more reliable assessment of the interpolated data should be conducted on a seasonal basis to determine the season that drives the overall behavior of the interpolated high wind-speed data to fail. Table 3-7 shows the Chi-square test results for high wind speeds for the four seasons in 1975. As expected, this method produced biased estimates in the winter, and the test failed in the winter due to the high daily variation in wind speed in the interpolated cities. However, test results were acceptable in the rest of the seasons.

Table 3-6 Chi-Square Goodness of fit results all year-groups

Year group	High wind speed			Mean wind speed		
	χ^2	$\chi^2_{,Df,\alpha}$	Decision	χ^2	$\chi^2_{,Df,\alpha}$	Decision
1975-1979	179.88	146.6	Reject	146.34	146.6	Accept
1980-1984	164.06	146.6	Reject	63.71	146.6	Accept
1985-1989	113.96	146.6	Accept	76.80	146.6	Accept
1990-1994	111.28	146.6	Accept	59.08	146.6	Accept
1995-1999	237.17	146.6	Reject	89.27	146.6	Accept
2000-2004	120.01	146.6	Accept	82.41	146.6	Accept
2005-2009	166.04	146.6	Reject	104.48	146.6	Accept
2010-2014	250.54	146.6	Reject	110.21	146.6	Accept
2015-2019	219.54	146.6	Reject	67.71	146.6	Accept

Table 3-7: Chi-Square Goodness of fit results for all seasons in 1975

Season	High wind speed		
	χ^2	$\chi^2_{,Df,\alpha}$	Decision
Winter	87.50	43.8	Reject
Spring	27.58	43.8	Accept
Summer	21.14	43.8	Accept
Autumn	43.65	43.8	Accept

Needed functional validation and assessment of the interpolated values were done by comparing the resulting wind records against a county's known measured wind speeds. A deep online search revealed mean and high wind-speed records for Sedgwick County (for January at discrete 5-year interval between 1975–2015) in the online Farmer's Almanac [28]. Sedgwick County, which is in zone 10, is bounded by Wichita, Chanute, Topeka, and Manhattan, with Wichita being the closest city. Figure 3.22 to Figure 3.24 compares the county's measured and predicted high and mean wind speeds for the mentioned time intervals. Overall, the global trend of the predicted values captured the measured values but presented relatively higher peak-speeds for the year 1990, lower peaks in years 2000 and 2005, and nearly identical values for the rest of the years. Based on the interpolation technique, the closest city to the interpolated location has a significant contribution; therefore, Wichita had the most significant effect on the interpolated values (higher weight function). Compared to 2000 and 2005, higher values were observed in 1990 because

Wichita had higher values in 1990 than 2000 and 2005. Adequate care should be given during the meshing of the study area since it is a highly spatial dependent interpolator.

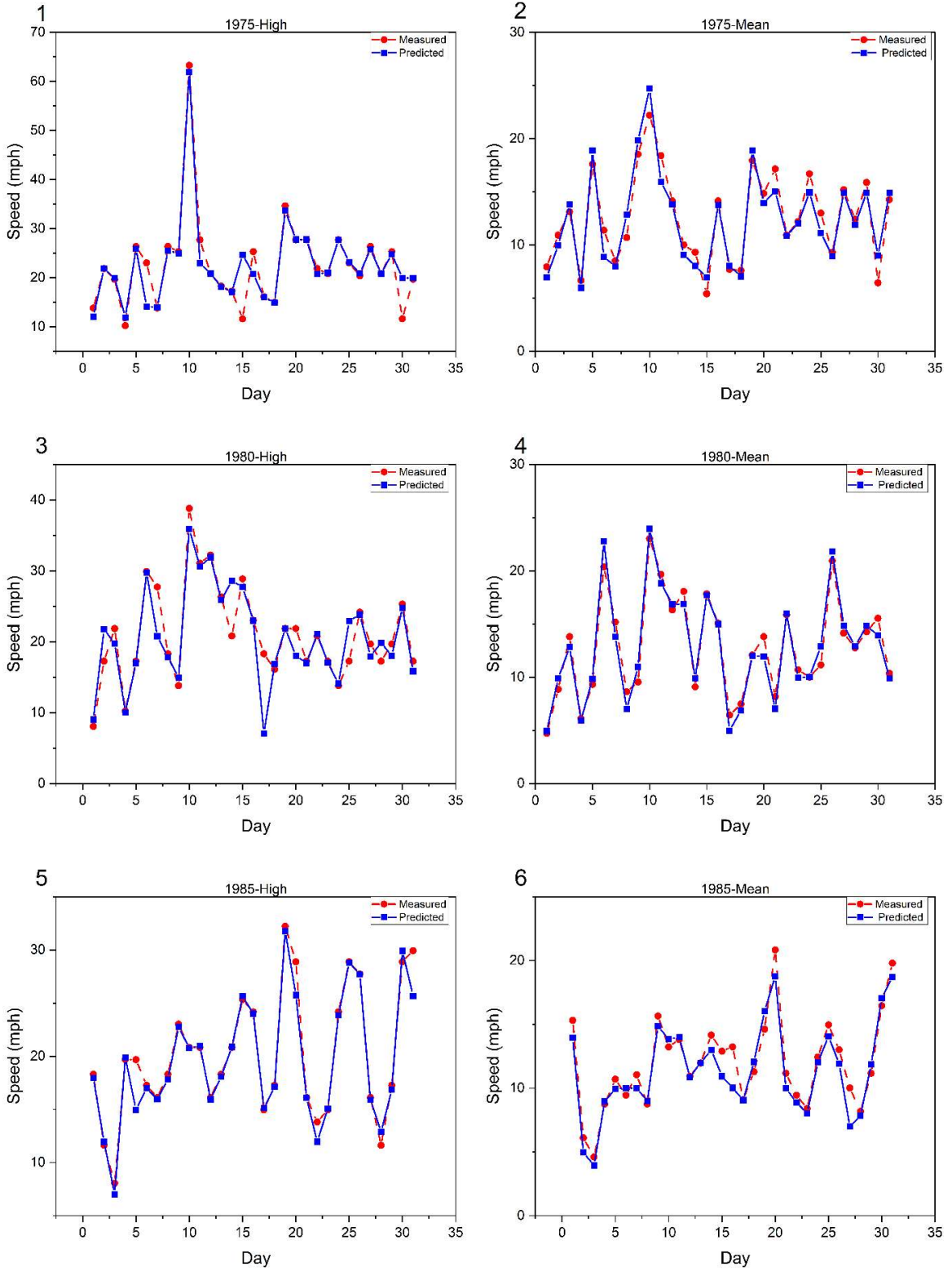


Figure 3.22 Measured vs. Predicted High and Mean Wind Speeds for Sedgwick County, 1975, 1980, 1985

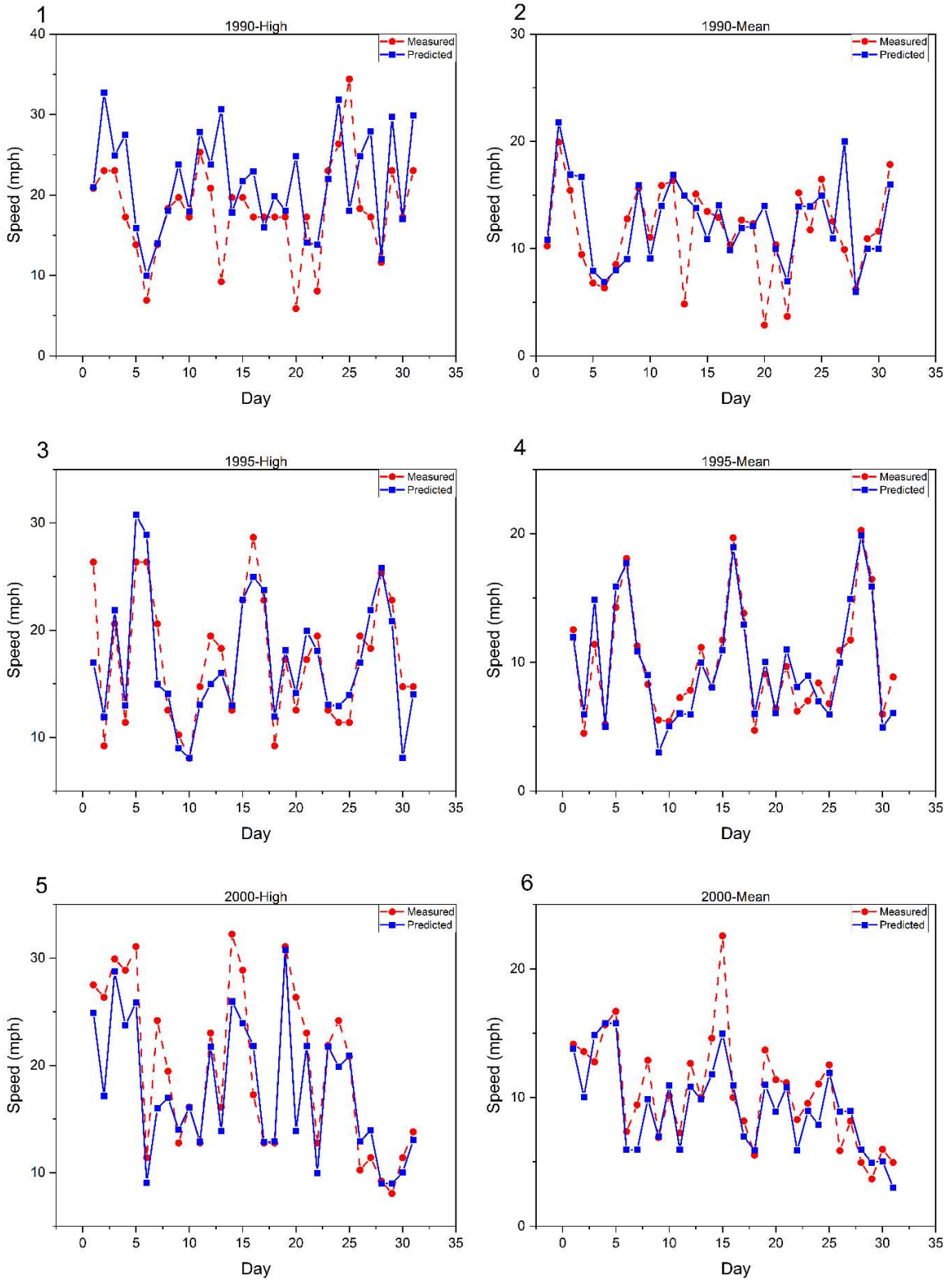


Figure 3.23 Measured vs. Predicted High and Mean Wind Speeds for Sedgwick County, 1990, 1995, 2000

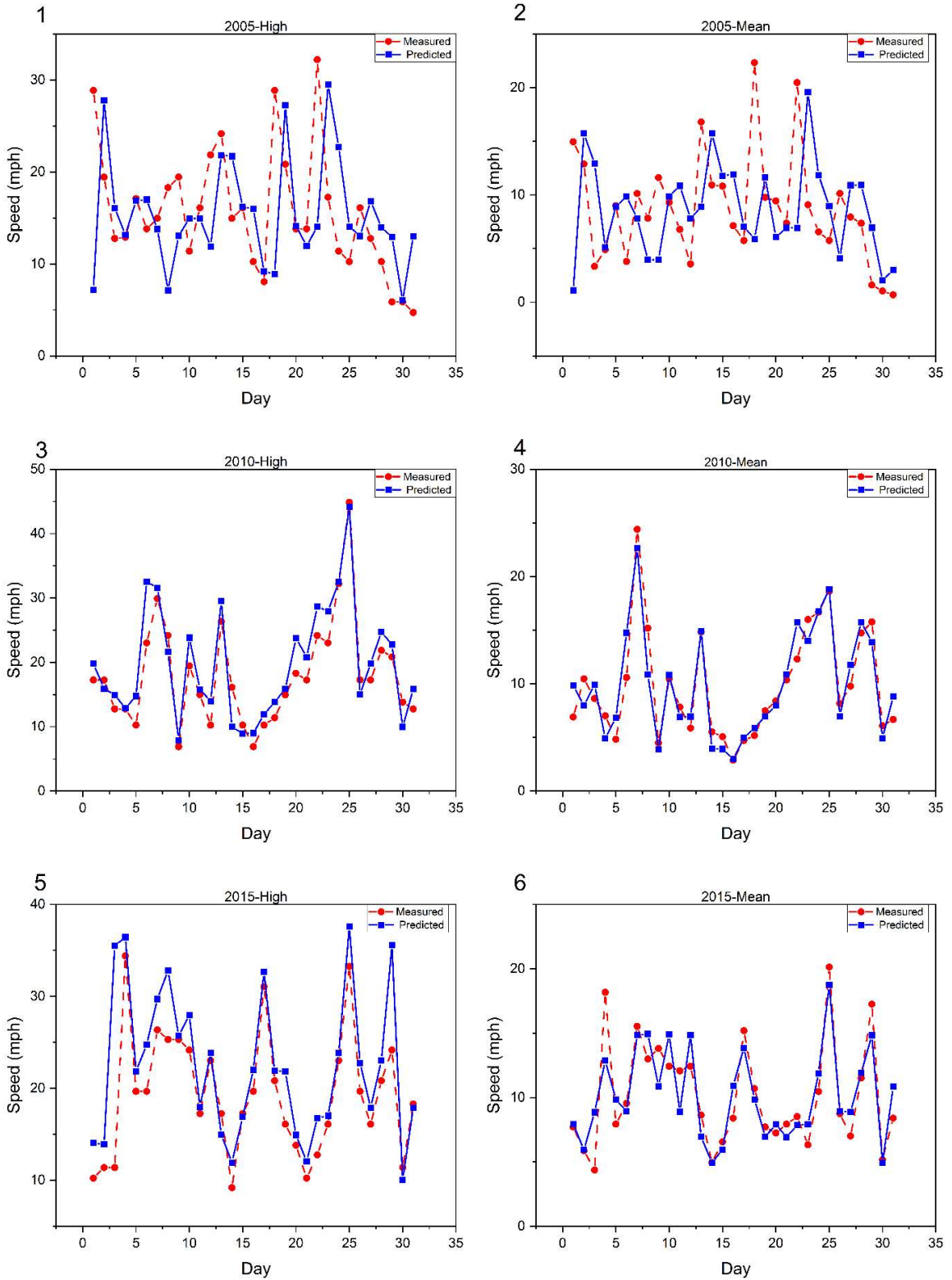


Figure 3.24 Measured vs. Predicted High and Mean Wind Speeds for Sedgwick County, 2005, 2010, 2015

3.7 Results and Discussion

This section provides results for counties and cities in Kansas. For example, as shown in Figure 3.25, zone 8 is a quadrilateral element consisting of four nodal cities: Ponca City, OK; Monett, MO; Chanute, KS; and Wichita, KS. Based on the earlier approach, interpolation of the wind-speed data for Cowley County assumed that significant data contribution would come from Wichita and Ponca City since they are closest to the center of Cowley County. At the same time, the cities that contribute more to Labette county's results would be Monette and Chanute. Global coordinates were obtained for the four cities and the counties center to calculate each city's weight function.

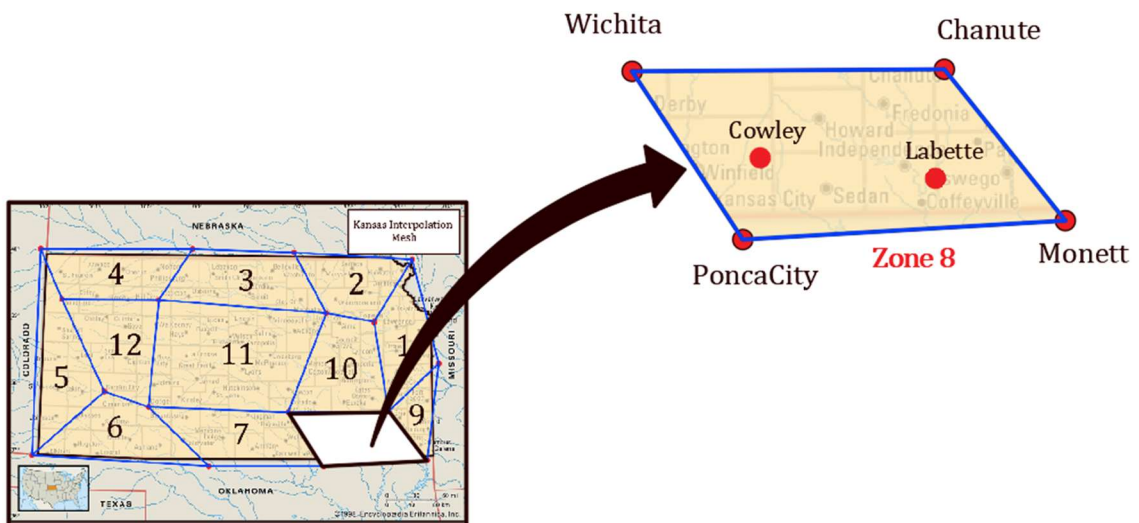


Figure 3.25 Zone 8

For Cowley County, the weight functions were obtained by solving Eq. (4), resulting in $\{N_1 = 0.40864, N_2 = 0.108845, N_3 = 0.10149, N_4 = 0.381025\}$. On the other hand, these weights were $\{N_1 = 0.03807, N_2 = 0.45162, N_3 = 0.470621, N_4 = 0.039681\}$ for Labette County. Which correspond to city contributions (Ponca City, Monett, Chanute, and Wichita), respectively. For any given day, the county's generated medium or high wind speed is equal to the city's weight function multiplied by the corresponding wind speed for

that city in that day. Figure 3.26 shows the high and medium wind-speed variations for the cities surrounding zone 8 for four key months in 1975. The red line graph represents the variation in wind speed for interpolated Cowley County. The overall trend of the derived data followed the cities' trend, and the values represent the weighted average levels.

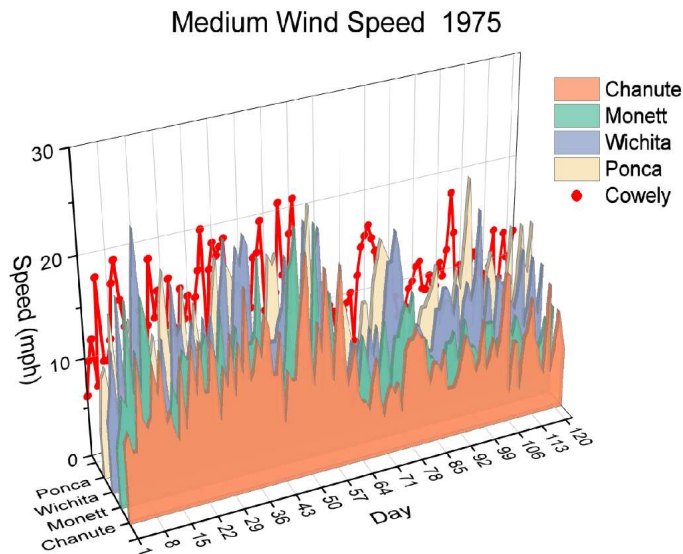
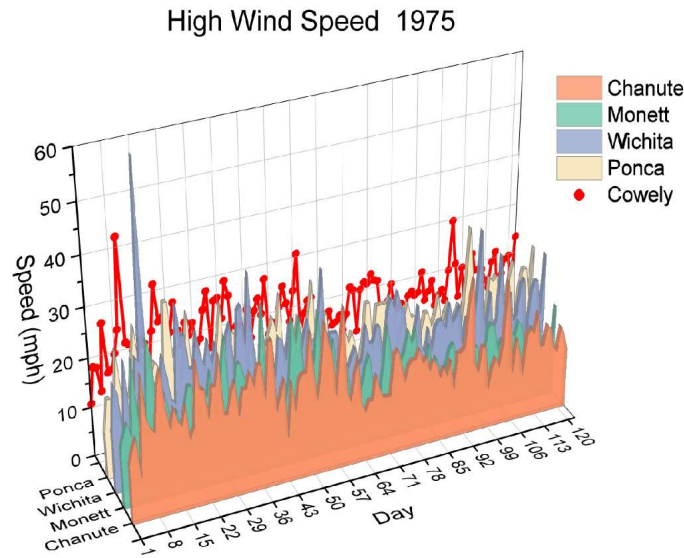


Figure 3.26 (A) High wind speeds for zone 8; (B) Medium wind speeds for zone 8
 Figure 3.27 also compares between the interpolated wind speed records for Cowley and Labette County based on the temporal scale (daily). As it is obvious, the global trend for

both records high and mean matches each other closely. However, the pointwise values for the high and mean records vary as it is expected based on the spatial location.

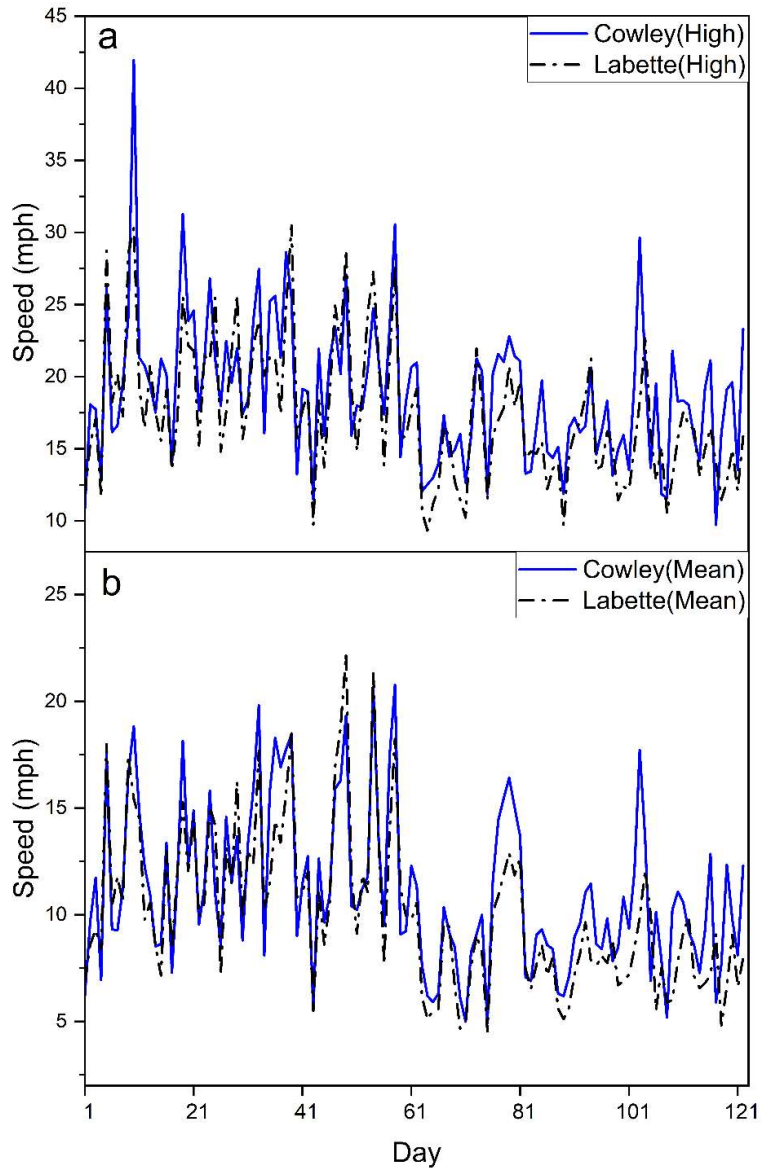


Figure 3.27 Comparison between the interpolated values for Cowley and Labette County (a) high speed (b) mean speed.

Figure 3.28 illustrates the total cycles over the entire 45 years for the City of Wichita as an example of the developed approach. The number of cycles follows a gaussian distribution with R^2 (0.9767) since the developed method assumed harmonic excitations in a range of

3-300 Hz, and the derived time histories resulted from superimposing eighty incremental cosine waves.

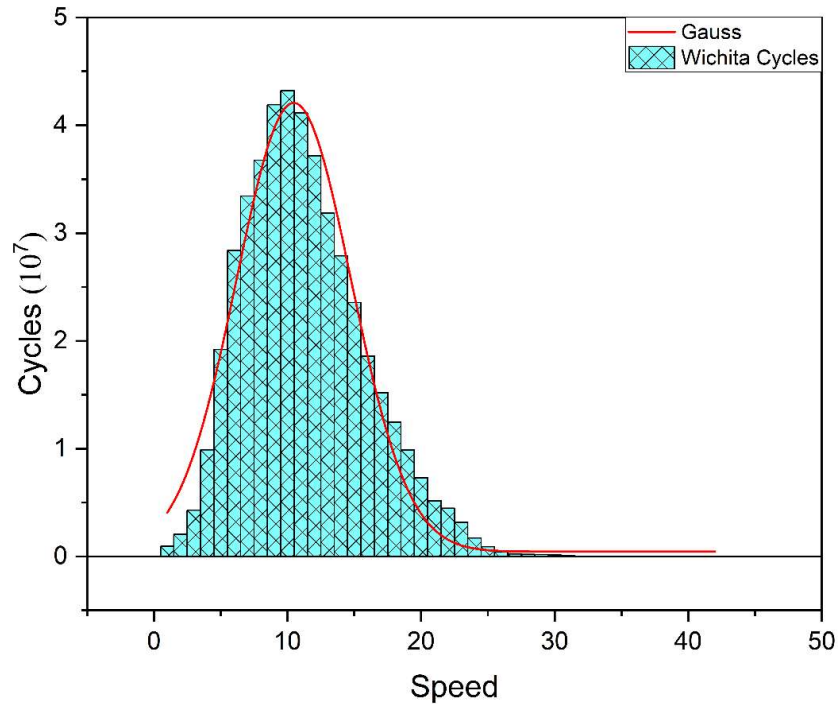


Figure 3.28 Wichita cycles distribution

3.8 Software Development

The proposed procedures require massive calculations prior to producing the wind-cycle profile for any given county. A database for all counties and cities was generated for 1975–2019 and stored in a matrix format to effectively produce any county profile for any given period. Then a user-friendly interpolation software was built to compute the complete wind-cycle profile for any given county in any time range. Cycles Generation software is an object-oriented program written in C# language to efficiently generate wind-cycle profiles from a previously developed database. This software requires Microsoft Excel to be installed on the working machine since the generation process requires access to an Excel file that contains all the background data. Moreover, the software can present a graph showing the wind-cycle distribution and text file as an external file. The software interface

contains two parts: the input part provides the required information for any county or city, and the output part displays the results for the county or the city.

3.8.1 Input Interface

The software input screen was divided into one section that displayed the Kansas state map and another section with the time selection section to specify the starting and ending interpolation date. Figure 3.29 shows the software input interface. The core cities shown in brown on the Kansas map are the cities that use the actual measured wind speeds, while the counties shown in black represent the interpolated counties. The speed-cycle profiles for a county were quickly produced by clicking on the desired county in the map and selecting the starting date from the "Year Built" box and the end date from the "Inspection Year" box. The software then grouped all the wind speed-cycles in that given time span and displayed them on the results screen. The inspection year must be greater than the year built, otherwise the software displays an error message. The interpolation date began in 1975 and ran until the year 2035. While the inspection years ran from 2010 to 2064. The most extended period the software can handle is 1975–2064.

3.8.2 Results

After specifying the input data, clicking the "Generate" button from the control box produced speed-cycle data based on the given information. The results were shown as a list in a white box and a histogram representation, as shown in Figure 3.30. The user could then save the results in a separate file on the hard disk, and the output file was formatted to be used in other software, such as the cantilever and butterfly fatigue simulators. Figure 3.31 shows the saving screen and sample output file. This software generated the results for the period 1975–2019 and extrapolated the results for the time interval 2020–2064 by

mirroring the data from the end of December 2019 to the beginning of the January 2020 timeline. Figure 3.32 demonstrates the mirroring technique.

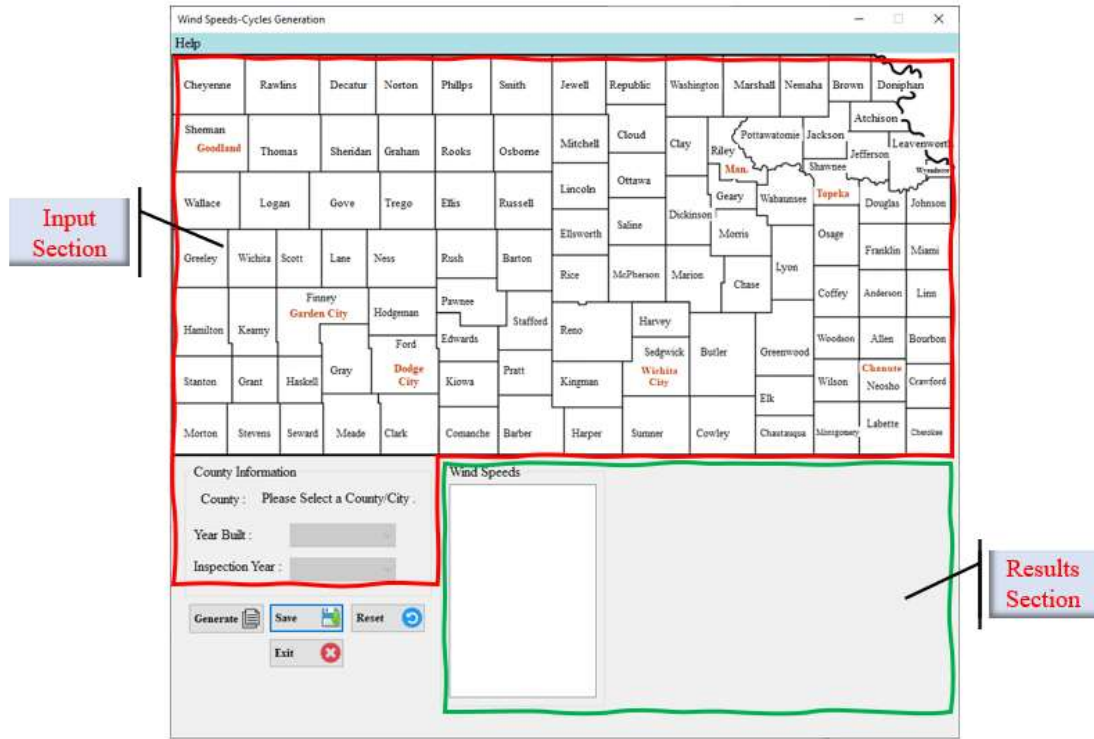


Figure 3.29 Speed-Cycle Generation interface

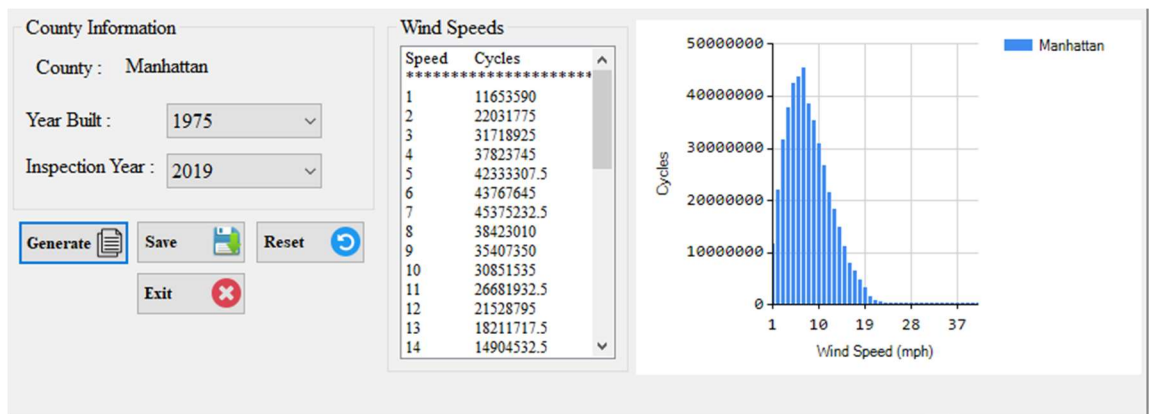


Figure 3.30 Results Screen

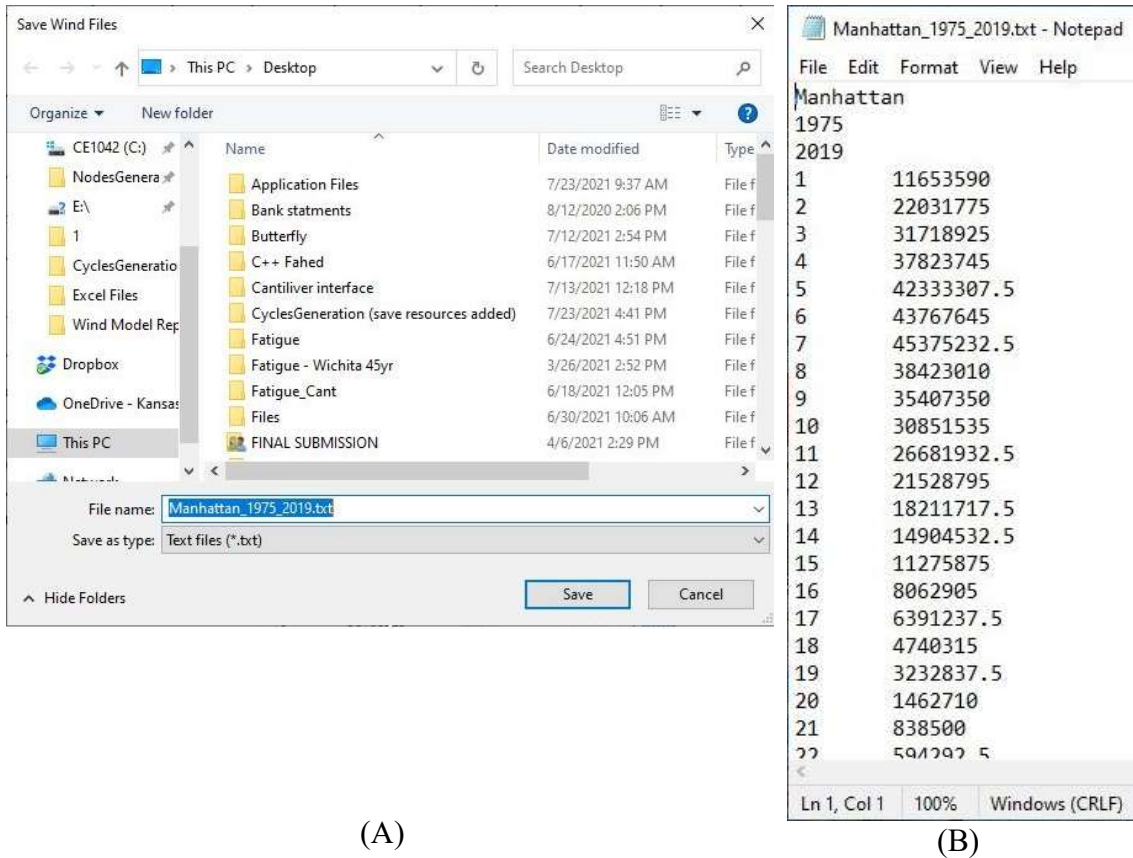


Figure 3.31 (A) Save Box Screen; (B) Sample File

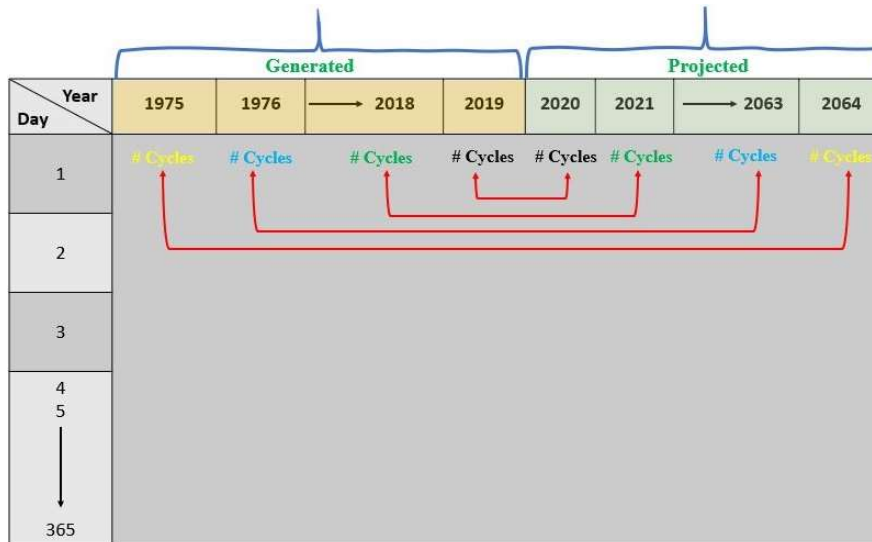


Figure 3.32 Database Mirroring

3.9 Comparison of Kansas Cities

This section compares wind speed cycles for main cities in Kansas to guide the highway agency (KDOT) to prioritize their fatigue inspection plans. Comparing the corresponding number of cycles for similar wind speeds indicates the wind loading differences for any cities under investigation since higher wind cycles produce more significant fatigue damage. However, if the wind speed values differ, comparing the number of cycles provides no measure on which city would experience more damage since the fatigue damage is a function of stress and the number of cycles. Lower wind speeds with a higher number of cycles could produce damage equivalent to higher wind speeds with a lower number of cycles since the stress experienced by the structure increased with increasing wind speed. To measure the damaging effect for a wind speeds content, the wind speed and number of cycles effect should be combined to yield a representative damaging index. The damaging index depends implicitly on the wind speed and could be expressed as follows:

$$\begin{aligned}\sigma &= f(V) \\ D &= f(\sigma, N) \\ N_f &= \frac{A}{\sigma^3} \\ \sigma &= CV^2 \\ D &= CNV^6\end{aligned}$$

Where V is the wind speed, σ is the stress produced by wind speed, N_f number of cycles to failure, D is the damaging index. A higher damaging index indicates more significant damage in the structures in any given city. The cumulative 45-years damaging index produced for the eight main cities in Kansas and plotted as in Figure 3.33. as indicated from the plot, the sign structures located in Dodge City and Goodland are expected to

experience more damage in the 45-years period, and more in-depth investigation should be made to evaluate the structures in these cities.

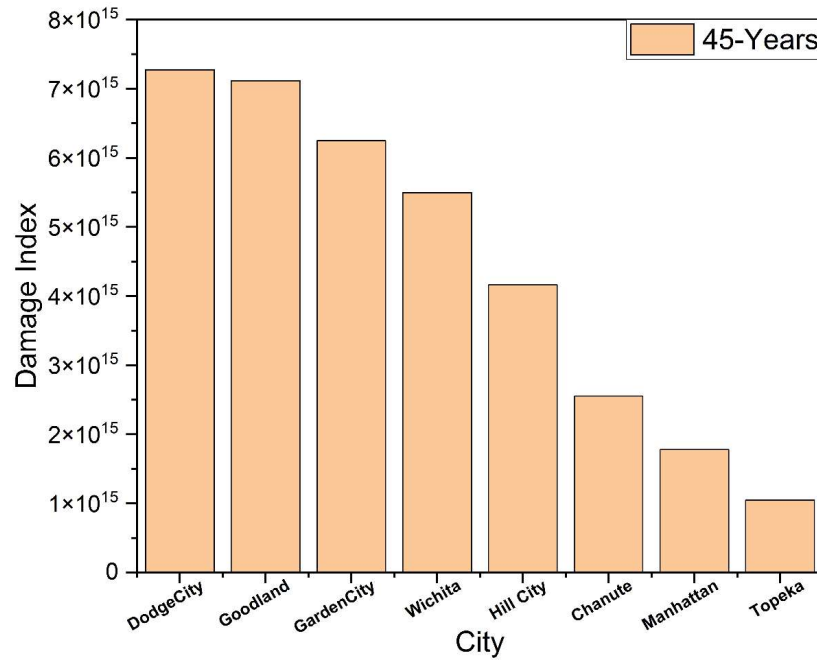


Figure 3.33 45-Years Damaging Index for Main Cities in Kansas

The 10-years damaging index plotted in Figure 3.34 for the main cities in Kansas from 1980-2019 to examine the period in which the higher damaging effect might occur.

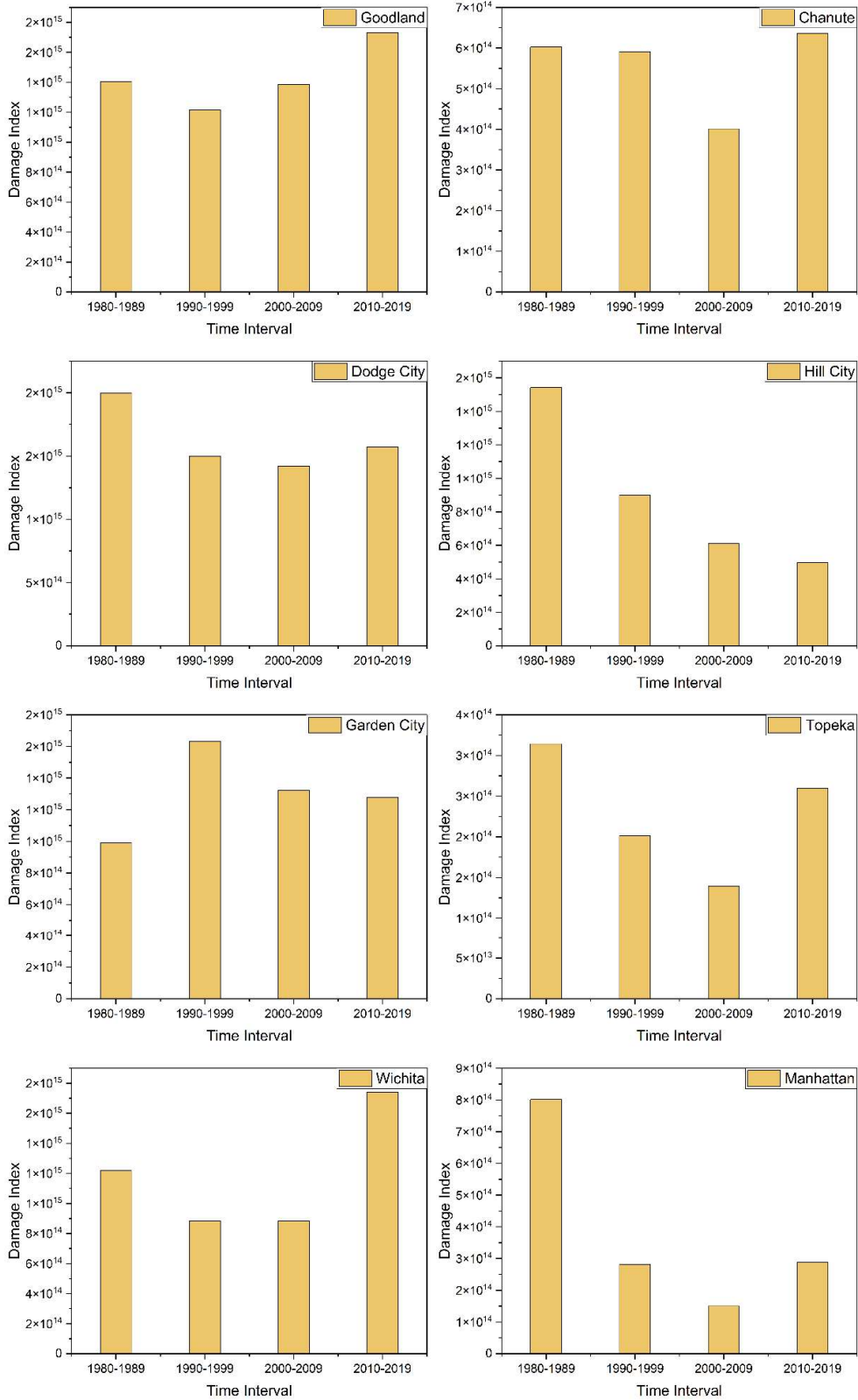


Figure 3.34 The 10-Years Damaging Index for Main Cities in Kansas

3.10 Tracking of Wind Speed Trend

The developed wind speed-cycle database was done for the years 1975-2019, where most of the needed wind speed data is available. This allows fatigue life procedures to utilize these records for the analytical fatigue life inspection from 1975-2019. The fatigue problem depends mainly on the cycle count at each stress level, accumulating over time. For this reason and to make the developed fatigue algorithm reliable, the wind speed data should be available for an extended period to allow for future inspection. A simplified yet accurate method is ensuring this wind-speed data set is projectable into the future by mirroring the data about the end of December 2019 / the beginning of January 2020 timeline, which allows for a 45-years extension. This could be done safely if the wind speed variation has an almost constant trend over the 1975-2019 period. Figure 3.35 and Figure 3.36 show the average high and mean wind speeds variation for the winter and spring, respectively, for four key cities in Kansas over the 1975-2015 timeline. It could be seen from the graphs that the long-term average mean wind speed variation trends are notably different from the average high wind speed trend. Mean wind speed can be characterized by temporally coherent wind speed trends while there is a slight fluctuation in the average high wind speed trend. This testifies to the possibility of mirroring the wind speed records about the end of December 2019 / the beginning of January 2020 timeline further to extend the wind speed-cycles record for future fatigue inspection.

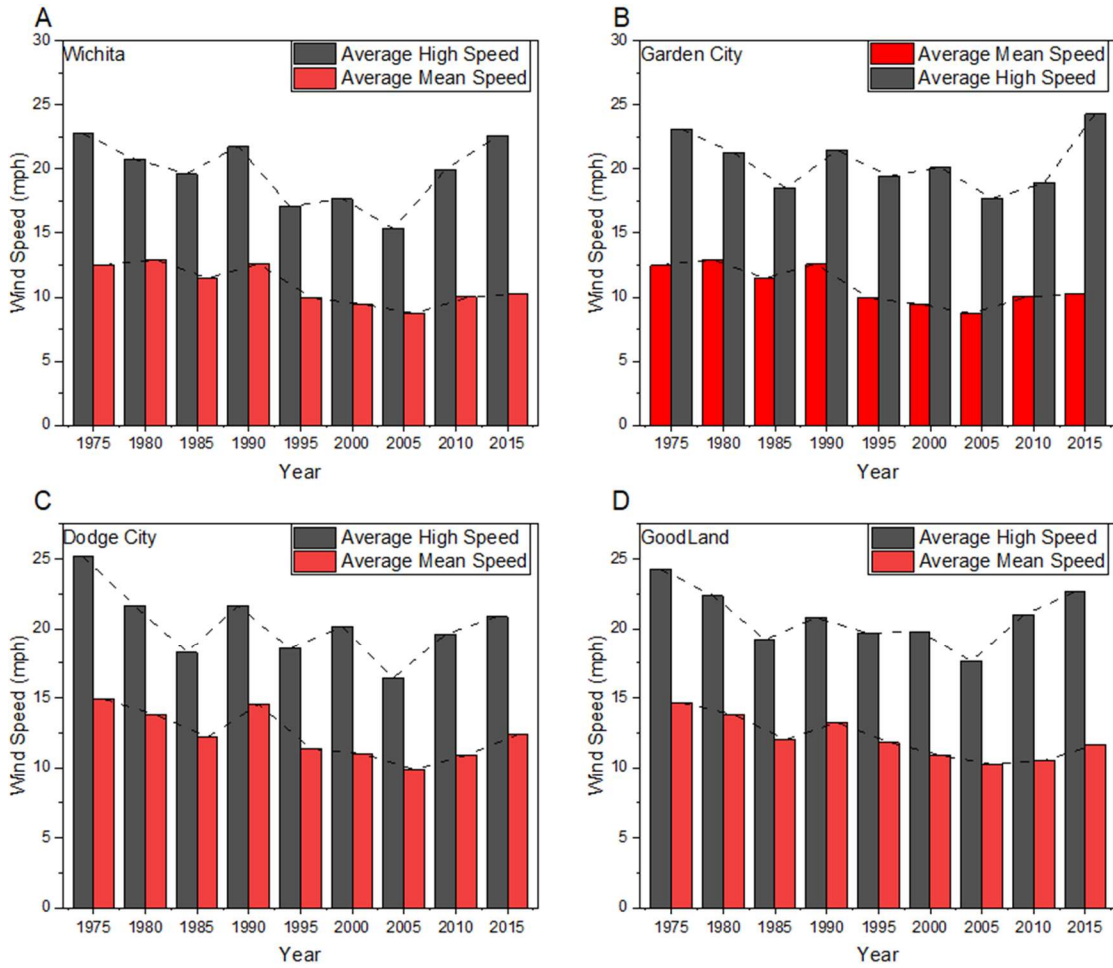


Figure 3.35 Average mean and high wind speeds in winter from 1975-2015 for (A) Wichita (B) Garden City (C) Dodge City (D) Goodland

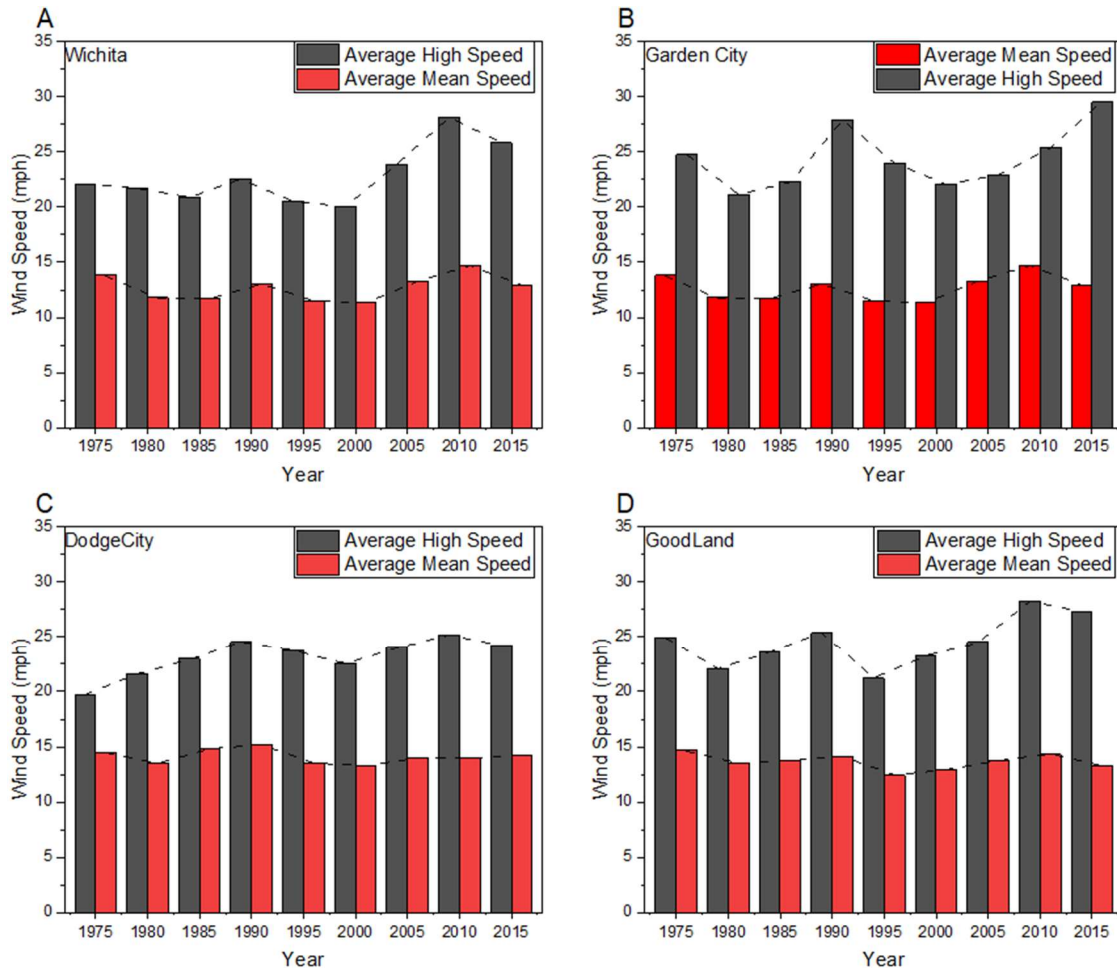


Figure 3.36 Average mean and high wind speeds in spring from 1975-2015 for (A) Wichita (B) Garden City (C) Dodge City (D) Goodland

3.11 Conclusions and Recommendations

This study used finite element shape functions to perform spatial interpolation of wind-speed records for all Kansas counties. This method considered spatial correlations among boundary sites. Synthetic wind-time histories were constructed for each day for the entire 45-year study period, and the number of cycles developed through the Rainflow analysis was used to provide descriptive wind loading for civil engineering applications. User-friendly software was produced using C# to extract the interpolated wind-speed cycles for any given county during 1975-2019. The following conclusions and findings were drawn from this study:

1. The finite element spatial interpolation technique accurately estimates spatially continuous phenomena from measured values at limited sample points.
2. Adequate care should be given during the meshing of the study area since this method is highly spatially dependent.
3. The FE interpolation technique proved to be an excellent spatial interpolator for recovering Wichita records based on statistical assessment.
4. The global trend of predicted values in Sedgwick County captured the measured wind records for most of the studied years while it admitted some relatively high peak wind-speed values for 1990 and low corresponding values in 2000 and 2005.

3.12 References

- [1] Ginal S. Fatigue Performance of Full-Span Sign Support Structures Considering Truck-Induced Gust And Natural Wind Pressures. MS Thesis 2003:393.
- [2] Bai Y, Nardi DC, Zhou X, Picón RA, Flórez-López J. A new comprehensive model of damage for flexural subassemblies prone to fatigue. *Comput Struct* 2021;256:106639. <https://doi.org/10.1016/J.COMPSTRUC.2021.106639>.
- [3] Yang DY, Frangopol DM. Probabilistic optimization framework for inspection/repair planning of fatigue-critical details using dynamic Bayesian networks. *Comput Struct* 2018;198:40–50.
- [4] Al Shboul KW, Rasheed HA, Alshareef HA. Intelligent approach for accurately predicting fatigue damage in overhead highway sign structures. *Structures* 2021;34:3453–63. <https://doi.org/https://doi.org/10.1016/j.istruc.2021.09.090>.
- [5] Chryssanthopoulos MK, Righiniotis TD. Fatigue reliability of welded steel structures. *J Constr Steel Res* 2006;62:1199–209.

- <https://doi.org/https://doi.org/10.1016/j.jcsr.2006.06.007>.
- [6] Zheng R, Ellingwood BR. Stochastic fatigue crack growth in steel structures subject to random loading. *Struct Saf* 1998;20:303–23. [https://doi.org/https://doi.org/10.1016/S0167-4730\(98\)00020-4](https://doi.org/https://doi.org/10.1016/S0167-4730(98)00020-4).
- [7] Roy S, Kundu CK. State of the art review of wind induced vibration and its control on transmission towers. *Structures* 2021;29:254–64. <https://doi.org/https://doi.org/10.1016/j.istruc.2020.11.015>.
- [8] Davenport AG. The spectrum of horizontal gustiness near the ground in high winds. *Q J R Meteorol Soc* 1962;88:197–8. <https://doi.org/https://doi.org/10.1002/qj.49708837618>.
- [9] Kaimal JC, Wyngaard JC, Izumi Y, Coté OR. Spectral characteristics of surface-layer turbulence. *Q J R Meteorol Soc* 1972;98:563–89. <https://doi.org/https://doi.org/10.1002/qj.49709841707>.
- [10] Iannuzzi A, Spinelli P. Artificial wind generation and structural response. *J Struct Eng* 1987;113:2382–98.
- [11] Webster R, Oliver MA. *Geostatistics for environmental scientists*. John Wiley & Sons; 2007.
- [12] Luo W, Taylor MC, Parker SR. A comparison of spatial interpolation methods to estimate continuous wind speed surfaces using irregularly distributed data from England and Wales. *Int J Climatol A J R Meteorol Soc* 2008;28:947–59.
- [13] Krige DG. Two-dimensional weighted moving average trend surfaces for ore-evaluation. *J South African Inst Min Metall* 1966;66:13–38.
- [14] Li L, Zhang X, Holt JB, Tian J, Piltner R. Spatiotemporal interpolation methods for

- air pollution exposure. Ninth Symp. Abstr. Reformul. Approx., 2011.
- [15] Yu Z, Song Y, Song D, Liu Y. Spatial interpolation-based analysis method targeting visualization of the indoor thermal environment. *Build Environ* 2021;188:107484. <https://doi.org/10.1016/J.BUILDENV.2020.107484>.
- [16] Ma X, Xu F, Chen B. Interpolation of wind pressures using Gaussian process regression. *J Wind Eng Ind Aerodyn* 2019;188:30–42. <https://doi.org/10.1016/J.JWEIA.2019.02.002>.
- [17] Ye W. Spatial Variation and Interpolation of Wind Speed Statistics and Its Implication in Design Wind Load 2013.
- [18] Flay RGJ, King AB, Revell M, Carpenter P, Turner R, Cenek P, et al. Wind speed measurements and predictions over Belmont Hill, Wellington, New Zealand. *J Wind Eng Ind Aerodyn* 2019;195:104018. <https://doi.org/10.1016/J.JWEIA.2019.104018>.
- [19] Stohl A, Wotawa G, Seibert P, Kromp-Kolb H. Interpolation Errors in Wind Fields as a Function of Spatial and Temporal Resolution and Their Impact on Different Types of Kinematic Trajectories. *J Appl Meteorol Climatol* 1995;34:2149–65. [https://doi.org/10.1175/1520-0450\(1995\)034<2149:IEIWFA>2.0.CO;2](https://doi.org/10.1175/1520-0450(1995)034<2149:IEIWFA>2.0.CO;2).
- [20] National Weather Service NW. Kansas Historical Weather Data. *Weather Undergr* 2015.
- [21] Rao SS. Chapter 2 - Discretization of the Domain. In: Rao SSBT-TFEM in E (Fifth E, editor., Boston: Butterworth-Heinemann; 2011, p. 53–73. <https://doi.org/https://doi.org/10.1016/B978-1-85617-661-3.00002-7>.
- [22] Kattan PI. The Quadratic Quadrilateral Element BT - MATLAB Guide to Finite Elements: An Interactive Approach. In: Kattan PI, editor., Berlin, Heidelberg:

Springer Berlin Heidelberg; 2003, p. 303–28. https://doi.org/10.1007/978-3-662-05209-9_14.

- [23] (ESRI) ESRI. ArcGIS Release 10.1 2021.
- [24] Ben-Israel A, Greville TNE. Generalized inverses: theory and applications. vol. 15. Springer Science & Business Media; 2003.
- [25] Cochran L. Wind issues in the design of buildings. 2012. <https://doi.org/10.1061/9780784412251.ch01>.
- [26] ASTM E1049. Standard practices for cycle counting in fatigue analysis. ASTM Stand 2017;85:1–10. <https://doi.org/10.1520/E1049-85R17.2>.
- [27] Matsuishi M, Endo T. Fatigue of metals subjected to varying stress. Japan Soc Mech Eng Fukuoka, Japan 1968;68:37–40.
- [28] ALmanac TOF. Almanac 2021. <https://www.almanac.com/weather/history/KS/Sedgwick/1975-01-01>.

Chapter 4 - Intelligent Approach for Accurately Predicting Fatigue Damage in Overhead Highway Sign Structures

Khalid W. Al Shboul¹, Hayder A. Rasheed², Husam A. Alshareef³

4.1 Abstract

Full-span overhead sign support structures can be found along any major highway across the US. Such structures experience different wind loading scenarios varying with time. As a result, these structures start to build up fatigue cracks within their members near the end of their fatigue life. Due to economic realities, the needed routine fatigue inspections on such highway structures cannot be performed regularly. This paper is intended to present a comprehensive tool to accurately predict the remaining fatigue life of full-span overhead highway sign support structures subjected to a long and sustained wind fluctuation. Synthetic wind time histories were developed by superimposing cosine waves over a range of frequencies of 3-300 Hz and randomly generated phase angles. Kaimal spectrum was utilized to build a database of wind time histories for each daily mean wind speed along a period of 45 years in the State of Kansas. Moreover, each wind time history was modified to capture both the mean speed and high speed in each given day. After that, the wind speed vs. the number of cycle relationship, for a given time span, was extracted from the synthetic wind time history using the Rain Flow counting technique. Fatigue evaluations were conducted using axial truss member stresses extracted from a finite element solution

¹ Ph.D. Candidate, Department of Civil Engineering, Kansas State University, Manhattan, KS

² Professor, Department of Civil Engineering, Kansas State University, Manhattan, KS

³ Assistant Professor, Department of Engineering Technology & Construction Management, Colorado State University Pueblo, Pueblo, CO, USA,

corresponding to each wind speed in any given time range. Potential fatigue failure was assessed for each structural member after amplifying the stress range using an average dynamic amplification factor generated by integrating the frequency-response curve of harmonic excitations. These assessments evaluate the ratio of consumed fatigue cycles to ultimate fatigue cycles using Miner's rule to estimate the fatigue life. A computationally affordable simulation package was developed to carry out the generation of wind time histories, cycle counting, structural modeling, and fatigue life calculations. This package was used to evaluate the fatigue life of a non-cantilever sign structure in Wichita, Kansas. The software predicted the end-of fatigue life of two members in this structure. Accordingly, inspections of these two members revealed the existence of unnoticed severe fatigue cracks while other members did not show any sign of distress.

4.2 Introduction

Full-span overhead sign support structures are considered important ancillary systems that provide help and guidance for the drivers through a set of mounted highway signs. In addition to these structures, cantilever and butterfly structures can be found along any major highway across the United States. Attributable to their functionality, highway sign structures must support large truss spans to provide the needed information for the passengers without disturbing their way and introducing any possible hazard that may result from any intermediate supports. Due to their long spans and the use of hollow circular tubes with a relatively small mass, these structures are considered semi-rigid with a low natural frequency and damping ratio [1–3]. As a result, they experience fatigue failure due to various fatigue loading scenarios, which include natural wind gust, galloping, vortex shedding, and truck-induced vibrations [4].

Inspection of sign structures is crucial to ensure their safety. As a result, it is vital to perform a complete investigation that covers every member within the structure and perform routine fatigue inspections in order to ensure the integrity of these structures. This is a cumbersome, costly, and time-consuming process that many state highway agencies avoid, thereby increasing the potential for unnoticed fatigue cracking and potential catastrophic failures.

In order to ensure that the support structures are proportioned to withstand all wind-induced loading scenarios and the wind-induced stresses are below the constant amplitude fatigue threshold (CAFT), AASHTO 2013 specifications [5] require the support structures to be designed for fatigue using two approaches: the nominal stress-based classifications of typical connection details or experiment-based methodologies. Past research studies were conducted to provide reasonably detailed methods of quantifying fatigue damage in highway sign structures. Fatigue simulations were also performed by many researchers using different wind loading scenarios, types of structures, and analysis methods [6–13]. Ginal [14] investigated the fatigue performance of three full-span overhead sign support structures using ANSYS considering natural wind load and truck-induced pressures. It was concluded that the truck-induced pressure has minimal damaging effect in most full-span overhead sign structures. On contrary, the natural wind loading ranging from 20-50 mph has the most damaging effect for these structures and the predicted remaining life for these structures under investigation ranged from 4-27 years. Kacin et al. [1] performed fatigue analysis of pristine and damaged overhead four-chord truss sign structure using stress histories obtained from finite element solution to identify the critical structural members, using the Kaimal wind spectrum for base wind speeds in the range of 5-25 mph. Infinite

fatigue life was predicted for the welded diagonal members, however, they recommended that field monitoring of the real structure and accurate field measuring of the wind loading should be necessary to confirm the exact conditions of the structures. Although wind is dynamic in nature, as a structural loading, its effect could be represented by mean speed plus fluctuating speeds [15]. Wind recording stations typically do not report instantaneous wind speeds but rather they report average speeds. Accordingly, the fluctuating part of the wind spectrum for practical engineering applications is usually simulated using either the Davenport spectrum [16] or the Kaimal spectrum [17].

This study is intended to build a comprehensive tool to accurately predict the remaining fatigue life of full-span overhead highway sign support structures subjected to long and sustained wind fluctuations. Synthetic wind time histories were developed by adapting Kaimal power spectral density function of naturally occurring winds [17]. This was conducted to build a wind time history dataset for each daily mean wind speed along a period of 45 years in the State of Kansas. Moreover, each time history was modified to capture both the mean speed and high speed in each given day. After that, the wind speed versus the number of cycles relationship was extracted from the synthetic wind time history using the Rain Flow counting technique. Fatigue evaluations were then conducted using axial member stresses corresponding to each wind speed in the ensemble and hundreds of structural simulations. Potential fatigue failure was assessed for each structural member after amplifying the stress range using an average dynamic amplification factor (DAF). These assessments evaluate the ratio of consumed fatigue cycles to ultimate fatigue cycles using Miner's rule to estimate the fatigue life. A computationally affordable simulation package was developed using object-oriented programming language C# to carry out the

generation of wind spectra, cycle counting, structural modeling, and fatigue life calculations. The package was produced as a backbone application interacting with the finite element software STAAD pro.

4.3 Overhead Sign Structure Model and Automation

4.3.1 Structural Modeling

In this paper, Staad Pro V8i SS6 [18] was used to model different overhead sign structures and perform first-order static analysis. Simulations were performed as many times as the wind speeds vary in the chosen period. Nodes and members were built using model generator C# code written for this purpose. The aluminum members were modeled using a 2-node frame element. Both the upper and lower chord members were modeled as continuous members while their intermediate nodes were connected to secondary members as pinned connections, as shown in Figure 4.1 Furthermore, the upper and lower chord members were rigidly connected to the columns with appropriate offsets. The material used is considered to be 6061 aluminum alloy with modulus of elasticity of 68.9 GPa. The base supports are considered to be completely fixed due to the usage of base plate with four corner anchor bolts.

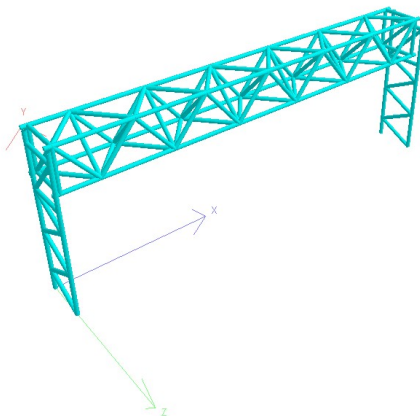
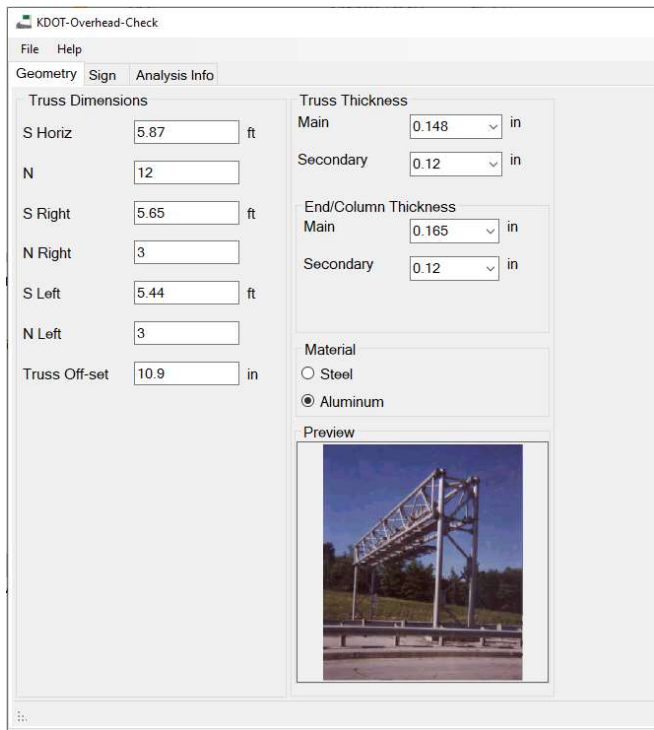


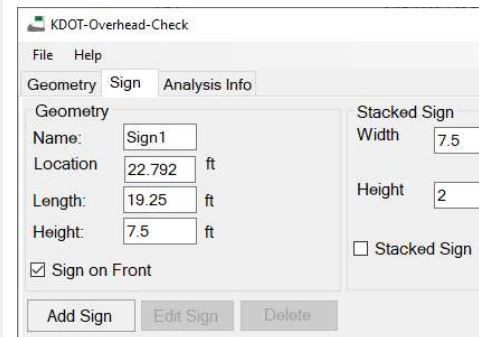
Figure 4.1 Model of four-chord box truss

4.3.2 Model Automation

To facilitate modeling the 4-chords box structures using Staad Pro, a user-friendly software was written and programmed using the object-oriented programming language C# as shown in Figure 4.2. The software can generate Staad Pro-based structural models easily and quickly for any structure with different geometry. The input parameters required for modeling are the panel size, the number of panels, truss offsets, member thicknesses, sign dimensions, and wind speed. This software plays a vital role in structural modeling as well as simulating the wind pressure at any wind speed and applying it to the sign (s) and structural members normal or transverse to the plane of the sign.



(A)



(B)

Figure 4.2 (A) The modeler interface, (B) adding sign(s) option interface

4.3.3 Dynamic Amplification Factor (DAF)

In this study, the static analysis was performed for any given structural model, then, the generated stresses were amplified using an overall blanket average (DAF) to account for

the dynamic nature of the wind load. The average DAF was calculated assuming harmonic excitations as in Eq. (1), which requires calculating the frequency-response curve for the range of frequencies used in the wind spectrum generation [3-300 HZ], as shown in Figure 4.3.

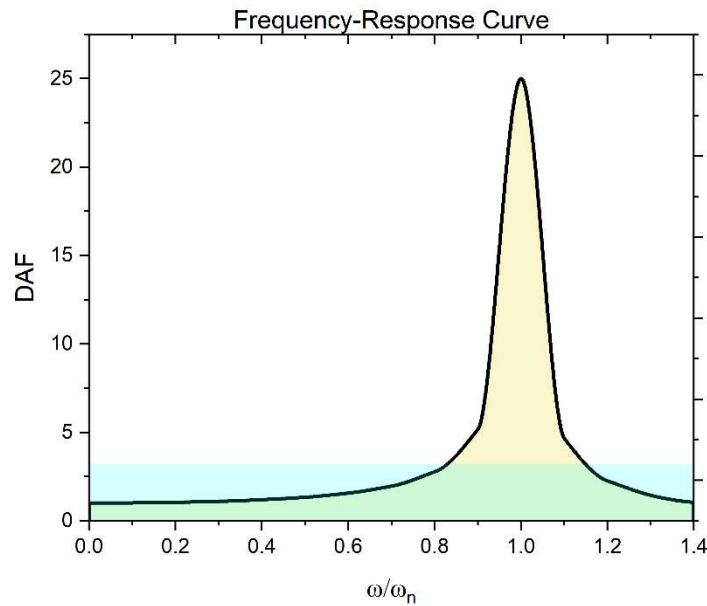


Figure 4.3 Frequency-response curve and average DAF ($\xi = 0.02$)

$$DAF = \frac{\int_0^{1.4} \frac{dR}{\sqrt{(1-R^2)^2 + (2\xi R)^2}}}{1.4} \quad (1)$$

Where ξ is the damping ration and $R = \frac{\omega}{\omega_n}$, ω : the excitation frequency, ω_n : natural frequency of the Structure, it is important to note that the average DAF was calculated in Eq. (1) by integrating the area under the curve across an excitation ratio of (0-1.4) where the value of the DAF exceeds unity.

4.4 Wind Loading on Overhead Sign Structures

4.4.1 Wind Speed Raw and Extended Data

The framework of the developed analysis requires wind speed data for the entire time span under investigation. To build a comprehensive 45-year database of high and mean

windspeeds, the state of Kansas was divided into eight regions, a representative city was chosen for each region, as shown in Table 4-1. Due to some gaps in the collected data, from the National Weather Service [19] for the cities cited above, the complete wind speed data sets were repeated to fill the gaps in a more reliable way. Therefore, the 45 years of data was subdivided into nine groups, each group consisting of five years of repeated data. For example, 1975-1979 was the first group of the wind speed data, and the first year of data 1975 was repeated to represent the remaining four years in the group. The same process was followed for the rest of the groups within the 45-year period. Each year consists of four seasons, one-month was selected from each season, and its data was repeated for the other two months in the season.

Table 4-1: Representation of Kansas regions using eight cities

City	Manhattan	Hill City	Wichita	Garden City	Dodge City	Topeka	Chanute	Goodland
Region	Northeast	North	South	West	Southeast	East	Southeast	Northwest

4.4.2 Synthetic Wind-Time Histories

The spatial and temporal variation of wind velocity has been characterized as having two components: a daily mean component $U(z)$, and daily fluctuating component $u(z, t)$, expressed through $U(z, t) = U(z) + u(z, t)$ [15,20], where $U(z, t)$ is the varying wind speed profile during the day. For a specific structure, a reference height (z) could be established, and the spatial dependency could be removed. The wind is a random process whose dynamic behavior cannot be entirely predicted. The well-established Kaimal spectrum [17] was utilized to generate the daily spectrum for the entire 45 years, using the following relationship:

$$S_K(f) = \frac{200U_*^2 z}{U_z(1 + 50\frac{fz}{U_z})^{5/3}} \quad (2)$$

where S_K is the Kaimal spectrum, z is the height above the ground 10 m (33 ft.), U_* is the shear velocity, U_z is the mean wind velocity at z , f is the specified frequency. From Eq. (3), the shear velocity is defined as:

$$U_* = \sqrt{\frac{\sigma_u^2}{6}} \quad (3)$$

Where the variance of the turbulent wind component is expressed as: (4)

$$\sigma_u^2 = 6KU_z^2$$

The surface drag coefficient K (0.005) is valid for open terrain [14]. The wind turbulence time history simulated using weighted amplitude wave superposition by superimposing cosine waves over a range of frequency of 3-300 Hz and randomly generated phase angles, Eq.(5) [21].

$$u(t) = \sum_{i=1}^N \sqrt{2S_i f_i \Delta f} \cdot \cos(2\pi f_i t + \phi_i) \quad (5)$$

Where ϕ_i is a randomly generated phase angle between 0 and 2π .

The resulting time history yields the following equation once it combined with the daily wind speed:

$$U(t) = U_z + \sum_{i=1}^N \sqrt{2S_i f_i \Delta f} \cdot \cos(2\pi f_i t + \phi_i) \quad (6)$$

After generating the turbulence time history, this fluctuating function combined with the mean wind speed in any given day to produce a complete wind time history Eq. (6). It should be noted that the fully produced time history, Eq. (6), is controlled by the mean speed, and does not necessarily capture a specific high speed. To account for the high wind speed in any given day, a scale-up factor (γ) was calculated and applied to Eq. (6) for each day to bring the maximum wind speed in the synthetic time history equal to the actual measured high speed for that day.

$$\gamma = \frac{(U_{max} - U_z)}{(U_{Kmax} - U_z)} \quad (7)$$

Where U_{max} is the actual maximum wind speed in the day, U_z is the mean wind speed, U_{Kmax} is the maximum calculated wind speed in the synthetic time history. After that, the new full time -wind history is reproduced using Eq. (8).

$$U(t) = U_z + \sum_{i=1}^N \gamma \sqrt{2S_i f_i \Delta f} \cdot \cos(2\pi f_i t + \phi_i) \quad (8)$$

Each wind speed value results from adding many cosine waves over the frequency content in addition to the mean value. This operation requires massive calculations even when using a high-speed computer if the frequency increment is too small. The wind time history generation is performed on a 1-second scale in each day. This results in 86400 discrete speed values in each day that should be calculated to generate a single wind time history while each speed is computed from imposing many cosine waves. This requires extremely massive computations for building a 45-year database. Before proceeding with the thorough analysis, a sensitivity calculation was performed in which (798, 80 and 40 cosine waves) were used to build the synthetic wind speeds for city of Wichita over a 45-year period to extract the number of wind cycles corresponding to each speed. This was performed using the Rainflow method, explained in details later, to establish the speed vs. the number of cycles distribution for the three different cosine waves, Figure 4.4 It is clear that the overall distribution is precisely the same, and the cycle variation follows a Gaussian distribution. The discretization using 80 waves is considered an excellent tradeoff between computational speed and accuracy of results to generate the 45-year wind database.

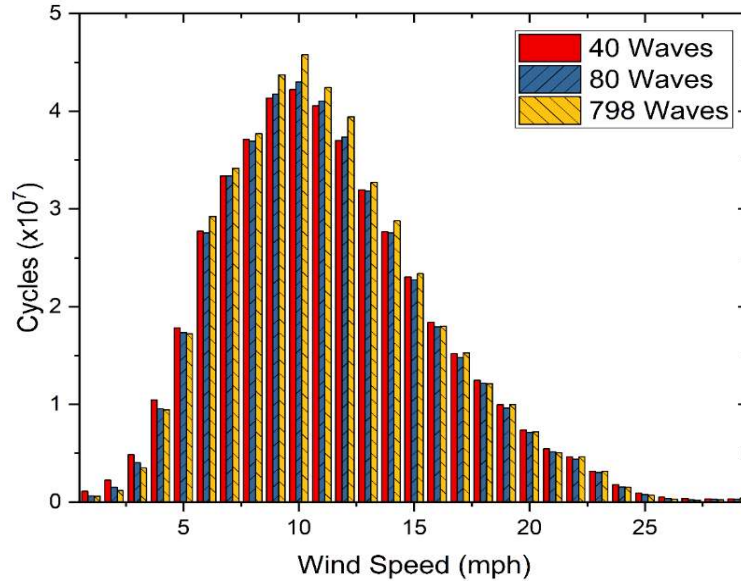


Figure 4.4 Speed vs. number of cycles for 45-years in City of Wichita

It is important to note here that large trucks passing underneath sign structures produce vertical and horizontal pressure. The horizontal gust could be ignored because it is much smaller than the horizontal natural wind component [1]. Nevertheless, the effect of horizontal component is implied with averaged dynamic amplification factor applied to the stress caused by natural wind. On the other hand, the vertical component effect is questionable as it varies with the truck speed, height of the sign, and sign geometry [6]. There are two types of sign geometries that are mounted on the overhead sign structures, namely, flat aluminum signs and VMS (Variable message signs). This work focuses on the flat aluminum signs which have very small horizontal projection area for vertical component of the truck induced vibration to excite. Therefore, this vertical component produces a negligible amount of stress in and around the flat sign (vertical pressure is parallel to the flat sign) [14] As a result, the truck induced vibration effects are not independently included in this wind loading model.

4.4.3 Validation of The Synthetic Time-History

The wind model established above is now validated against a real wind speed profile obtained for city of Manhattan from the National Oceanic and Atmospheric Administration (NOAA) through WillyWeather.com [22]. The average wind speed for the day of September 23rd 2020 was 11.2 km/h (7 mph), and the highest wind speed was 22.3 km/h (13.8 mph). The wind profile was built by applying these parameters into the proposed wind model for validating the fluctuation behavior, as shown in Figure 4.5a. It is essential to clarify that the time history was plotted by picking the wind speed values corresponding to the time step depicted in the actual wind time profile. It is clear from the plot that simulated wind histories accurately reflect the characteristics of the actual measured natural wind records. To further confirm this observation, the time-history profile was transformed to frequency domain using non-uniform discrete fast Fourier transform function in MATLAB, Figure 4.5b. These simulations produce a wind time profile that adheres closely to the fluctuations of the natural one. In conclusion, it was felt that the simulated wind histories would provide an accurate representation of actual in-service loading conditions for the sign support structures.

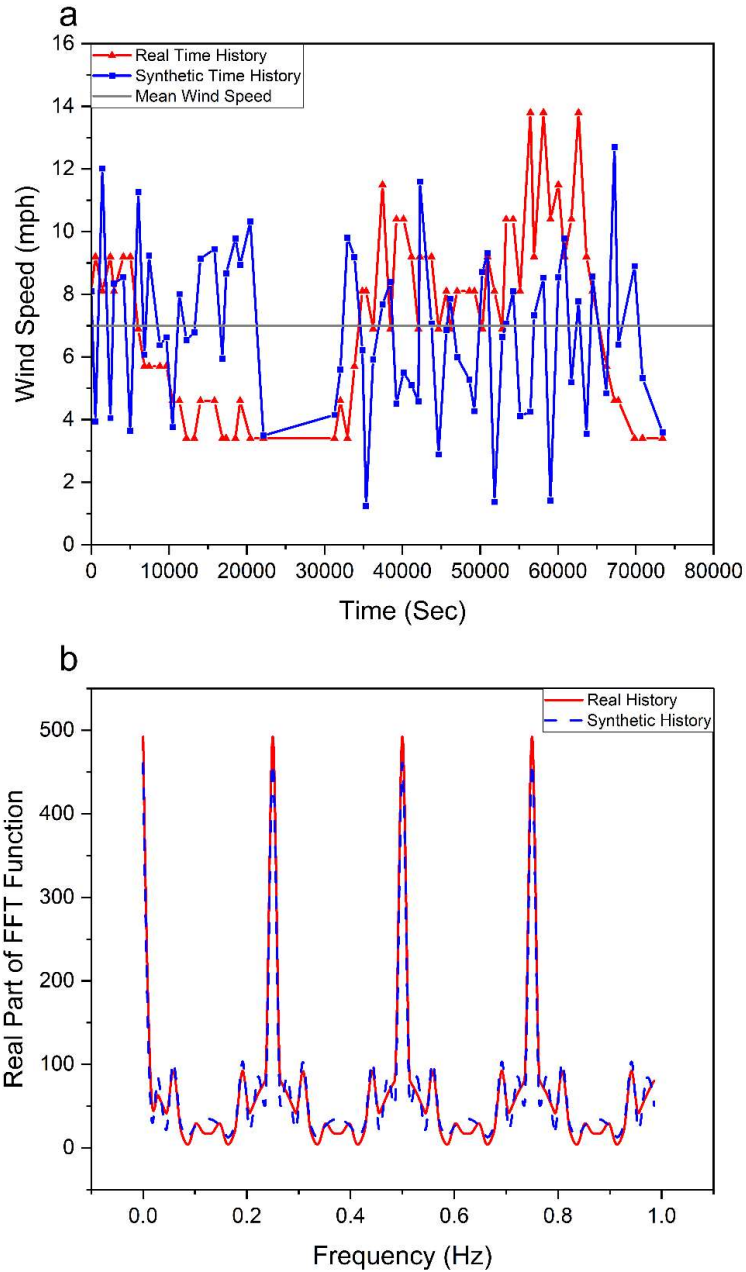


Figure 4.5 Real and synthetic wind comparison for mean 7 mph and high 13.8 mph, (1 mph = 1.609 km/h). (a) Time domain (b) Frequency domain

4.4.4 Wind Loading on The Structure

The effect of the natural wind was simulated using the developed software by specifying a certain wind speed. The software can generate the wind loading and populate it to the Staad Pro models. Both effects of wind loading on signs and members were considered. First, the wind pressure was calculated using the following expression [5]

$$P_z = 0.00256K_zGV^2I_rC_d \text{ (psf)} \quad (9)$$

Where K_z is the height and exposure factor calculated based on the height of the member using Eq. (10), G is the gust factor taken to be 1.14, V is the applied wind velocity (mph), I_r is the importance factor taken to be 1.0.

$$K_z = 2.01\left(\frac{Z}{Z_g}\right)^{\frac{2}{\alpha}} \quad (10)$$

Z is height above the ground at which the pressure is calculated, $Z_g=274.3$ m (900 ft.), $\alpha=9.5$.

The drag coefficient (C_d) was considered based on the object size and shape. For the truss members, the value of C_d was taken to be 1.2, while for the signs, the value of C_d was determined based on the aspect ratio (width/height). After generating the pressure from each wind speed in the time span under investigation, the pressure is converted to force by multiplying it by the gross area over which the pressure is applied.

4.5 Fatigue Analysis and Life Prediction

4.5.1 S-N Curve Implementation

The stress life method was used in the scope of this paper to evaluate the fatigue life of different structural elements. AASHTO 2015 manual [5] provides $S-N$ curves for different connection types based on a wide range of laboratory fatigue tests of full-scale structures. However, an experimental $S-N$ curve for the welded aluminum was used here to determine the number of cycles to failure at each stress value on the member level using Eq. (11).

$$N_i = \left(\frac{\sigma_i}{A}\right)^{\frac{1}{B}} \quad (11)$$

Where N_i is the number of cycles to failure at i -th stress range, σ_i is the member stress value corresponding to a wind speed level, A and B are constants to be determined from a log-log plot of the $S-N$ curve.

The stress amplitude vs. the number of cycles to failure for the welded aluminum obtained from [23] is plotted on a log-log scale to find the values of A and B as shown in Figure 4.6. Furthermore, this $S-N$ curve is compared with AASHTO 2015 $S-N$ curve evaluated for a typical connection for a column component of the sign structure analyzed reflecting very good correspondence, Figure 4.6.

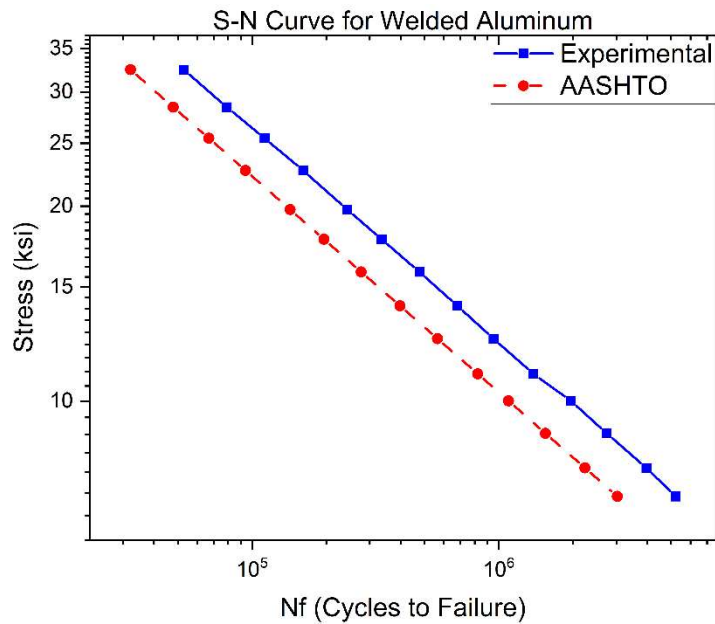


Figure 4.6 S-N curve for welded aluminum adapted from [23]

The $S-N$ curve was extrapolated to extend it to lower stress values to cover a broader range of stresses that might affect overhead structures assuming that aluminum does not have a threshold stress. The plotted data on a log-log scale seem to fall along a straight line. Therefore, Eq. (11) is used to calculate A and B values from two points along the curve

4.5.2 Rainflow Counting and Palmgren-Miner Rule

Wind time histories were generated for the 45 years of data. These histories represent highly irregular variations of speed with time. To identify how each wind speed cycle is extracted, Rainflow counting technique, developed by Endo et al. [24], is adapted here to convert the irregular time histories to cycles. The algorithm of this technique was borrowed from ASTM E1049 [25] and implemented in a computer code to extract the cycle database for 45 years. After building the cycles database, the simulator software mentioned earlier build the structural models for all the wind speeds in the time span under consideration then for each member in the structure, the stress is extracted at each loading level after performing the analysis and the number of cycles to failure under this stress level interpolated from the $S-N$ curve. The linear damage formula known as Miner rule is used to assess the fatigue condition of each member by using Eq. (12).

$$D_i = \frac{n_i}{N_i} \quad (12)$$

Where D_i is the damage in a specific member at a particular stress range, n_i is the number of cycles at i -th stress range, obtained from Rainflow analysis, N_i is the number of cycles to failure at the same stress range that could be obtained from Eq. (10). After assessing the damage at each stress level resulted from applying all the wind speeds in the time span under consideration, the total damage could easily be computed using Eq. (13)

$$D = \sum_i D_i \quad (13)$$

According to the miner rule, fatigue failure is expected when such life fractions sum to a unity, when 100% of the life is exhausted ($D=1$).

4.5.3 Fatigue Life Calculation Automation

A comprehensive tool to accurately predict the remaining fatigue life of full-span overhead sign support structures subjected to a long and sustained wind fluctuation was developed in conjunction with building 45-year wind database histories. This effort yielded a computationally affordable simulation package to evaluate the fatigue life of the structural members and detect members that are prone to fatigue failure. The user in the software interface will select the city, define the structural geometry and select the time span that the structure has been in service. This could be defined as the year that the structure was built and how long the structure has been in service at the time of evaluation, as shown in Figure 4.7 the software will extract the wind speeds and the number of cycles for each speed for that time span from the database which has been established earlier. The finite element software Staad Pro [26] runs a number of analyses to cover all wind speeds, and the post-processing engine calculates the damage index for each member in the structure using the rules mentioned earlier. Then a color index screen results pops-up for the user to facilitate detecting the damaged members. The color coding used in this software gives a range of lives for each member based on the miner rule as seen in Table 4-2

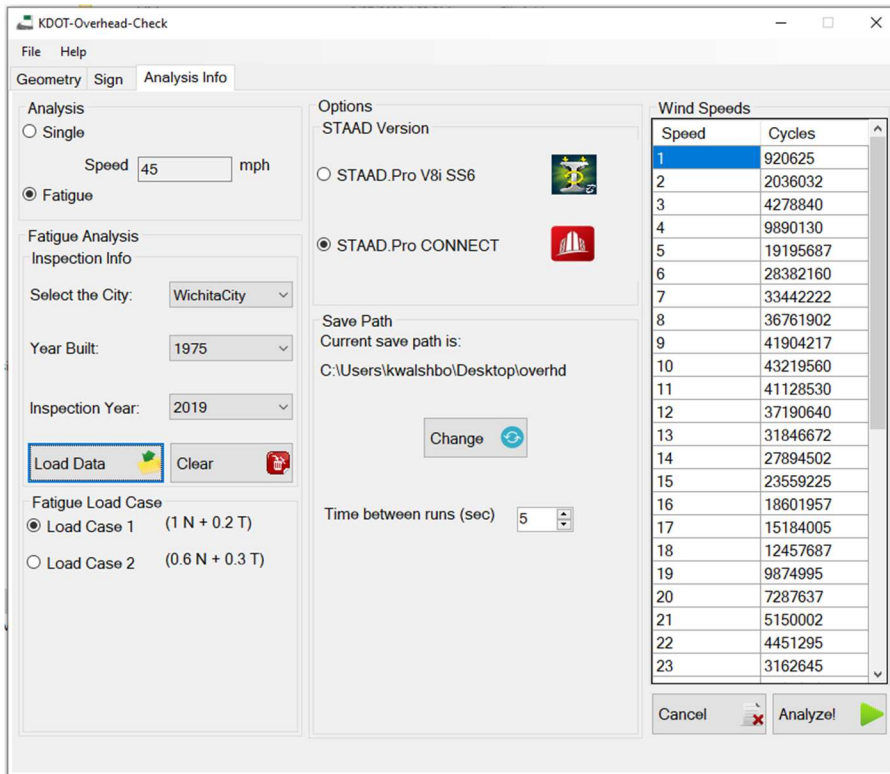


Figure 4.7 Fatigue life software interface

Table 4-2 Results color code

Fatigue life $D = \sum_i D_i$	Color
$D < 0.8$	Green
$0.8 \leq D < 1$	Yellow
$1 \leq D < 1.1$	Orange
$D \geq 1.1$	Red

4.6 Case Study

4.6.1 Results of a Sign Structure Analyzed

Figure 4.8 describes the methodology developed in this paper to evaluate and assess the overhead sign support structures in terms of remaining fatigue life. This procedure yielded a standalone software written in the C# programming language. In order to validate the

functionality and the algorithm used in this software, it was used as an inspection tool to evaluate a four-chord box overhead truss in the city of Wichita, State of Kansas. The structure was modeled through the model generator developed earlier using the parameters in Table 4-3, see Figure 4.9. This structure was then exposed to 45 years of wind loading since it was built in 1975 and inspected in 2019. It should be noted that the present methodology and procedure could be followed to produce such similar tool to account for different geometries and wind raw records.

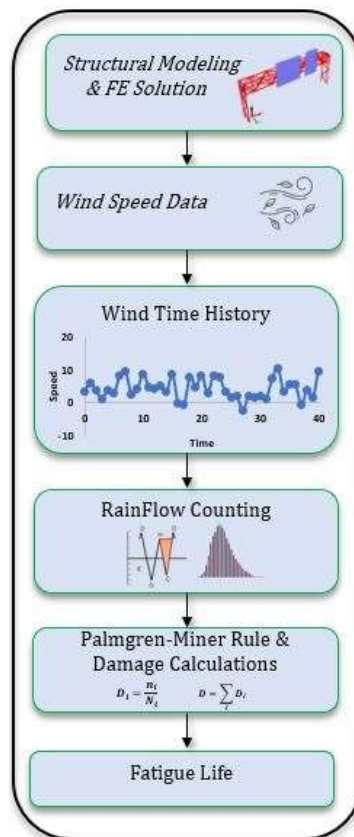


Figure 4.8 Fatigue life calculation flowchart

Table 4-3 Case study model information

Geometry									
Main truss dimension		Right truss dimension		Left truss dimension		Sign information			
Span	1.79 m	Span	1.72 m	Span	1.75 m	Sign1	Sign2		
Number of panels	12	Number of panels	3	Number of panels	3	Location	6.94 m	14.7 m	
Main wall thick.	3.75 mm	Main wall thick.	7.08 mm	Main wall thick.	7.08 mm	Height	2.2 m	2.43 m	
Secondary wall thick.	3.04 mm	Sec. wall thick.	3.04 mm	Secondary wall thick.	3.04 mm	Width	5.86 m	3.50 m	
$\omega_n = 5.4Hz$									
Material (Aluminum)									
Parameter	Value								
Young's Modulus	6.89 GPa								
Poisons ratio	0.35								
Density	2574.3kg/m ³								

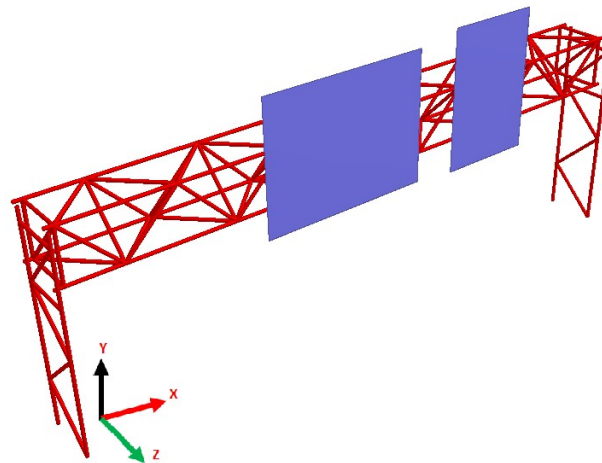


Figure 4.9 Wichita Staad model (Model 2)

Upon performing a set of subsequent 45 analyses (1-45 mph) by Staad Pro and reading back-sorting the analysis results, the fatigue engine performed the needed calculations to evaluate the fatigue life consumption in all members in the analytical model. It is worth mentioning that the model consisted of 161 members. Thus, evaluating the fatigue life for

all members would be computationally cumbersome without using such software. After finishing the analysis, the results window indicated the fatigue life for all model members. Figure 4.10 shows the results obtained from the software. According to Figure 4.10, two members reached their end of fatigue life, members 258 and 259 (red-colored). Both of them reached a damage index of 1.1. Based on Miner's rule, a member reaches the end of its fatigue life when the damage index surpasses unity. Since those two members exceeded a damage index of unity, it was expected that both members reached their ultimate fatigue failure or have the tendency to develop visible fatigue cracks. It is worth mentioning that both distressed members (258 and 259) are adjacent to each other, while member 260 in their vicinity, reflected a damage index of 0.918, see Figure 4.11.

Wichita

Member	Fatigue Life	Color	Member	Fatigue Life	Color	Member	Fatigue Life	Color	Member	Fatigue Life	Color	Member	Fatigue Life	Color
5	0.4428	Green	41	0.4507	Green	116	0.0659	Green	151	0.0001	Green	236	0.1286	Green
6	0.4510	Green	42	0.4094	Green	117	0.1291	Green	152	0.1108	Green	237	0.4286	Green
7	0.3934	Green	43	0.3953	Green	118	0.0176	Green	153	0.4422	Green	238	0.1800	Green
8	0.4510	Green	44	0.4652	Green	119	0.0335	Green	154	0.0284	Green	239	0.0007	Green
9	0.3934	Green	45	0.4485	Green	120	0.4300	Green	155	0.0248	Green	240	0.0029	Green
10	0.3028	Green	46	0.4111	Green	121	0.1829	Green	156	0.0101	Green	241	0.0009	Green
11	0.0159	Green	47	0.4275	Green	122	0.2308	Green	157	0.0283	Green	242	0.2938	Green
12	0.2896	Green	48	0.4670	Green	123	0.2136	Green	158	0.1720	Green	243	0.0087	Green
13	0.0014	Green	49	0.4887	Green	124	0.3907	Green	159	0.0002	Green	244	0.4392	Green
14	0.2036	Green	50	0.4827	Green	125	0.4655	Green	160	0.4063	Green	245	0.3989	Green
15	0.0011	Green	51	0.4853	Green	126	0.4454	Green	161	0.0417	Green	246	0.4059	Green
16	0.0010	Green	52	0.4585	Green	127	0.0529	Green	162	0.0083	Green	247	0.3989	Green
300	0.7639	Green	53	0.4827	Green	128	0.5463	Green	163	0.4099	Green	248	0.4396	Green
19	0.9453	Yellow	54	0.4845	Green	129	0.0050	Green	164	0.0170	Green	249	0.4675	Green
20	0.9414	Yellow	55	0.4576	Green	130	0.4621	Green	165	0.4339	Green	250	0.4396	Green
21	0.3430	Green	56	0.4603	Green	131	0.0014	Green	166	0.0000	Green	255	0.4195	Green
22	0.5660	Green	57	0.4612	Green	132	0.2411	Green	167	0.1306	Green	256	0.5889	Green
23	0.4049	Green	58	0.4755	Green	133	0.5074	Green	168	0.4548	Green	257	0.3910	Green
24	0.1647	Green	59	0.4476	Green	134	0.0012	Green	169	0.0000	Green	258	1.1084	Red
25	0.0844	Green	60	0.4142	Green	135	0.4525	Green	170	0.4567	Green	259	1.1160	Red
26	0.0398	Green	61	0.4591	Green	136	0.2314	Green	171	0.1260	Green	260	0.9183	Yellow
27	0.0213	Green	62	0.4777	Green	137	0.0051	Green	172	0.0000	Green			
28	0.1656	Green	63	0.4678	Green	138	0.4774	Green	173	0.3904	Green			
29	0.0916	Green	64	0.4162	Green	139	0.0003	Green	174	0.0077	Green			
30	0.0427	Green	65	0.4024	Green	140	0.4192	Green	175	0.4240	Green			
31	0.2144	Green	66	0.4355	Green	141	0.0022	Green	176	0.0174	Green			
32	0.1696	Green	67	0.4421	Green	142	0.2149	Green	177	0.3527	Green			
33	0.4178	Green	68	0.3925	Green	143	0.4413	Green	178	0.5201	Green			
34	0.4238	Green	69	0.3937	Green	144	0.0060	Green	179	0.0010	Green			
35	0.2097	Green	70	0.4392	Green	145	0.4451	Green	180	0.4871	Green			
36	0.4207	Green	71	0.4300	Green	146	0.1199	Green	181	0.4258	Green			

Figure 4.10 Fatigue life results sample for Wichita model

4.6.2 Further Results and Discussion

As mentioned before, AASHTO provides a set of $S-N$ curves for different types of connections. The potential number of cycles to failure (N_i) could be obtained per AASHTO using Eq. (14)

$$N_i = \frac{A'}{\Delta\sigma_i^3} \quad (14)$$

Where A' is a constant associated with the member connection, $\Delta\sigma$ is the stress value acting on the detail at cycle i . Both failed members fall under the slotted tube-to-gusset connections category, as shown in Figure 4.12. The fatigue life for damaged members was re-calculated using Eq. (13) to compare the results shown earlier. For brevity, the results

here are reported just for member 259 since both members 259 and 258 showed almost the same damage value. The total damage in member 259, calculated based on the AASHTO $S-N$ equation, was 1.078, where the value obtained from the program was 1.1, which is almost identical. Figure 4.13 presents a comparison of the variation in the damage corresponding to each wind speed as obtained from the program versus AASHTO equation. It is evident from this figure that the damage variation between the two approaches is in excellent agreement. Nevertheless, one may observe that at certain wind speeds the damage experienced by the member based on the AASHTO equation is slightly higher while it is slightly lower than the program's prediction for other wind speeds.

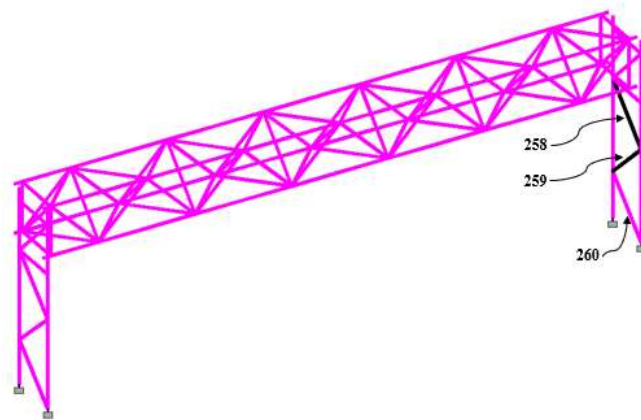


Figure 4.11 Damaged members in the model

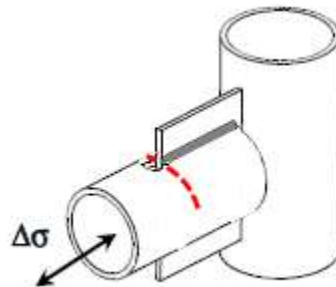


Figure 4.12 Member's connection type per AASHTO

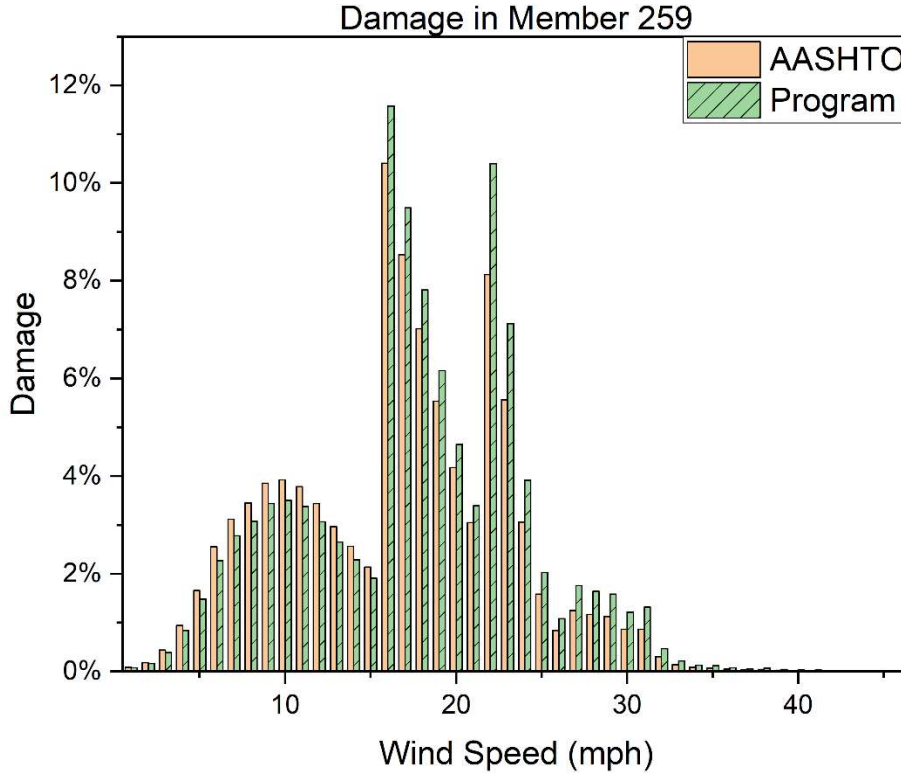


Figure 4.13 damage variation with speed in member 259

As for the other members in the model, they showed a damage index ranging from very low value (no damage) to 0.945 (highly damaged). Some critical members are observed on the left side of the truss (members 19 and 20) with damage percentage of 94.5% and 94.14%, respectively, indicating that these diagonal welded members are nearing their fatigue life. To estimate the remaining life in these two members, the current damage value was subtracted from unity while estimating linear extrapolation rate from the last five years. For example, the total damage in member 260 over the entire 45 years was 0.9183 and it was 0.814 over the first 40 years resulting in a localized average damage per year of $\left(\frac{(0.9183 - 0.814)}{45 - 40}\right) = 0.02086/\text{year}$. Therefore, the average remaining life could be calculated as follows: $\frac{(1 - 0.9183) \text{ damage}}{0.02086 \frac{\text{damage}}{\text{year}}} = 3.916 \cong 4.00 \text{ years}$. This implies that after approximately 4 years the member 260 would experience full damage. To verify this

expectation, the last 5 years of wind data were populated to fill extra 4 years. This assumption is expected to be accurate to a great extent. This was implemented by simply multiplying the number of cycles corresponding to each wind speed (in the last five years) by a ratio of (4/5). After that, the newly computed number of cycles was added to the original number of cycles in the database. Upon re-calculating the damage in member 260 using the extended cycles database, it was found that the damage in member 260 reached the unity mark after four extra years meaning that it attained the end of its fatigue life as seen in Figure 4.14. It is worth mentioning that the performed calculations resulted in an even higher damage index for members 258 and 259 since their fatigue life index was not reset to zero as a result of replacing these two members.

Member	Fatigue Life	Color
258	1.2082	Red
259	1.2164	Red
260	1.0020	Yellow

Figure 4.14 damage in member 260 after exposing it to extra 4 years of wind speeds
 These exciting results motivated the KDOT team (Kansas Department of Transportation) to investigate the truss in situ. On 9/9/2019, a field inspection of the truss under concern has been made. Interestingly enough, a complete fatigue damage (fatigue cracking) was found in the two indicated members only, as shown in Figure 4.15.



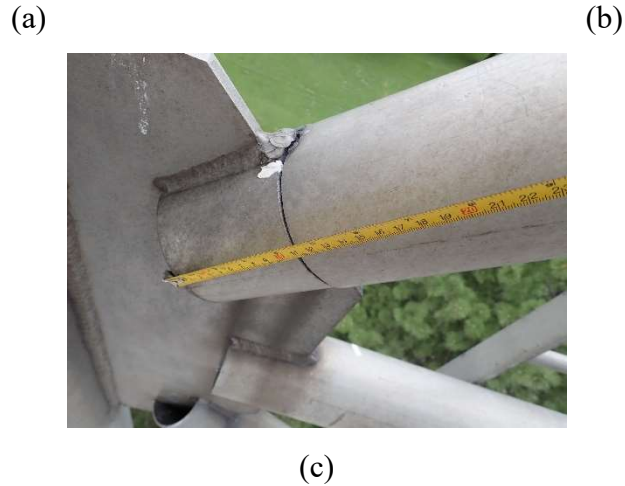
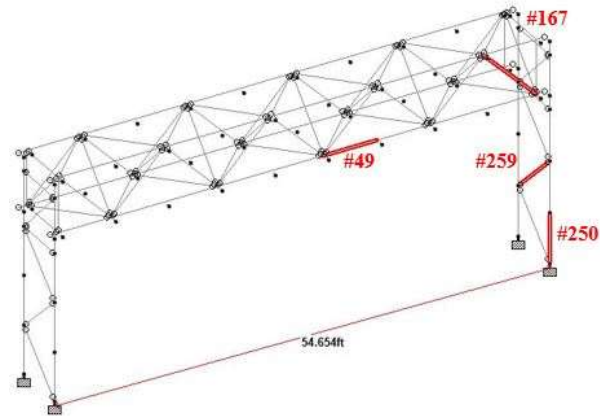


Figure 4.15 damaged members in the overhead sign truss under investigation (Wichita) courtesy of KDOT (Bureau of structural and geotechnical services).

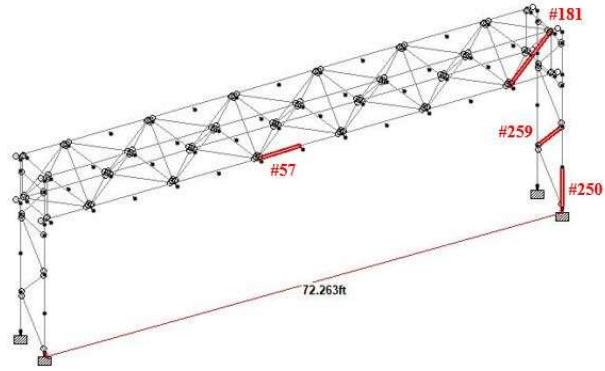
4.7 Additional Examples

In this section, additional two examples along with the case study, discussed earlier, were carried out using the same software to allow for a comparison. All the geometric properties, spacing and sign dimensions were kept the same as the Model 2 in Figure 4.9 except for the span of the structure (number of panels). Figure 4.16 shows the three models. In order to better understand the procedure adopted in this study the stress variation with wind speed was extracted from the software for four critical members, namely, column main member (CMM), column secondary member (CSM), truss main member (TMM) and truss secondary member (TSM). The location for each one of the members and member numbering is also indicated in Figure 4.16. Upon calculating the stresses in the four members, the damage was then evaluated using a 45-years of wind loading. Figure 4.17 shows the stress variation and the damage in the members. Among all the member locations, the column secondary member (CSM) shows higher damage because it is highly stressed element and this damage increased with increasing the span length and that make sense due to increasing the loading. CSM in both models 2 and 3 experienced total damage

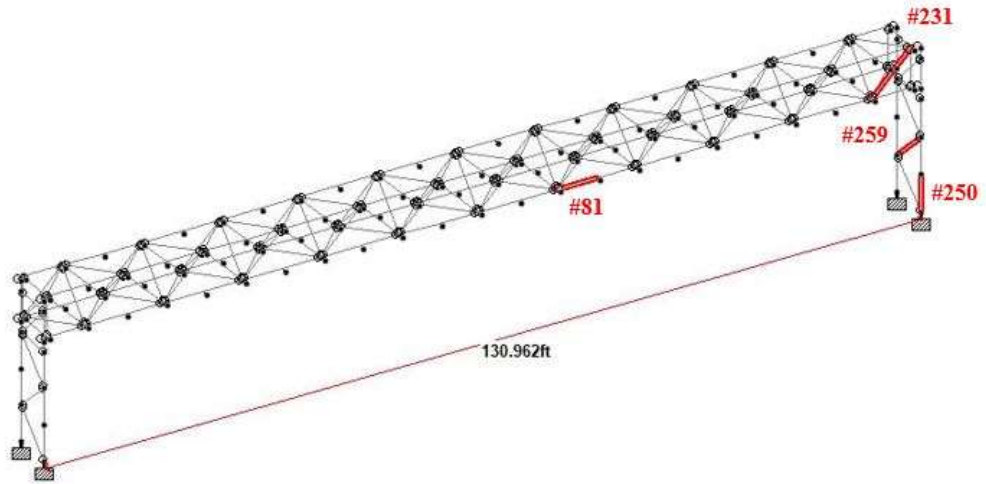
index greater than 1 indicating the end of their fatigue life. Furthermore, the other three members showed close damage values to each other in case of model 1 and model 2, Figure 4.17.



A (Model 1, N=9)

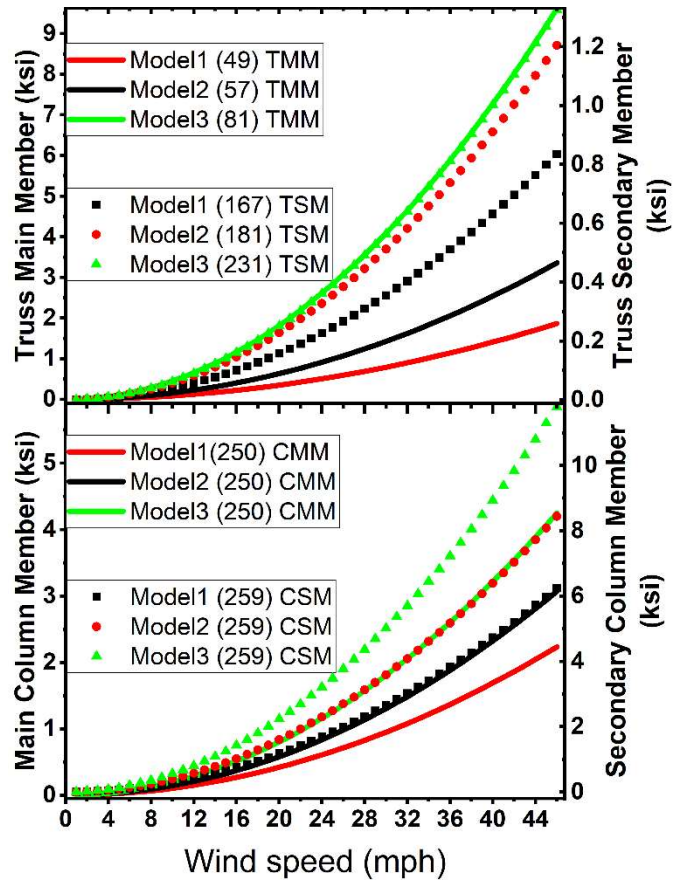


B (Model 2, N=12)

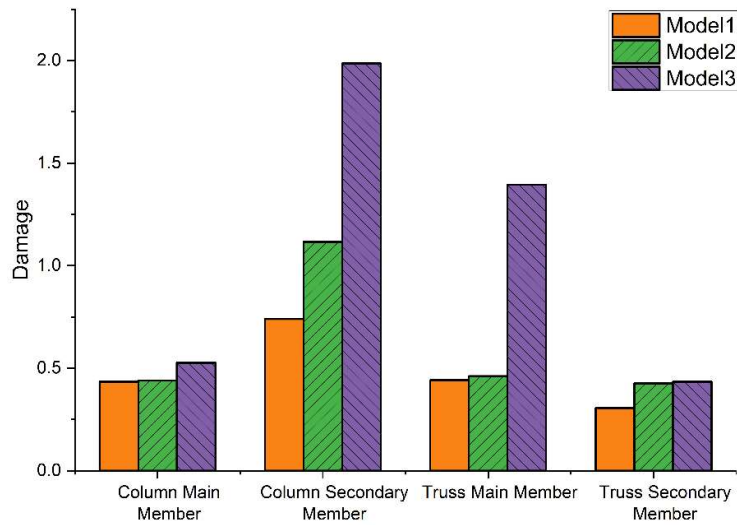


C (Model 3, N=22)

Figure 4.16 Examples for three models and location of the evaluated members



(A)



(B)

Figure 4.17 (A) Stress variation in the critical members with wind speed (B) Damage index for the critical members resulted from 45 years of wind loading

4.8 Conclusions

This paper presents a framework to develop an inspection tool to assess overhead sign structures with respect to remaining fatigue life. The structure was modeled using the Finite element software Staad Pro, through a software shell developed to facilitate the modeling, the running of hundreds of simulations, as well as post fatigue calculations. A 45-year wind time history database was established for the State of Kansas to allow for fatigue inspection of any given period of service span. Kaimal wind spectrum was adopted to generate wind histories, and then the rainflow counting technique was performed to extract the number of cycles for each wind speed over the service time span. The developed software was used to inspect a four-chord overhead truss structure in the city Wichita exposed to 45 years of wind loading history. Based on the results obtained from the analysis, it was shown that the overhead truss structure in Wichita experienced some full fatigue damage in two members (damage index = 1.1). Interestingly, a follow up inspection performed by KDOT indicated that these two members were specifically subject to severe fatigue cracking. Further analysis of the same truss using the AASHTO fatigue $S-N$ equation confirmed this finding. Furthermore, some of the other diagonal members in the vertical trusses showed high damage values (damage index = 0.91830-0.9453). Upon extrapolating the remaining fatigue life into the future, it was estimated that one of the members would reach its end of fatigue life within four years. This was further confirmed to be the case with a scaled-up wind analysis. It is important to alert the highway agencies to high likelihood of attracting fatigue damage in the diagonal welded members in the vertical trusses. It is worth concluding that this developed software is expected to significantly influence the state

highway decision-making and prioritization of repair plans, as it provides a framework that could be applied in any state or region after updating the wind records for that state.

4.9 References

- [1] Kacin J, Rizzo P, Tajari M. Fatigue analysis of overhead sign support structures. *Eng Struct* 2010;32:1659–70. <https://doi.org/10.1016/j.engstruct.2010.02.014>.
- [2] Li X, Whalen TM, Bowman MD. Fatigue Strength and Evaluation of Double–Mast Arm Cantilevered Sign Structures. *Transp Res Rec* 2005;1928:64–72. <https://doi.org/10.1177/0361198105192800107>.
- [3] Arabi S, Shafei B, Phares BM. Fatigue analysis of sign-support structures during transportation under road-induced excitations. *Eng Struct* 2018;164:305–15. <https://doi.org/10.1016/j.engstruct.2018.02.031>.
- [4] Hosch IE, Fouad FH. Design Fatigue Load of Sign Support Structures Due to Truck-Induced Wind Gust. *Transp Res Rec* 2010;2172:30–7. <https://doi.org/10.3141/2172-04>.
- [5] AASHTO. 2015 Interim Revisions to Standard Specifications for Structural Supports for Highway Signs , Luminaires , and Traffic Signals Sixth Edition 2013. 2015.
- [6] Creamer BM, Frank KH, Klingner RE. Fatigue loading of cantilever sign structures from truck wind gusts. 1979.
- [7] DeSantis P V, Haig PE. Unanticipated loading causes highway sign failure. *Proc. ANSYS Conv.*, 1996.
- [8] Chen G, Wu J, Yu J, Dharani LR, Barker M. Fatigue Assessment of Traffic Signal Mast Arms Based on Field Test Data Under Natural Wind Gusts. *Transp Res Rec*

- 2001;1770:188–94. <https://doi.org/10.3141/1770-24>.
- [9] Dexter RJ. Fatigue-resistant design of cantilevered signal, sign, and light supports. vol. 469. Transportation Research Board; 2002.
- [10] Letchford C, Cruzado H. Risk assessment model for wind-induced fatigue failure of cantilever traffic signal structures. 2008.
- [11] Fouad FH, Hosch IE. Design of Overhead VMS Structures for Fatigue Loads. University Transportation Center for Alabama; 2011.
- [12] Hong HP, Zu GG, King JPC. Estimating fatigue design load for overhead steel sign support structures under truck-induced wind pressure. *Can J Civ Eng* 2016;43:279–86. <https://doi.org/10.1139/cjce-2015-0158>.
- [13] Roy S, Kundu CK. State of the art review of wind induced vibration and its control on transmission towers. *Structures* 2021;29:254–64. <https://doi.org/https://doi.org/10.1016/j.istruc.2020.11.015>.
- [14] Ginal S. Fatigue Performance of Full-Span Sign Support Structures Considering Truck-Induced Gust And Natural Wind Pressures. MS Thesis 2003:393.
- [15] Cochran L. Wind issues in the design of buildings. 2012. <https://doi.org/10.1061/9780784412251.ch01>.
- [16] Davenport AG. The spectrum of horizontal gustiness near the ground in high winds. *Q J R Meteorol Soc* 1962;88:197–8. <https://doi.org/https://doi.org/10.1002/qj.49708837618>.
- [17] Kaimal JC, Wyngaard JC, Izumi Y, Coté OR. Spectral characteristics of surface-layer turbulence. *Q J R Meteorol Soc* 1972;98:563–89. <https://doi.org/https://doi.org/10.1002/qj.49709841707>.

- [18] Bentley. Staad Pro V8i SS6 2016.
- [19] National Weather Service NW. Kansas Historical Weather Data. Weather Undergr
2015.
- [20] Solari G. Wind Loading of Structures: Framework, Phenomena, Tools and
Codification. Structures 2017;12:265–85.
<https://doi.org/https://doi.org/10.1016/j.istruc.2017.09.008>.
- [21] Iannuzzi A, Spinelli P. Artificial wind generation and structural response. J Struct
Eng 1987;113:2382–98.
- [22] WillyWeather. Weather forecast 2020. [https://www.willyweather.com/ks/riley-
county/manhattan.html](https://www.willyweather.com/ks/riley-county/manhattan.html).
- [23] Sonsino CM. Course of SN-curves especially in the high-cycle fatigue regime with
regard to component design and safety. Int J Fatigue 2007;29:2246–58.
<https://doi.org/10.1016/j.ijfatigue.2006.11.015>.
- [24] Matsuishi M, Endo T. Fatigue of metals subjected to varying stress. Japan Soc
Mech Eng Fukuoka, Japan 1968;68:37–40.
- [25] ASTM E1049. Standard practices for cycle counting in fatigue analysis. ASTM
Stand 2017;85:1–10. <https://doi.org/10.1520/E1049-85R17.2>.
- [26] Bentley. Staad Pro V8i SS6 2016.

Chapter 5 - Evaluating Fatigue in Steel Cantilevered Sign Structures Under Service Life Wind Events Through a Comprehensive Tool for Inspection

Khalid W. Al Shboul¹ and Hayder A. Rasheed^{2*}

*Corresponding author: Tel. +1(785) 341-6220. Email: hayder@ksu.edu

5.1 Abstract

Fatigue failure of cantilevered highway sign structures have been recognized in many states due to sustained wind loading events. AASHTO specifies that the structural component should be designed for infinite life by maintaining the wind induced stress below their constant amplitude fatigue threshold (CAFT). However, for the existing structures, that are typically not designed for fatigue, it is essential to evaluate the condition of all the critical and fatigue prone components for safety considerations. The visual inspection consumes a lot of time and effort and may not detect unnoticed fatigue cracks. A need for analytical inspection tools to examine all the critical members and connections in terms of remaining fatigue life has received a growing attention to ensure public safety. This paper introduces a simplified analytical inspection tool implemented into a computer software to assess all the critical components according to AASHTO specifications for fatigue. A failed structure

¹ Ph.D. Candidate, Department of Civil Engineering, Kansas State University, Manhattan, KS, USA, Email: kwalshbo@ksu.edu

² Professor, Department of Civil Engineering, Kansas State University, Manhattan, KS, USA, Email: hayder@ksu.edu

has been examined using this software and the results showed a fatigue damage crack in the vertical weld of mast-to-arm box connection at the upper chord level reflecting the in-situ condition of the structure.

Keywords: Cantilever Structures; Butterfly Structures; Fatigue analysis; AASHTO; Connections.

5.2 Introduction

Cantilever and butterfly sign support structures are assemblies used to promote the highway accessibility, efficiency, and safety of the traffic flow. They support large signs with needed information to guide the motorist in their trips. Unexpected fatigue damage within the structure's connection details can lead to catastrophic failure causing injuries, property damage, traffic closures [1]. The damage raised the need to address the safety issues related to the highway system, prompted research and intensive field inspection, and drove most highway agencies to change the connection designs to Ring-stiffened box connections in new projects due to their superiority in resisting fatigue loading. This recommendation is based on various experimental testing performed under the NCHRP projects [2–4]. However, fillet-welded mast-to-arm connection details are still a widely attractive alternative for some highway agencies due to the cost-effectiveness and lower fabrication effort. These connections are classified as the most fatigue-prone details. The stress fluctuations due to natural wind loading may cause fatigue cracks at these locations. Computing the whole wind-induced stresses during lifetime loading events is impractical. To overcome the unreliability in designing the highway structures for finite fatigue life, AASHTO recommends an infinite life fatigue design approach. Each component shall resist the equivalent static wind load to maintain a stress level below the constant amplitude

fatigue threshold (CAFT) yielding infinite fatigue life. AASHTO 2013 *Structural Supports for Highway Signs, Luminaires, and Traffic Signals* [5] implemented the findings from the NCHRP project [2] to identify CAFT required for infinite life design. Each connection detail is associated with certain CAFT in a tabulated format. Extensive research has been done to evaluate the highway sign structures' response and provide a reasonable understanding of the fatigue failure in terms of critical spots, crack growth, and mitigation [6–9]. Barele et al. [10] developed a finite element failure analysis of cantilever sign structure by modeling the extreme monotonic wind load and stress spectra of the variable service loads. This study revealed estimated fatigue life and design improvements. Choi et al. [11] conducted a comparison study and improvement evaluations between AASHTO 2015 standards and AASHTO 2001 by providing two design examples of overhead and cantilever highway structures. The study concluded that AASHTO 2015 guideline uses reliability methods and statistical data to introduce resistance factors for the applied loads and is a more rational design approach. The fatigue loads are based on more available data and rational probability and risk models. Rice et al. [12] performed a full-scale experimental approach to capture the structural response of four representative sign trusses and conducted an analytical study to assess the response of the trusses at full design wind loads. Li [13] carried out finite element analysis using ANSYS to model and analyze different highway sign structures, including single mast-arm and double mast-arm cantilever structures. According to the transient study that was performed, it was found that the double mast-arm cantilever sign structure is the most critical among the other non-cantilevered structures. However, all the structures had infinite life. Tsai and Alipour [14] performed a long-term health monitoring for a traffic signal structure to characterize the

wind-induced behavior and the fatigue damage parameters. They concluded that the monitored structure cannot dampen out the in-plane vibration easily resulting in fatigue-stress accumulation. Choi and Najem [15] conducted a reliability-based fatigue assessment for the potential crack initiation in cantilevered sign structure connection details. They developed probability curves which can be used to determine the inspection frequencies or maintenance strategies.

Most of the departments of transportation, including KDOT, perform the inspection of highway sign structures in typical site visits and produce an inventory for each structure. However, these inspections were not performed on a regular basis and might introduce a hazard for the inspector. In addition to that, it is hard to perform routine fatigue inspections for all the structure members since it is costly and time-consuming. This increases the possibility of unnoticed fatigue damage and possibly failure of the assembly. The Federal Highway Administration (FHWA) does not regulate sign inspections like highway bridges. The agency leaves this up to each state. Over time, the DOT's developed their own procedures for inventory management and outlined the inspection parameters. Even though the fatigue characteristics of highway sign structures have been widely investigated, and various critical spots have been identified, fatigue behavior is highly variable and encompasses many uncertainties resulting from the service load, environmental conditions, material properties, and pre-existing imperfections [16]. Accurate lifetime wind loading event approximation is one of the critical factors for minimizing the unreliability of fatigue life calculations. It is impractical to characterize the wind load events experienced by the structures during their service life which makes the life calculations hard due to the lack of stress fluctuations spectrum. In this study, analytical natural wind-time histories developed

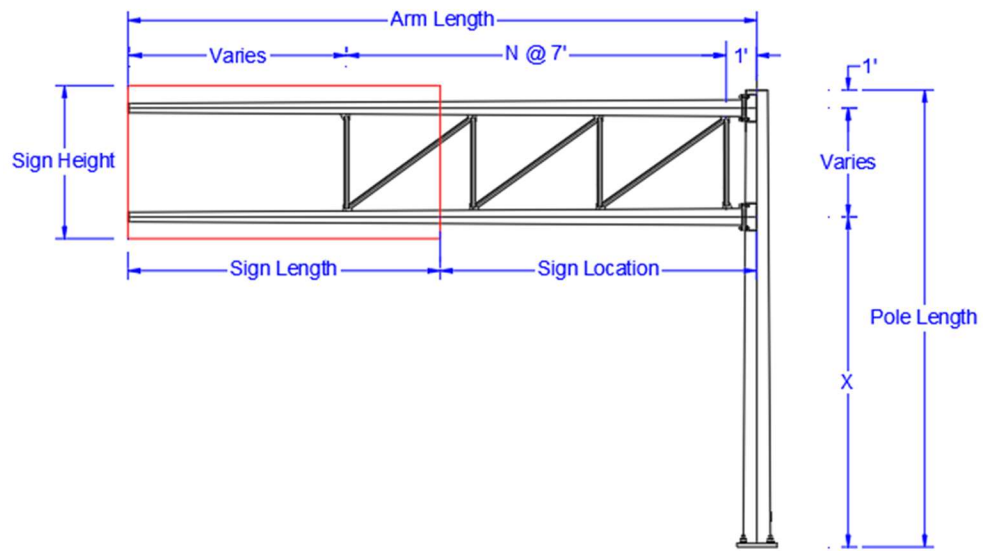
earlier for the state of Kansas along with AASHTO fatigue life calculation procedures were used to produce an inspection tool to calculate the fatigue life consumption in different critical spots in cantilevered and double cantilevered (Butterfly) structures. This article summarizes the analytical inspection procedures, emphasizing analytical modeling, structural assessment, and software development. Additional details on wind load event development may be found in [17].

5.3 Sign Structures Modeling

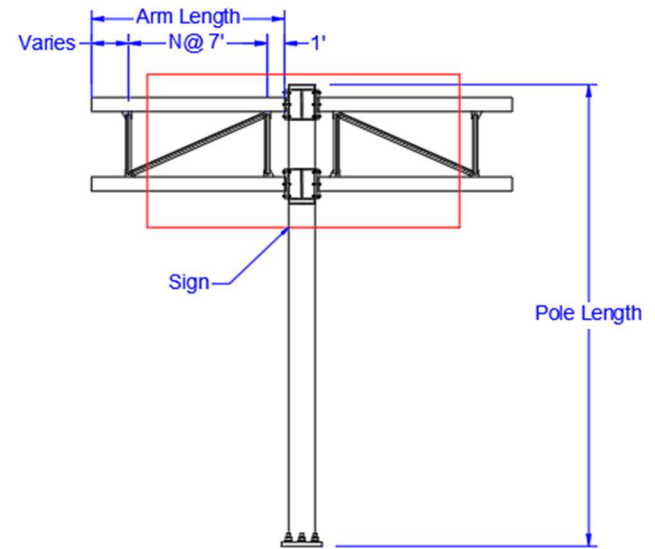
5.3.1 KDOT Highway Structures

The Kansas Department of Transportation utilized the cantilever and balanced doubled cantilever (butterfly) sign trusses in their highway transportation system in various sizes, which are shown in Figure 5.1, most of which have been in service for 30-45 years. These structures are characterized by having a hollow circular single post, either uniform or tapered, to reduce their own weight. The post mounts a two-chord steel truss made up of multiple angle sections ($3'' \times 3'' \times \frac{3}{8}''$). These angle sections are connected to the main chords by welded angle-to-gusset connections. The geometry of the structures varies based on the design models. Eight standard models are depicted in KDOT standards and classified as retired or new designs. The key detail that has been changed between both model designs is the mast-to-arm connection. In the old designs, the mast arm connection consists of a horizontal gusseted box connection fillet welded to the pole and connected to the main chords through a bolted plate, Figure 5.2a. On the other hand, the new designs consist of the ring stiffened connections that encircle the pole entirely, as shown in Figure 5.2b. In addition to the mast- arm-connection, the design models vary in terms of the detail

dimensions, including the wall thicknesses, the diameter of the pipes, and the size of the plates. Table 5-1 summarizes the geometric properties for the eight design models.



(a) Cantilever Model



(a) Butterfly Model

Figure 5.1(a) Cantilever model (b) Butterfly model

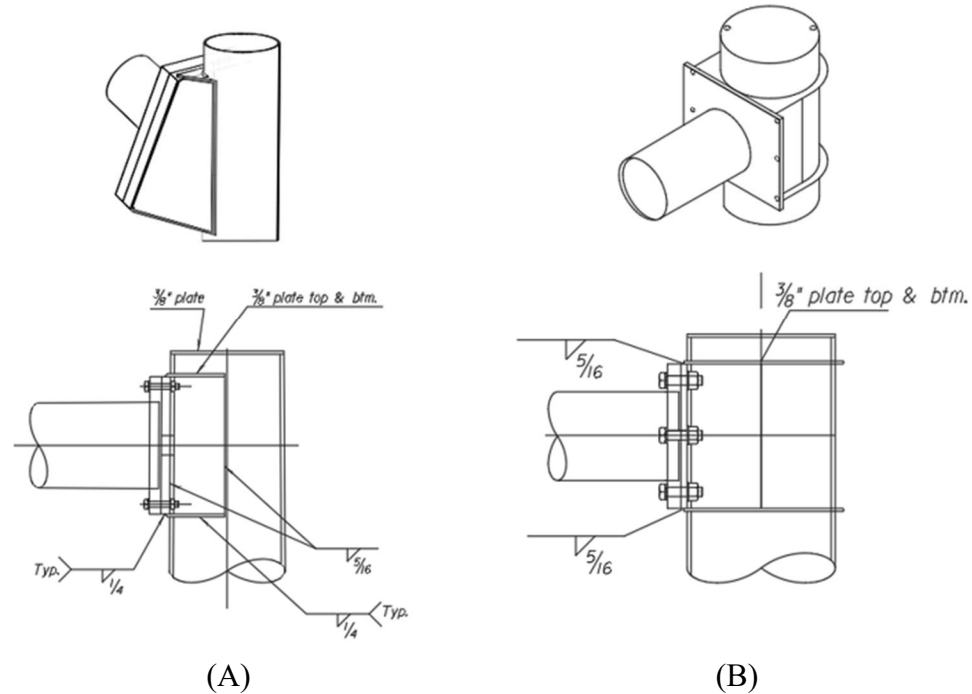


Figure 5.2 Support Connection, (A) Gusseted box connections. (B) Ring-stiffened box connection

Table 5-1 Geometric properties for cantilever models

Model	Pole dimension	Arm dimension	A	Pole uniformity	Arm to column connection
1	15" O.D × 3 Ga. wall	9.2" O.D × 3 Ga. wall	4'	Tapered / Uniform	Gusseted box connections
2	18" O.D × 3 Ga. wall	11.0" O.D × 7 Ga. wall	6'	Tapered / Uniform	Gusseted box connections
3	18" O.D × 3 Ga. wall	12.5" O.D × 7 Ga. wall	6'	Tapered / Uniform	Gusseted box connections
4	18" O.D × 3 Ga. wall	12.5" O.D × 7 Ga. wall	6'	Tapered / Uniform	Gusseted box connections
5	18" O.D × 3 Ga. wall	12.5" O.D × 3 Ga. wall	6'	Tapered / Uniform	Gusseted box connections
6	18" O.D × 3 Ga. wall	13.0" O.D × 3 Ga. wall	6'	Tapered / Uniform	Gusseted box connections
7	18" O.D × 3 Ga. wall	14.0" O.D × 5/8"	6'	Uniform	Ring-stiffened connections
8	20" O.D × 3 Ga. wall	14.0" O.D × 3/4"	6'	Uniform	Ring-stiffened connections

5.3.2 FE Modeling

5.3.2.1 Structure

The finite element software Staad Pro V8i SS6 [18] was chosen to model the flexible sign structures and execute the static analysis. The structures were modeled using a combination of beam elements, truss elements, and plate elements with appropriate cross-sectional dimensions. The upper and lower main chords were modeled using a 2-node frame element, and they ran continuously. At the same time, the secondary members were connected at the intersection nodes and released to act as a pin connection. Moreover, the main truss chords are connected to the plates that makes up both types of connections, old and new. The base support is simulated as a fixed support. In addition to that, the material used is steel with an elastic modulus of 29000 ksi.

5.3.2.2 Mast-to-Arm connection

The gusseted box connection was used in KDOT standards in models 1-6, while the ring stiffened connection was used for models 7 and 8. A 4-noded plate elements were used to model all the plates in the connection and attached directly to the main upper and lower chords at the center node. The steel plates have the same thicknesses as the actual structures and are connected to the pole through another plate with the same fillet weld thickness and properties. The pole was divided into sub-elements, and the plate nodes merged with pole nodes, as shown in Figure 5.3. In order to verify that the connections were modeled correctly, the critical node deflections were calculated for nodes (18, 19, 24, 25, 26, and 27) for a specific model and compared to the same model results but with assuming that the truss-pole connected rigidly. Beam elements are used to connect the pole with the cantilevered truss. The length of each beam is the pole's radius at the connection level (in

the tapered case). The properties of the beams are $\text{Area} = 1 \times 10^6 \text{ in}^2$ $I_x = I_y = I_z = 1 \times 10^8 \text{ in}^4$
 Geometry data are shown in Table 5-2.

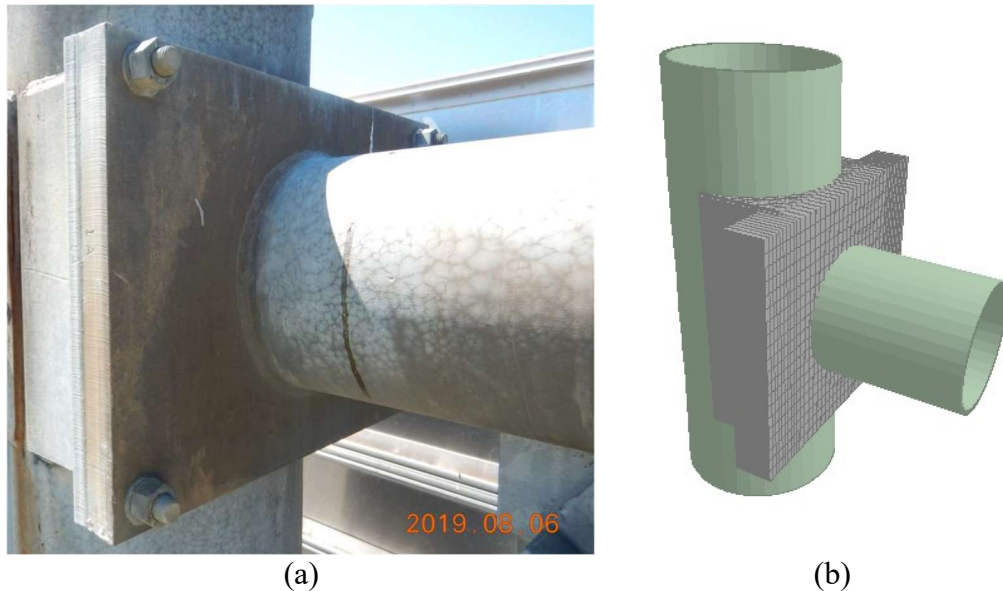


Figure 5.3 (a) post-to-chord connection (b) The model

Table 5-2 Geometry and loading data for the test model.

Truss information		Sign information	
N	3	Location	2 ft.
S	7 ft.	Length	10 ft.
Pole height	10 ft.	Height	8 ft.
Wind speed		45 mph	

First-order structural analysis was performed to the rigid structure, Gusseted box connection model, and ring stiffened model, and the resulted response was compared.

Figure 5.4 shows the deflected shapes for the three models.

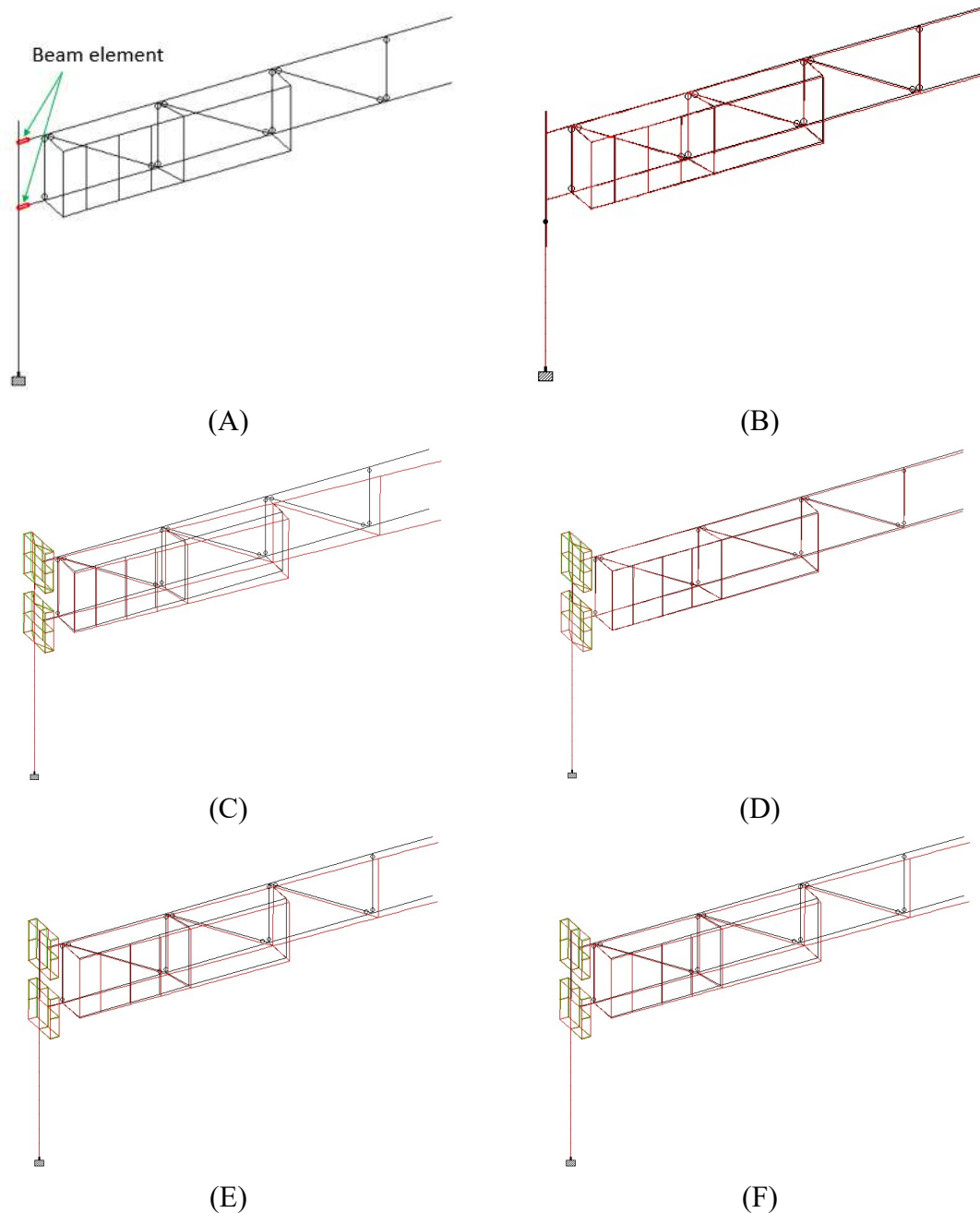


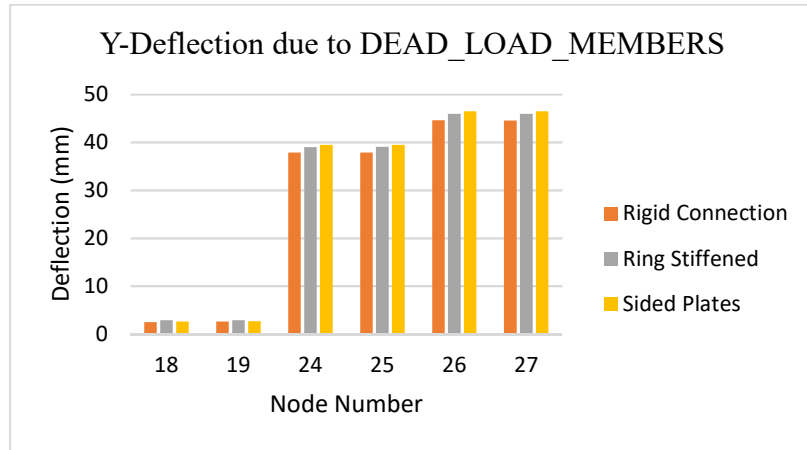
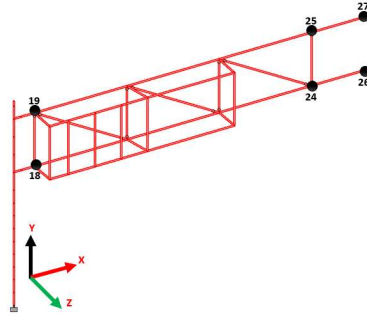
Figure 5.4 (A) rigid model (B) rigid-dead load (C) gusseted-normal wind (D) gusseted-dead load (E) ring stiffened-normal wind (F) gusseted-dead load.

The analysis considered two load cases, the dead load and the normal wind load on members, and the joints displacement were recorded for 6 nodes, near the pole and at the tip of the cantilever. Results are shown in Table 5-3 and Figure 5.5. From the preceding analysis, it is shown that the ring stiffened connection and the gusseted box connection

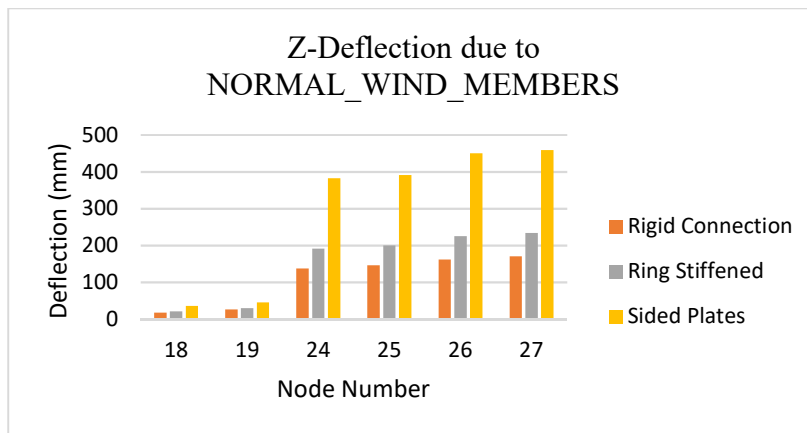
gave almost the same response as the rigid theoretical connection in the Y direction due to the dead load. At the same time, there are differences in the Z- direction deflection due to the flexible nature of these connections. As a result, it was felt that the modeling of the connection is reasonable.

Table 5-3 Key nodes deflection for the three models.

Model	Node	Load Case	X(mm)	Y(mm)	Z(mm)
Rigid connection	18	DEAD LOAD MEMBERS	7.186	-2.471	0.404
		NORMAL WIND MEMBERS	-0.000	0.003	17.307
	19	DEAD LOAD MEMBERS	13.724	-2.583	0.777
		NORMAL WIND MEMBERS	0.001	0.008	25.830
	24	DEAD LOAD MEMBERS	7.101	-37.859	0.271
		NORMAL WIND MEMBERS	0.102	0.298	137.162
	25	DEAD LOAD MEMBERS	13.762	-37.863	0.783
		NORMAL WIND MEMBERS	0.077	0.298	145.601
	26	DEAD LOAD MEMBERS	7.101	-44.604	0.243
		NORMAL WIND MEMBERS	0.102	0.319	161.640
	27	DEAD LOAD MEMBERS	13.762	-44.596	0.769
		NORMAL WIND MEMBERS	0.077	0.320	169.972
The gusseted box connection	18	DEAD LOAD MEMBERS	7.143	-2.612	0.380
		NORMAL WIND MEMBERS	-0.003	0.008	36.082
	19	DEAD LOAD MEMBERS	13.968	-2.686	0.801
		NORMAL WIND MEMBERS	-0.014	0.008	44.838
	24	DEAD LOAD MEMBERS	7.059	-39.462	0.285
		NORMAL WIND MEMBERS	0.089	0.258	382.543
	25	DEAD LOAD MEMBERS	14.005	-39.466	1.017
		NORMAL WIND MEMBERS	0.258	391.453	391.453
	26	DEAD LOAD MEMBERS	7.059	-46.490	0.278
		NORMAL WIND MEMBERS	0.089	0.274	450.178
	27	DEAD LOAD MEMBERS	7.143	-2.612	0.380
		DEAD LOAD MEMBERS	-0.003	0.008	36.082
The ring stiffened connection	18	DEAD LOAD MEMBERS	7.143	-2.612	0.380
		NORMAL WIND MEMBERS	-0.003	0.008	36.082
	19	DEAD LOAD MEMBERS	13.968	-2.686	0.801
		NORMAL WIND MEMBERS	-0.014	0.008	44.838
	24	DEAD LOAD MEMBERS	7.059	-39.462	0.285
		NORMAL WIND MEMBERS	0.089	0.258	382.543
	25	DEAD LOAD MEMBERS	14.005	-39.466	1.017
		NORMAL WIND MEMBERS	0.258	391.453	391.453
	26	DEAD LOAD MEMBERS	7.059	-46.490	0.278
		NORMAL WIND MEMBERS	0.089	0.274	450.178
	27	DEAD LOAD MEMBERS	7.143	-2.612	0.380
		DEAD LOAD MEMBERS	-0.003	0.008	36.082



(A)



(B)

Figure 5.5 Key nodes deflection for three models (A) Dead load case (B) Normal wind load case

After that, a convergence study was conducted to verify that the model converged and to find out the mesh size that provides a mesh-independent solution for the critical stress. This was done by comparing the stresses obtained by different mesh densities. Figure 5.6 shows the stress for different mesh densities vs. mesh sizes. It was concluded from the graph that

the mesh size with three elements across the height/width provides a stable solution. Since the developed approach will be capable of generating different models with varying parameters and the STAAD Pro will perform the analysis for multiple wind speeds, the 3-element model was reproduced in such a way to yield the same results with less computational time. The three-element plate model was replaced by two plates only along the height of the connection, and beam elements were connected to the two-sided plates at three locations, namely, the top, middle, and bottom. Figure 5.7 shows the location of the beams and the beam connections. The beams properties in the new support model were calibrated against the three-meshed support to yield the same stress at different spots and ensure that the structure's global response is identically the same.

Figure 5.8 compares the stress values for different locations in both models under various loading to ensure that the beam model will yield the same response. Clearly from the graph, the stress in both models is identical to each other, and the beam model connection provides satisfactory results. It is considered an excellent tradeoff between the accuracy of the results and computational time since multitude of simulations will be carried out during the structure's service life span.

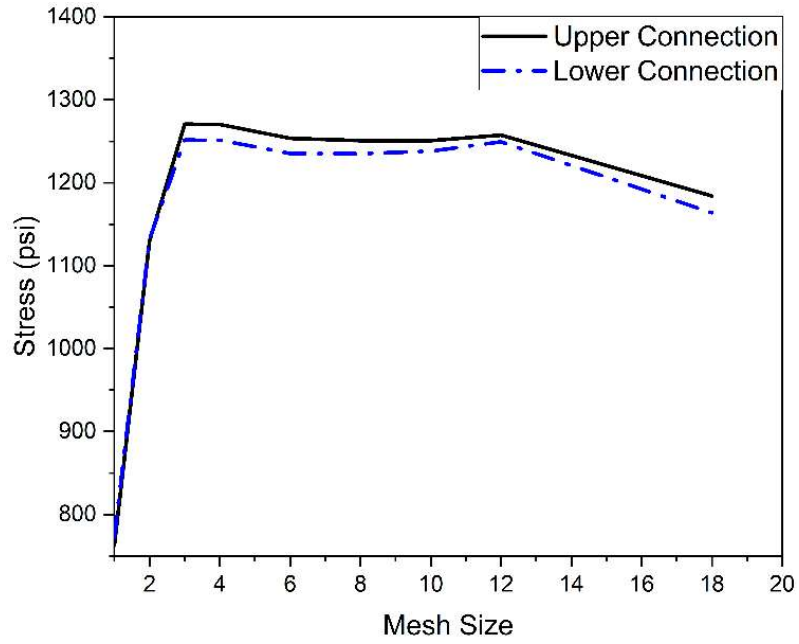


Figure 5.6 Stress at center of the plate vs. mesh density

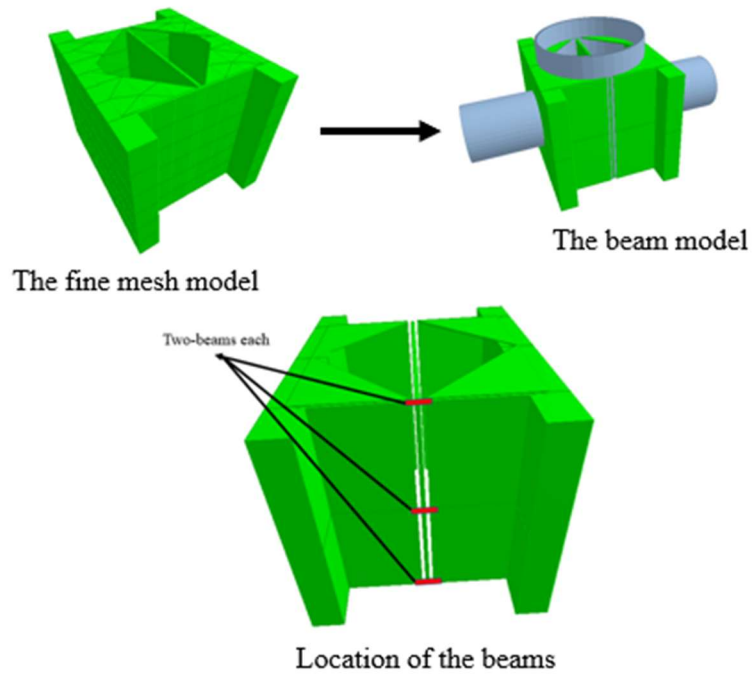


Figure 5.7 The calibrated beam connection

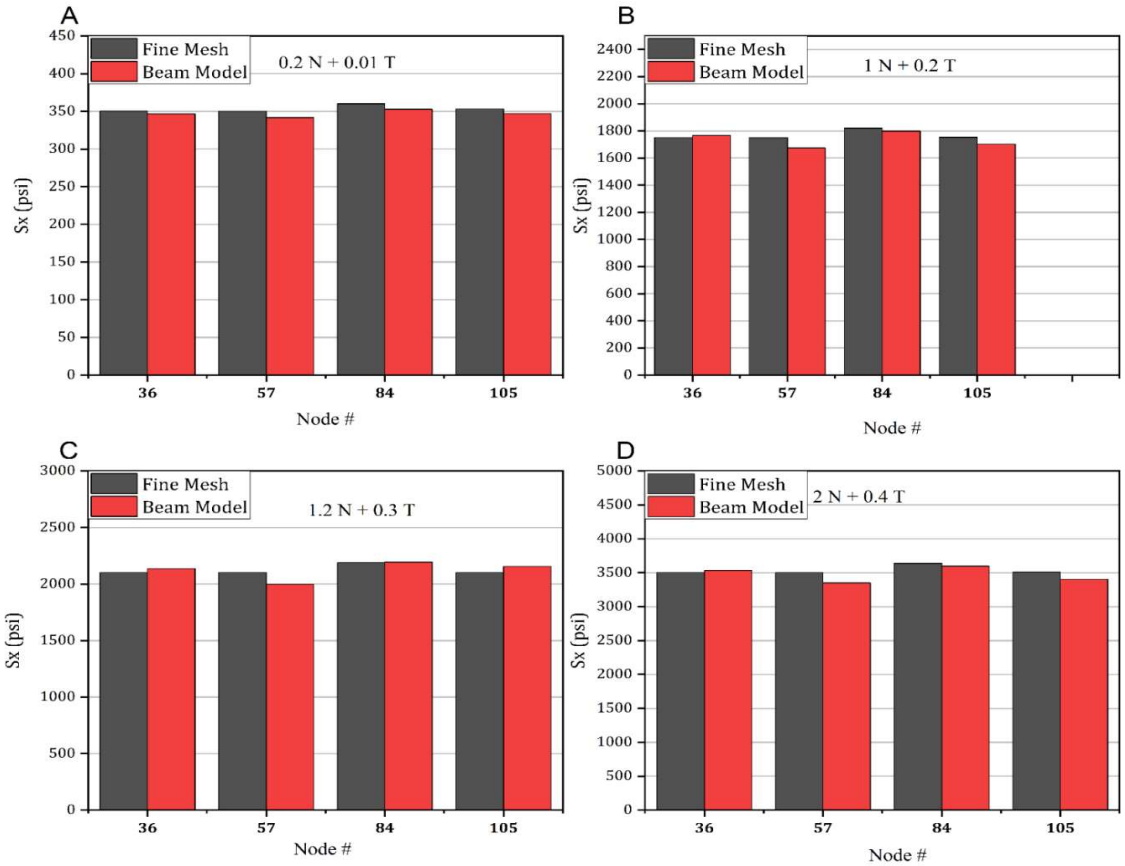


Figure 5.8 Stress comparison in different locations for the beam model vs. the fine-meshed model

5.3.2.3 Sign(s) Modeling

The cantilever and butterfly structures carry the sign(s) -if they exist -on the truss, and the sign placement varies with location, length, and height of the sign and the number of the total signs. The sign is modeled in the structure by creating a frame attached to the truss using four elements, and the sign ribs are distributed within the frame depending on the number and spacing of the ribs. The wind load was calculated based on the size of the sign then distributed equally over the ribs. Since the sign location is sensitive in the cantilever structure, the frame and the ribs are created on the cantilever truss at their respected location in the actual structure. The software will be capable of creating intermediate nodes if needed to connect the sign frame to the primary chords of the truss.

5.4 Dynamic Amplification Factor (DAF)

This study utilized the static solution for certain analytical model, due to the dynamic nature of the wind, the calculated stresses were amplified using an overall blanket average (DAF). The analytical wind modeling was carried out over a range of frequencies [3-300 HZ], assuming harmonic excitations the DAF was calculating by averaging the frequency-response curve, shown in Figure 5.9, for this particular range of frequencies as in Eq. (1).

$$DAF = \frac{\int_0^{1.4} \frac{dR}{\sqrt{(1 - R^2)^2 + (2\xi R)^2}}}{1.4} \quad (1)$$

Where ξ is the damping ratio and $R =$

$\frac{\omega}{\omega_n}$ ω : the excitation frequency, ω_n : natural frequency of the structure

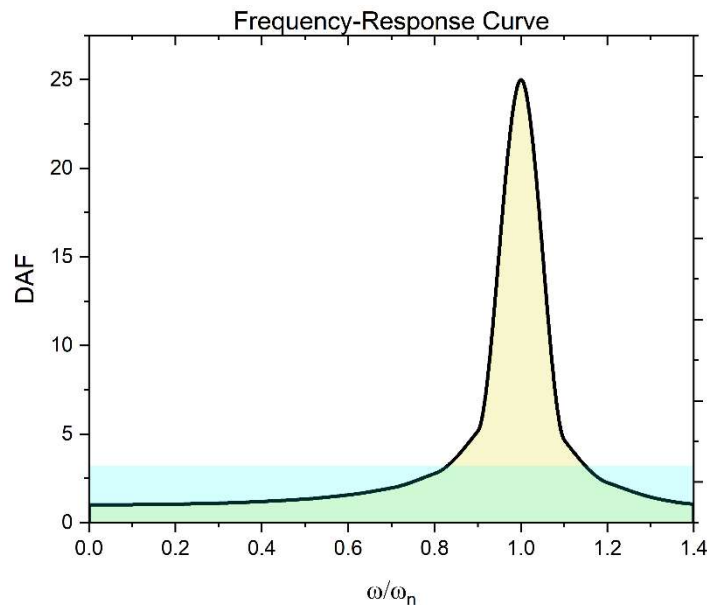


Figure 5.9 Frequency-response curve and average DAF ($\xi = 0.02$)

5.5 Wind Loading on Sign Structures

5.5.1 Synthetic Wind Time Histories

The wind speed records for the state of Kansas was developed earlier using Isoparametric finite element shape functions to derive wind speed records for all unsampled Kansas

counties from actual available data recorded at 17 city locations using the general interpolation formula as in Eq. (2) [17]

$$\hat{Z}(x_0, y_0) = \sum_{i=1}^n w_i Z(x_i, y_i) \quad (2)$$

Where $\hat{Z}(x_0, y_0)$ represents the predicated value at a specific location (x_0, y_0) , $Z(x_i, y_i)$ represents the measured value at the sample point (x_i, y_i) , w_i is the weight assigned to the sample point, and n is the number of sampling points used in the interpolation [19,20]. The developed wind speed records used to generate analytical wind-time histories to represent the actual natural wind events during the structures service life. The detailed interpolation method described in [17][21]. However, for convenience the analytical derivation of the wind-time histories will be summarized here. A computational method using Kaimal spectrum [22] was utilized in wind-time histories development to generate each daily spectrum using Eq.(3).

$$S_K(f) = \frac{200U_*^2 z}{U_z(1 + 50 \frac{fz}{U_z})^{5/3}} \quad (3)$$

where S_K is the Kaimal spectrum, z is the height above the ground 10 m (33 ft.), U_* is the shear velocity, U_z is the mean wind velocity at z , f is the specified frequency.

The fluctuation part of the wind-time history obtained by superimposing cosine waves over the entire frequency range and randomly generated phase angles, Eq.(4) [23,24].

$$u(t) = \sum_{i=1}^N \sqrt{2S_i f_i \Delta f} \cdot \cos(2\pi f_i t + \phi_i) \quad (4)$$

Where ϕ_i is a randomly generated phase angle between 0 and 2π .

After generating the turbulence time history, this fluctuating function combined with the mean wind speed in any given day to produce a complete wind time history. The full-time history is given by

$$U(t) = U_z + \sum_{i=1}^N \sqrt{2S_i f_i \Delta f} \cdot \cos(2\pi f_i t + \phi_i) \quad (5)$$

5.5.2 Wind Loading Calculation

The wind loading resulted from certain wind speed was evaluated through calculating the wind pressure using AASHTO 2015, Eq. (6).

$$P_z = 0.00256 K_z G V^2 I_r C_d \text{ (psf)} \quad (6)$$

Where K_z is the height and exposure factor calculated based on the height of the member and conservatively taken not to be less than 1.0, if the structure on a bridge this value taken to be 1.3. G is the gust factor =1.14, V is the applied wind velocity (mph), I_r is the importance factor = 1.0. The drag coefficient (C_d) was considered based on the object size and shape. For the truss members, the value of C_d was taken to be 1.2, while for the signs, the value of C_d was determined based on the aspect ratio. After generating the pressure resulted from each wind speed, the pressure is multiplied by the area where it is applied to generate wind force. The effect of the natural wind during the structure's service life was automated using the developed software. The software can generate the wind loading and populate it to the Staad Pro models. Both effects of wind loading on signs and members were considered using AASHTO fatigue load cases.

5.6 Fatigue Damage Evaluation

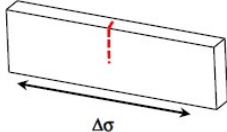
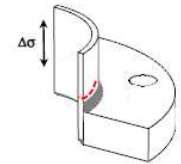
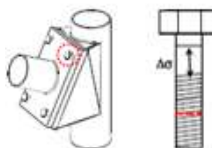
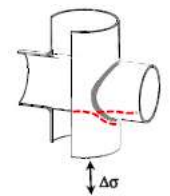
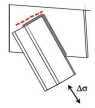
5.6.1 AASHTO S-N Curves

The $S-N$ method was used in the scope of this paper to evaluate the fatigue life of different structural components. AASHTO 2015 manual [5] provides $S-N$ curves for different connection types based on a wide range of laboratory fatigue tests of full-scale structures. Eq. (7) could express the number of cycles to failure, Where N_i is the number of cycles to failure at i -th stress range, $\Delta\sigma_i$ is the member stress value corresponding to a

wind speed value. A' is a constant associated with the component provided in AASHTO manual [5]. Table 5-4 describes the $S-N$ equation for different components that were used in this study. Each $S-N$ curve has a flat plateau described as the threshold in the table. Below this value, the stress is assumed to have no contribution to the cumulative damage and the components have infinite life.

$$N_i = \frac{A'}{\Delta\sigma_i^3} \quad (7)$$

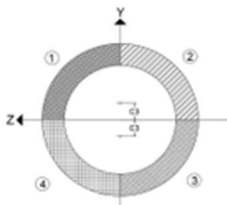
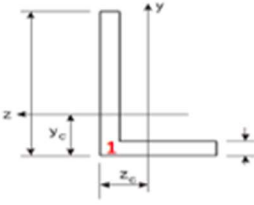
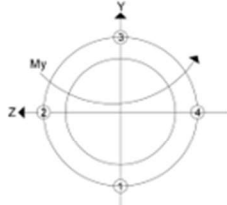
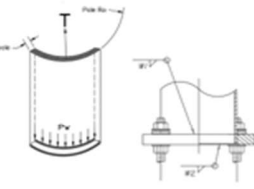
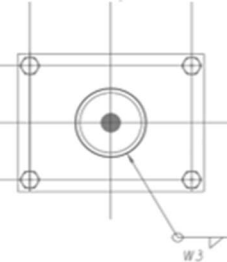
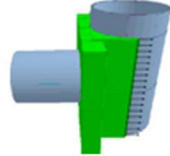
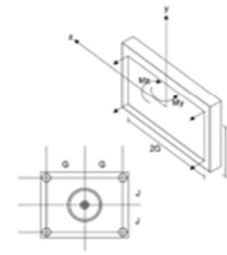
Table 5-4 S-N equations for different structure components used by AASHTO

Description	$A \times 10^8$ (ksi ³)	Threshold (ksi)	Example	Location	Description	$A \times 10^8$ (ksi ³)	Threshold (ksi)	Example	Location
Plain Material	250	24		Pole Members And truss main mem.	Fillet-welded tube-to-transverse-plate connections	3.9	2.6		Base plate
Gusseted box connections	Infinite life	--		Mast arm connection	Anchor bolts	22	7		Connection bolts
Ring-Stiffened box connections	Infinite life	--		Mast arm connection	Partial-penetration groove-welded mast-arm-to column pass-through connections	11	4.5		Arm weld
Angle-to-gusset connections	3.9	2.6		Secondary members Weld Connection					

5.6.2 Damage Assessment and Palmgren-Miner Rule

Once the structural analysis is completed for all the wind speeds in the time period where the structure is investigated, the member end forces resulted from the FE solution were collected for each structural component associated with a wind speed. The axial stress was calculated in each critical component, as indicated in Table 5-5. The resulting stress was amplified using the DAF. Then, each critical member is associated with an appropriate S-N curve from the AASHTO to calculate the needed number of cycles to failure. Moreover, the fractional damage was calculated by using Miner rule Eq. (8) to estimate the damage consumption by finding the ratio of the number

Table 5-5. Stress calculation in different structure spots.

Location	Example	Stress	Location	Example	Stress
Main members		$\sigma_{x1} = \frac{My}{2C_3 \frac{\pi}{2} (r_o^2 - r_i^2)} - \frac{Mz}{2C_3 \frac{\pi}{2} (r_o^2 - r_i^2)}$ $\sigma_{x2} = \frac{-My}{2C_3 \frac{\pi}{2} (r_o^2 - r_i^2)} - \frac{Mz}{2C_3 \frac{\pi}{2} (r_o^2 - r_i^2)}$ $\sigma_{x3} = \frac{-My}{2C_3 \frac{\pi}{2} (r_o^2 - r_i^2)} + \frac{Mz}{2C_3 \frac{\pi}{2} (r_o^2 - r_i^2)}$ $\sigma_{x4} = \frac{My}{2C_3 \frac{\pi}{2} (r_o^2 - r_i^2)} + \frac{Mz}{2C_3 \frac{\pi}{2} (r_o^2 - r_i^2)}$	Secondary members		$\sigma_{x1} = -y \frac{M_z I_{yy} + M_y I_{yz}}{I_{yy} I_{zz} - I_{yz}^2} + z \frac{M_y I_{zz} + M_z I_{yz}}{I_{yy} I_{zz} - I_{yz}^2} + \frac{Fx}{A}$
Pole		$\sigma_x = \frac{My \cdot r}{I} + \frac{Fx}{A}$	Base plate weld		$\sigma_x = \frac{\pm My}{2C_3 \frac{\pi}{2} (r_o^2 - r_i^2)} \pm \frac{Mz}{2C_3 \frac{\pi}{2} (r_o^2 - r_i^2)}$ $\sigma_w = \sigma_x \frac{t_p}{t_{w1} + t_{w2}}$
Arm weld		$\sigma_x = \frac{\pm My}{2C_3 \frac{\pi}{2} (r_o^2 - r_i^2)} \pm \frac{Mz}{2C_3 \frac{\pi}{2} (r_o^2 - r_i^2)}$ $\sigma_w = \sigma_x \frac{t_m}{t_{w2}}$	Connection Weld		$\sigma_w = S_x \frac{t_p}{t_w}$
Connection Bolts		$\sigma_x = \frac{My}{4G \frac{\pi}{4} d_b^2} + \frac{Mz}{4J \frac{\pi}{4} d_b^2} + \frac{T}{4 \frac{\pi}{4} d_b^2}$			

of stress cycles experienced by the structure to the number of cycles required for failure. As indicated by the $S-N$ curve, only the stresses greater than the threshold were assumed to contribute to the damage.

$$D_i = \frac{n_i}{N_i} \quad (8)$$

Where D_i is the damage in a specific member at a particular stress range, n_i is the number of cycles at i -th stress range, obtained from Rainflow analysis, N_i is the number of cycles to failure at the same stress range. In the scope of this work, wind time histories were generated for the 45 years of data [21] these histories represent highly irregular variations of speed with time. Rainflow counting technique [25] was used to convert the irregular time histories to cycles.

$$D = \sum_i D_i \quad (9)$$

The cumulative damage was determined by adding all the fractional damages associated to each wind speed using Eq. (9).

5.7 Analysis Automation

Figure 5.10 explains the flow chart for the developed procedures. The current environment requires certain inputs from the user regarding the structure geometry, the sign placement, and the wind data then the analysis should be carried out for the analytical model after exposing it to various wind speeds depending on the location of the structure, the built time, and the inspection year. Automation for the aforementioned steps was developed through user-friendly software written in C# to perform the simulations and damage calculations efficiently. The user can specify the type of the structure, provide the necessarily geometric parameters, execute the analysis, and display the results. Figure 5.11 shows the developed software interface and the main input parameters. The engineer can

also specify if any of the components experienced corrosion by selecting a thickness reduction factor to account for a different level of corrosion based on engineering judgment.

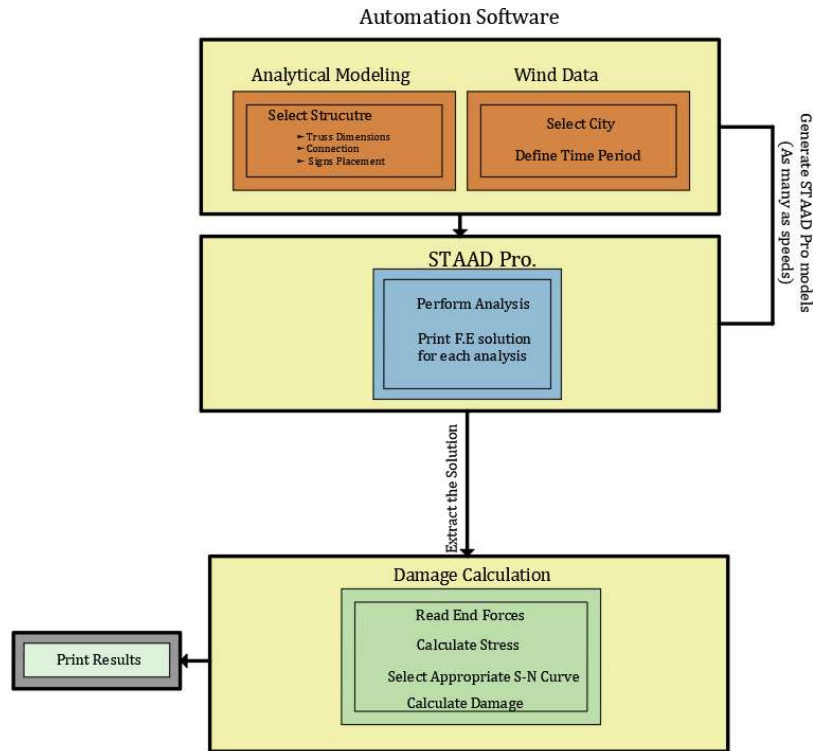


Figure 5.10 Flowchart of the automation algorithm

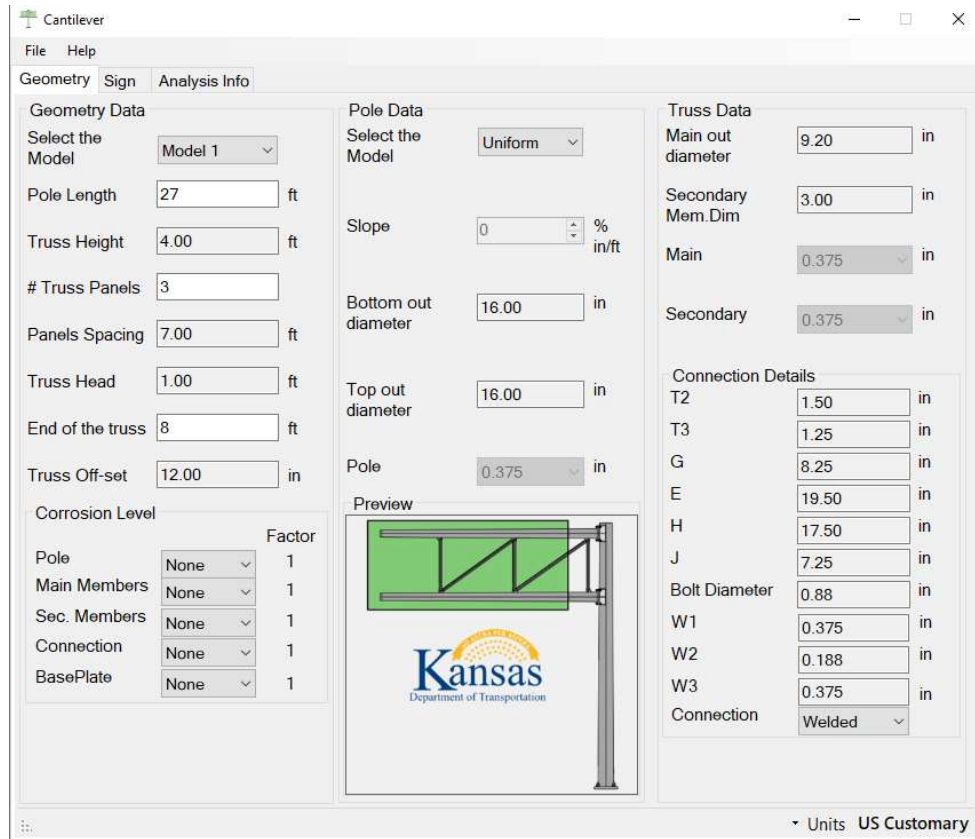


Figure 5.11 The modeling software interface

5.8 Evaluation of a Damaged Structure and Software Validation

5.8.1 Background

A cantilever highway sign structure that has been in service for 32 years was selected to test the validity of the developed approach. The structure is located in Sedgwick County, Kansas, over northbound I-235 at ramp to West Street. The structure consisted of 3 panels spaced at 7ft. (2133.6 mm) and supported over a single tapered pole that has a height of 27 ft. (8229.6 mm) and base outer diameter OD of 16 in. (406.4 mm). The main truss has design model 1 properties and consisted of multiple angle sections $3'' \times 3'' \times 3/8''$ connected by welded angle-to-gusset connections. The full geometric details are shown in Figure 5.12 and the general structure properties are presented in Table 5-6.

Table 5-6. Sedgwick structure information

Structural Data		Original project data		Sign and attachment		
Structure type	Cantilever	Date let	1987	Sign ID	Sign height (ft.)	Sign length (ft.)
Structure material	Galvanized Steel	Inspection Date	10/30/2019	12737	6.5	12.5
Arm truss span	30 ft.			12738	2.5	7.5
Vertical clearance	18 ft.					

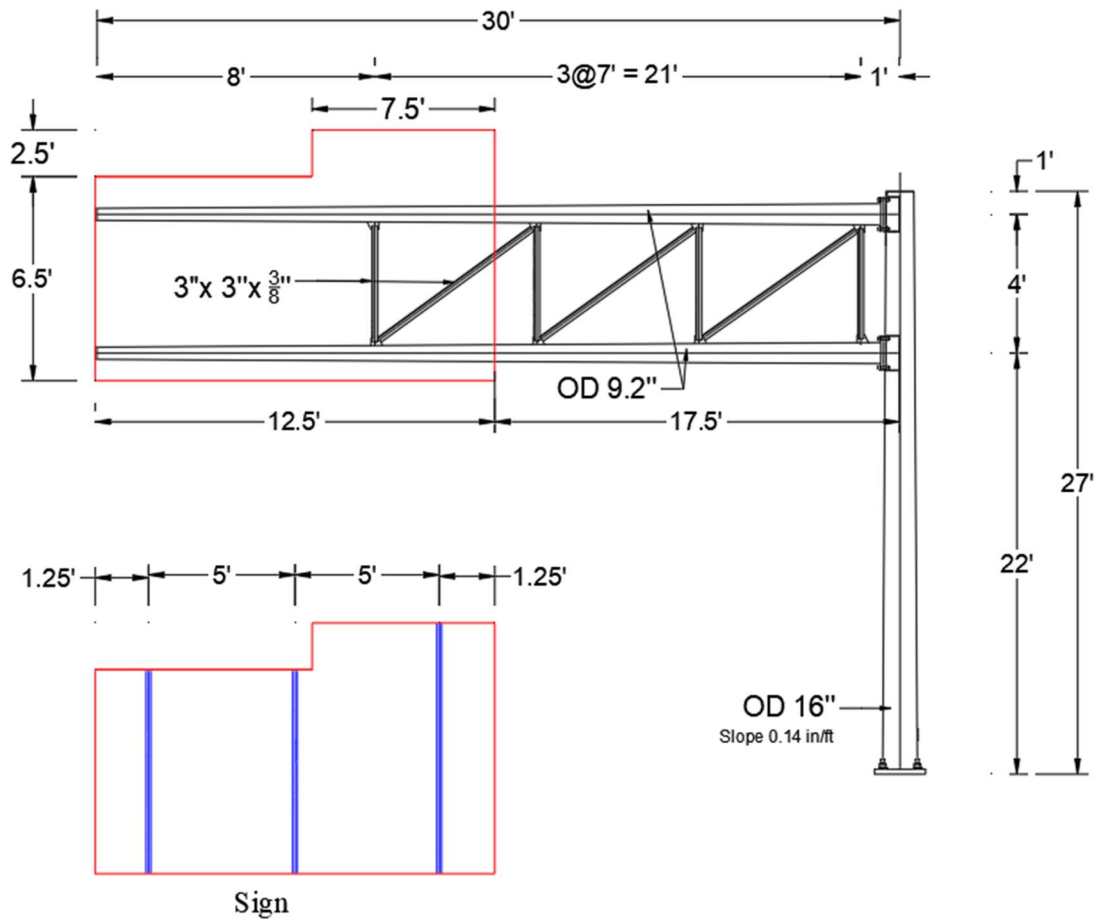


Figure 5.12 Sedgwick structure geometry (all dimensions are in feet/inches)

5.8.2 Field Inspection of the Structure

On October 30th, 2019, the KDOT had performed a comprehensive field inspection to assess the condition of all the structure components as part of their regular inspection plans.

The visual inspection revealed different corrosion levels for the entire structure, 50%

corrosion staining was observed on the anchor bolts hardware, and full corrosion staining on the full height of the column. In addition to that, the connection plates have corrosion staining reflected through corrosion bleed-out emanating from the weld copings. A complete fatigue crack in the vertical weld of mast-to-arm box connection at the upper chord level also was observed. Close-up view of the vertical column-to-mast arm connection is shown in Figure 5.13. Obviously, the crack occurred in the entire weld toe resulting in a complete separation of the vertical splice plate from the column.



Figure 5.13 Crack in the weld toe in Sedgwick structure, courtesy of KDOT (Bureau of structural and geotechnical services).

5.8.3 Analytical Investigation

AASHTO 2015 *Structural Supports for Highway Sign LTS* specifies an infinite life for the both mast-arm-to-pole connections; the fillet-welded, and the ring-stiffened box if they were detailed as per the recommendations in Article 5.14.7. These connections were tested experimentally in full size, and they did not develop any fatigue cracking under both in-plane and out-of-plane loading scenarios. However, in all the tested specimens the fatigue

cracking occurred in other critical locations such as the tube-to-transverse-plate welds in the mast arm and/or the pole, and/or hand holes [2,5]. The connection between the side plate and the pole falls under the category of E' details in AASHTO specification having a CAFT of 2.6 ksi (18 Mpa). The wind loading event for the whole structure life was revealed a range of wind speeds (1-33 mph) with the corresponding number of cycles that might the structure experience. After providing the software with the necessary information, including an approximated average corrosion reduction factor of about 17%, which reflects the existing conditions of this structure the software starts to build and run the analysis. Upon performing the required successive analysis by STAAD pro, the software read back and classified the end forces for each component. The fatigue engine evaluated the fatigue life consumption for each component in the model and displayed the results in the results screen, as shown in Figure 5.14. Based on Miner's rule, the stressed component approaches the end of its life when the cumulative damage index exceeds unity. Thus, the end of fatigue life was detected only for the Mast-to-arm connection colored in red with a damage index of 1.116. The stress variation with wind speed for the connection along with the wind speed cycles were plotted and shown in Figure 5.15. The stress life method assumed that the stresses greater than CAFT (2.6 ksi for this connection) contribute to the fatigue damage accumulation. From the plot, only the stresses resulting from the wind speeds (21-33 mph) will cause fatigue damage. The number of cycles to failure associated with each stress is calculated using the $S-N$ equation with $A' = 3.29 \times 10^8$ ksi. information shows the fatigue damage calculation as per Miner's rule. The possibility of this complete fatigue crack is likely due to the poor quality of the weld, some defects are very likely to exist resulting in local stress concentration yielding to rapid fatigue damage accumulation. Moreover, the

harsh corrosion environment introduced discontinuities along the weld length resulted in significant lower fatigue resistant. Another important reason, the geographical area plays a vital rule in the analysis results since the variation in fatigue life is extremely correlated to the difference in wind environment in various sites, Sedgwick County is known by the strong wind records and many ancillary structures have shown different level of wind related distress as per KDOT. In addition, the wind-induced fatigue damage was evaluated for all different critical spots in the structure, namely, pole-to-base plate weld connection, chord-to-transverse plate weld connection, anchor bolts, and all the truss members. the fatigue lives of all the previous details were found to be infinite for this particular structure. This attributed to that at lower wind speeds, all the stresses experienced by these details are below the threshold stress thus no fatigue damage was developed. At the same time, at higher wind speeds the stresses are higher than the threshold causing a tendency to develop fatigue damage, but the number of cycles is low to an extent not causing this damage to be significant resulting in infinite life.

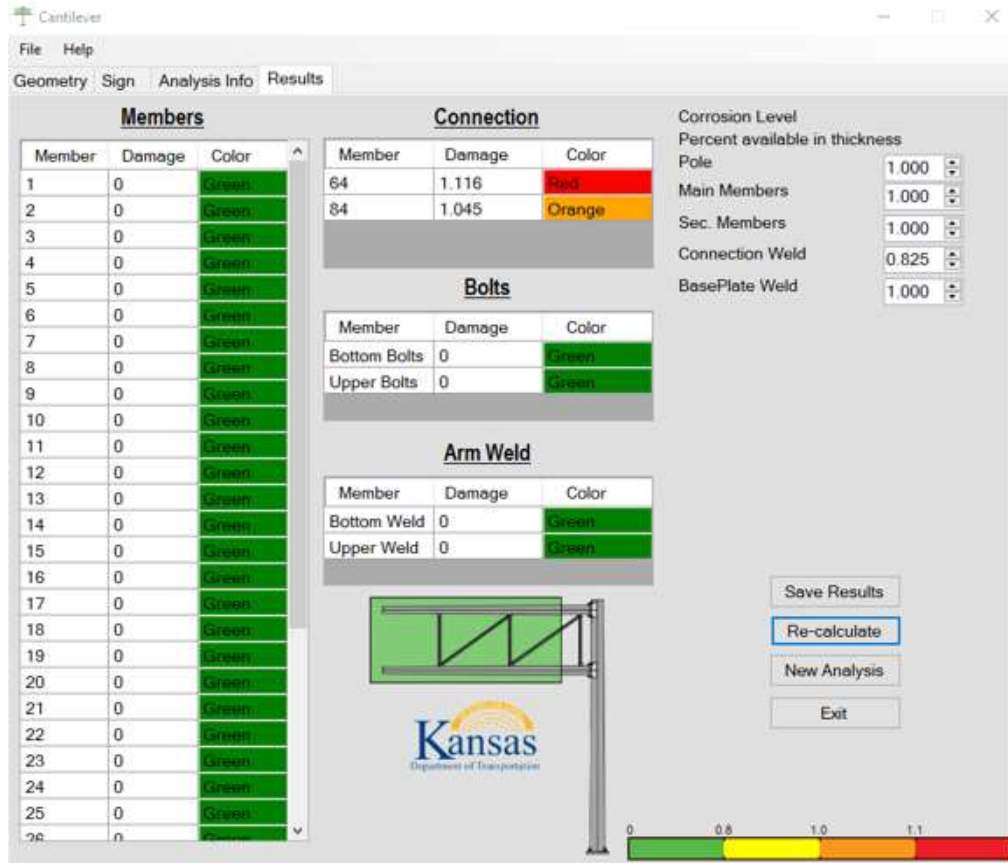


Figure 5.14 Fatigue life results in Sedgwick structure.

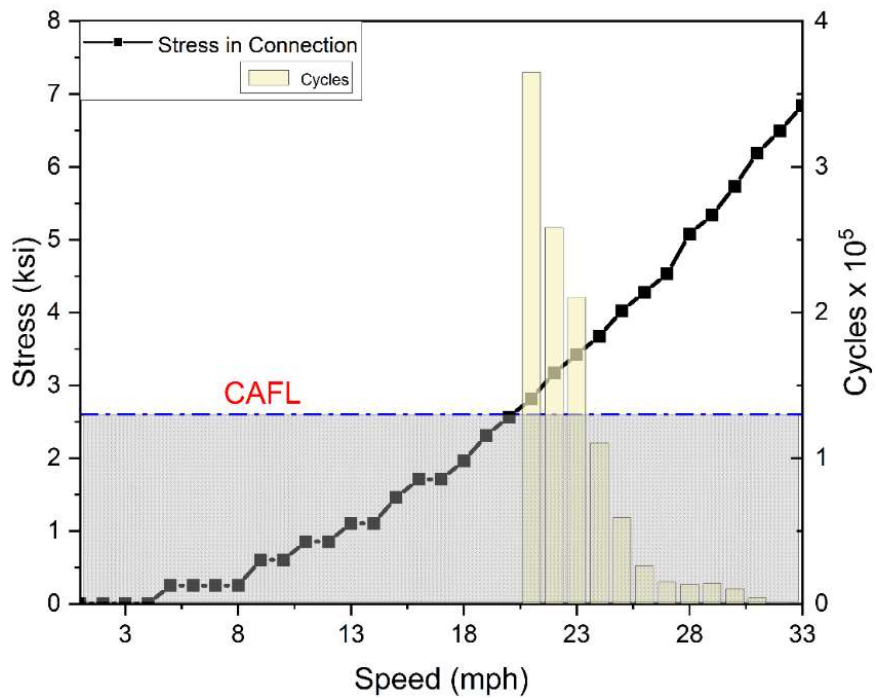


Figure 5.15 Stress variation with wind speed in the connection

Table 5-7. Stress and damage in connection associated to each wind speed

Speed (mph)	Stress (ksi)	N _i (Cycle)	n _i (Cycle)	D _i
21	2.82	17421692.22	3647732	0.2094
22	3.17	12235811.27	2582522	0.2111
23	3.42	9730332.478	2102996	0.2161
24	3.67	7864766.583	1105565	0.1406
25	4.03	5975640.433	590647.5	0.0988
26	4.28	4981930.229	260106	0.0522
27	4.53	4196883.267	149004	0.0355
28	5.08	2969547.639	133981.5	0.0451
29	5.33	2568838.623	138694.5	0.0540
30	5.74	2065094.187	102642	0.0497
31	6.19	1644141.092	40464	0.0246
32	6.49	1425231.089	4365	0.0031
33	6.84	1216291.56	405	<u>0.0003</u>
				Sum
				= 1.1

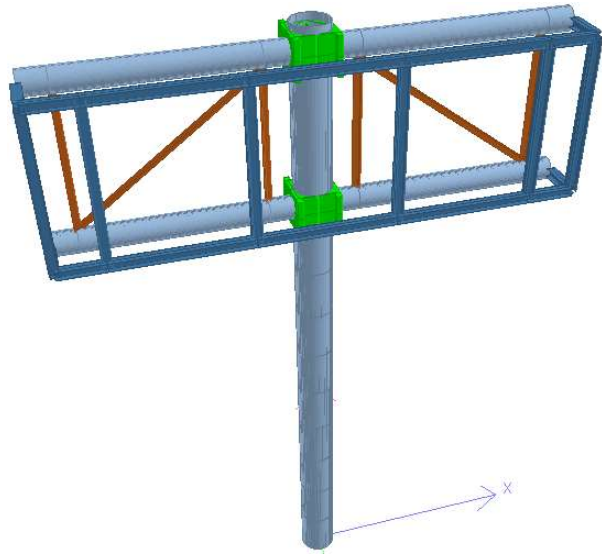
The same software was developed for the butterfly sign structures. The fatigue life for the butterfly truss members was re-calculated using the software to compare the analytical results with the actual condition of the structure. The structure is located in Wyandotte county, Kansas. The truss details and model shown in Table 5-8 and Figure 5.16, respectively. After completing the required analysis, the results screen indicated none of any component experienced fatigue damage as shown in Figure 5.17.

Table 5-8 Wyandotte structure information

Structural Data		Original project data		Sign and attachment		
Structure type	Butterfly	Date let	1985	Sign ID	Sign height (ft.)	Sign length (ft.)
Structure material	Galvanized Steel	Inspection Date	8/6/2019	---	8.5	18
Arm truss span	10 ft.					
Vertical clearance	0 ft.					



(a)



(b)

Figure 5.16 (a) the actual structure (b) the model

Members			Connection			Corrosion Level Percent available in thickness	
Member	Damage	Color	Member	Damage	Color	Pole	
1	0	Green	88	0	Green	1.000	
2	0	Green	124	0	Green	1.000	
3	0	Green				Main Members	1.000
4	0	Green				Sec. Members	1.000
5	0	Green				Connection Weld	1.000
6	0	Green				BasePlate Weld	1.000
7	0	Green					
8	0	Green					
9	0	Green					
10	0	Green					
11	0	Green					
12	0	Green					
13	0	Green					
14	0	Green					
15	0	Green					
16	0	Green					
17	0	Green					
18	0	Green					
19	0	Green					
20	0	Green					
21	0	Green					
22	0	Green					
23	0	Green					
24	0	Green					
25	0	Green					
26	0	Green					

Bolts		
Member	Damage	Color
Bottom Bolts	0	Green
Upper Bolts	0	Green

Arm Weld		
Member	Damage	Color
Bottom Weld	0	Green
Upper Weld	0	Green

Figure 5.17 Damage in the butterfly member's model

5.9 Conclusions

Analytical fatigue damage evaluation framework was developed and implemented in computer software to provide a cost-effective inspection tool to assess highway sign

structures. Analytical models were created for a cantilever structure based on past wind events history to simulate the damage in different critical truss components. The software showed its superior capability in calculating the fatigue damage by capturing the crack in the mast connection. The main conclusion is that the most critical fatigue detail is the connection since it has lower CAFT and is susceptible to being highly stressed. The ring stiffened connection replaces the gusseted box connection in KDOT standards due to its superiority in resisting fatigue damage. Accurate fatigue damage characterization is highly dependent on the actual past wind events during the service life of the structure. The fatigue failure has been widely noticed in flexible highway structures, and it is essential to alert the highway agencies to the faulty connections in an efficient and timely manner. For this reason, this developed software is projected to have a substantial impact on state highway decision-making and the development of inspection inventories.

Acknowledgment

This work was supported by Kansas Department of Transportation, Bureau of structural and geotechnical services through the grant KTRAN-Project-KSU-20-3 (KDOT)

5.10 References

- [1] Hosseini MS. Parametric study of fatigue in light pole structures 2013.
- [2] Roy S, Park YC, Sause R, Fisher JW, Kaufmann EJ. Cost-effective connection details for highway sign, luminaire, and traffic signal structures. 2011.
- [3] Hamilton III HR, Puckett JA, Gray B, Wang P, Deschamp B, McManus P. Traffic Signal Pole Research. 2004.
- [4] Puckett JA, Erikson RG, Peiffer JP. Fatigue testing of stiffened traffic signal structures. J Struct Eng 2010;136:1205–14.
- [5] AASHTO. 2015 Interim Revisions to Standard Specifications for Structural Supports for Highway Signs , Luminaires , and Traffic Signals Sixth Edition 2013. 2015.

- [6] DeSantis P V, Haig PE. Unanticipated loading causes highway sign failure. Proc. ANSYS Conv., 1996.
- [7] Kaczinski MR, Dexter RJ, Van Dien JP. Fatigue-resistant design of cantilevered signal, sign and light supports. vol. 412. Transportation Research Board; 1998.
- [8] Dexter RJ. Fatigue-resistant design of cantilevered signal, sign, and light supports. vol. 469. Transportation Research Board; 2002.
- [9] Creamer BM, Frank KH, Klingner RE. Fatigue loading of cantilever sign structures from truck wind gusts. 1979.
- [10] Barle J, Grubisic V, Vlak F. Failure analysis of the highway sign structure and the design improvement. Eng Fail Anal 2011;18:1076–84.
<https://doi.org/https://doi.org/10.1016/j.engfailanal.2011.02.006>.
- [11] Choi H, Roda AM, Najm H. Fatigue Study on Structural Supports for Luminaries, Traffic Signals, Highway Signs (LRFD LTS Specifications) 2015.
<https://doi.org/10.13140/RG.2.2.23638.24648>.
- [12] Rice JA, Foutch DA, LaFave JM, Valdovinos S. Field testing and analysis of aluminum highway sign trusses. Eng Struct 2012;34:173–86.
<https://doi.org/https://doi.org/10.1016/j.engstruct.2011.09.021>.
- [13] Li X. Fatigue strength and evaluation of highway sign structures 2005.
- [14] Tsai L-W, Alipour A. Studying the wind-induced vibrations of a traffic signal structure through long term health monitoring. Eng Struct 2021;247:112837.
- [15] Choi H, Najm H. Fatigue reliability assessment of potential crack initiation of tube-to-transverse plate connections for cantilever sign support structures. J Perform Constr Facil 2018;32:4018002.
- [16] Zheng R, Ellingwood BR. Stochastic fatigue crack growth in steel structures subject to random loading. Struct Saf 1998;20:303–23.
[https://doi.org/https://doi.org/10.1016/S0167-4730\(98\)00020-4](https://doi.org/https://doi.org/10.1016/S0167-4730(98)00020-4).
- [17] Al Shboul, Khalid W. Rasheed, Hayder A. AlKhiary A. Spatial Wind Speed Interpolation Using Isoparametric Shape Functions for Structural Loading. Wind Struct 2022.
- [18] Bentley. Staad Pro V8i SS6 2016.
- [19] Ye W. Spatial Variation and Interpolation of Wind Speed Statistics and Its

Implication in Design Wind Load 2013.

- [20] Ben-Israel A, Greville TNE. Generalized inverses: theory and applications. vol. 15. Springer Science & Business Media; 2003.
- [21] Al Shboul KW, Rasheed HA, Alshareef HA. Intelligent approach for accurately predicting fatigue damage in overhead highway sign structures. Structures 2021;34:3453–63. <https://doi.org/https://doi.org/10.1016/j.istruc.2021.09.090>.
- [22] Kaimal JC, Wyngaard JC, Izumi Y, Coté OR. Spectral characteristics of surface-layer turbulence. Q J R Meteorol Soc 1972;98:563–89. <https://doi.org/https://doi.org/10.1002/qj.49709841707>.
- [23] Iannuzzi A, Spinelli P. Artificial wind generation and structural response. J Struct Eng 1987;113:2382–98.
- [24] Bobillier B, Chakrabarti S, Christiansen P. Physical Modeling of Wind Load on a Floating Offshore Structure. J Offshore Mech Arct Eng 2001;123:170–6.
- [25] Matsuishi M, Endo T. Fatigue of metals subjected to varying stress. Japan Soc Mech Eng Fukuoka, Japan 1968;68:37–40.

Chapter 6 - Conclusions and Recommendations

6.1 Conclusions

Structural analysis software continuously benefits engineers in analyzing and designing complex systems subjected to various loading scenarios, which cannot be done without using such sophisticated tools. Most engineering software is based on the Finite element method, which is considered the most efficient method used for structural analysis tackling different analysis levels. This involves linear and nonlinear problems of systems with complicated geometries, material properties, loads, and boundary conditions. Using such software with proven algorithms saves time and cost due to its enormous capabilities and the high automation of individual tasks. Accordingly, most of the engineer tasks become easily approachable from design checks, optimization, cost estimation, rendering, and producing the final project drawings. The capabilities of widely used commercial structural engineering software are fundamentally the same and may vary between different software due to the customization made to meet the customer's needs. However, the cornerstone principle of the methodology remains the same. Nowadays, large full-span overhead sign support structures are widely used on any major highway to guide and help commuters. These highway sign structures must support large truss spans to provide the needed information for the passengers without disturbing their way and introducing any possible hazard that may result from any intermediate supports. Due to their long spans and the use of hollow circular tubes with a relatively small mass, these structures are considered semi-rigid with a low natural frequency and damping ratio. As a result, they experience fatigue failure, mainly due to natural wind loading. The demand for developing a systematic inspection tool to predict the condition of existing structures and connection

details is drastically increased by government officials due to the complexity of the inspection process. Moreover, it may involve human injuries. Also, besides the fact that physical inspection for the structural members at various locations in different cities is costly and time-consuming, it is inefficient and may include human errors. The initial idea for developing a new software tool for fatigue predictions for highway sign structures emerged from the lack of algorithmized framework deployed in standalone commercial software capable of such analyses

This research intends to develop an inspection framework along with windows desktop application to accurately simulate and calculate the fatigue damage of highway sign structures using AASHTO standards. The object-oriented programming concept was utilized in this work to develop the software for the state of Kansas. Moreover, it can be extended to different states and locations worldwide once the wind speed records have been populated.

The following significant findings were compiled from the current study.

- The finite element spatial interpolation technique accurately estimates spatially continuous phenomena from measured values at limited sample points.
- Adequate care should be given during the meshing of the study area since this method is highly spatially dependent.
- The FE interpolation technique proved to be an excellent spatial interpolator for recovering Wichita records based on statistical assessment.
- The global trend of predicted values in Sedgwick County captured the measured wind

records for most of the studied years while it admitted some relatively high peak windspeed values for 1990 and low corresponding values in 2000 and 2005.

- fatigue damage detection procedures were developed and implemented into computer software to quantify the cumulative damage in flexible highway sign structures.
- The developed software was used to inspect a four-chord overhead truss structure in the city Wichita exposed to 45 years of wind loading history. Based on the results obtained from the analysis, it was shown that the overhead truss structure in Wichita experienced some full fatigue damage in two members (damage index = 1.1).
- The follow up in-situ inspection performed by KDOT indicated that these two members were specifically subject to severe fatigue cracking. Further analysis of the same truss using the AASHTO fatigue $S-N$ equation confirmed this finding.
- The software showed its superior capability in calculating the fatigue damage by capturing the crack in the mast connection for a cantilever structure and the full fatigue life was reached after imposing corrosion factors which reflects the existing conditions of these structures.
- The most critical fatigue detail is the mast-arm-connection since it has lower CAFT and is susceptible to being highly stressed.
- The ring stiffened connection replaces the gusseted box connection in KDOT standards due to its superiority in resisting fatigue damage.
- Accurate fatigue damage characterization is highly dependent on the actual past wind events during the service life of the structure.

- The butterfly models showed no fatigue damage in any of their components, indicating that the torsional effect seems not affecting the cumulative fatigue damage.
- It may appear to be surprising to see the results agree well with the field conditions, although several assumptions and wind simulation approximations are made. This is attributed to the fact that the characteristics of the fatigue problem are a function of the cycle count at each stress range, making the variation effects an averaged one rather than a compounding error one.
- The fatigue life simulator software accepts the development and enhancement to add more extra options and analysis capabilities.